AD-A071 420 NATIONAL AEROSPACE LAB AMSTERDAM (NETHERLANDS) F/G 20/4
TRANSONIC WIND TUNNEL TESTS ON AN OSCILLATING WING WITH EXTERNA--ETC(U)
MAR 79 H TIJDEMAN, J W VAN NUNEN, A N KRAAN AFOSR 77-3233
UNCLASSIFIED NLR-TR-78106-U-PT-2 AFFDL-TR-78-194-PT-2 NL

1 OF 2
AD
A071420

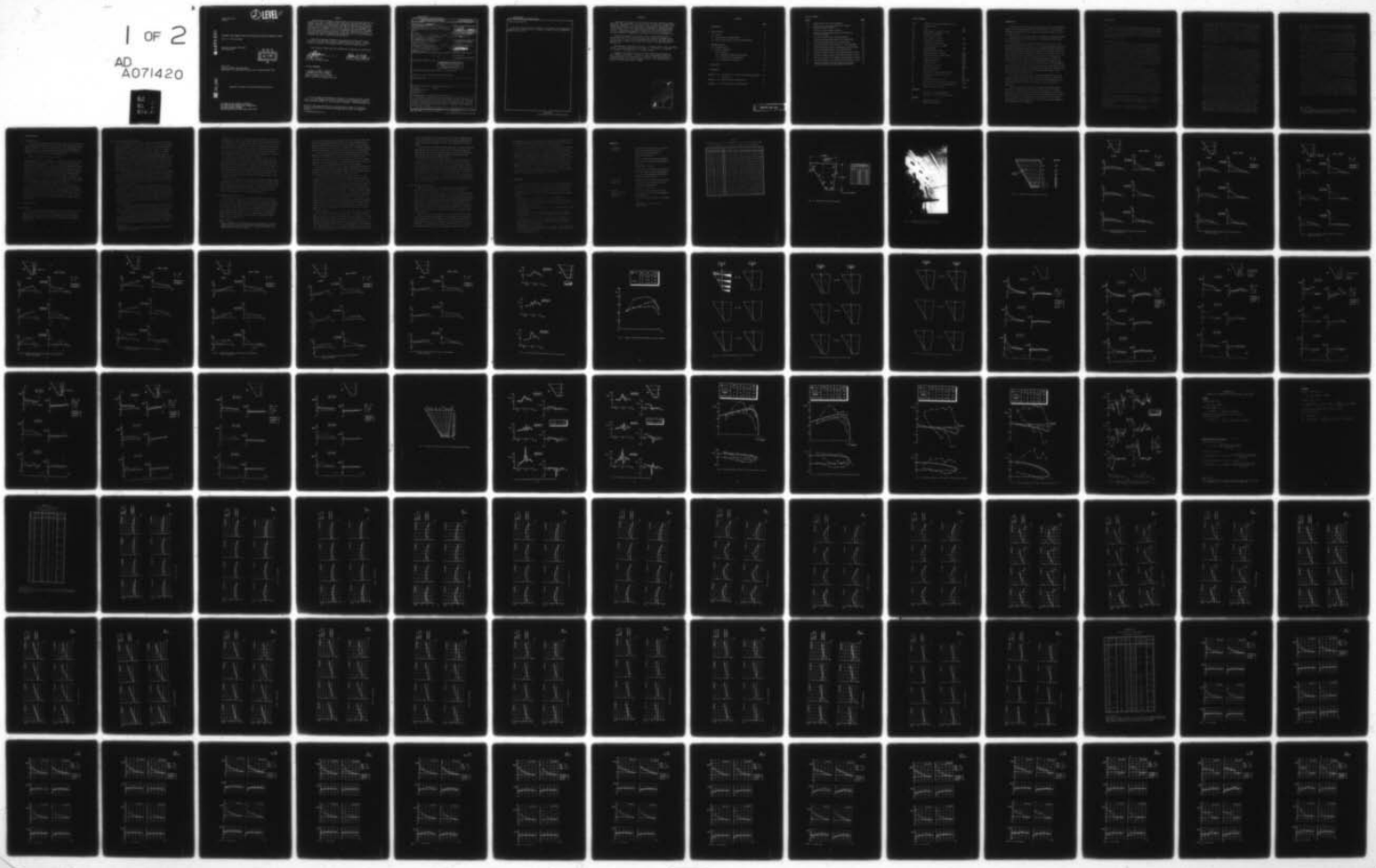

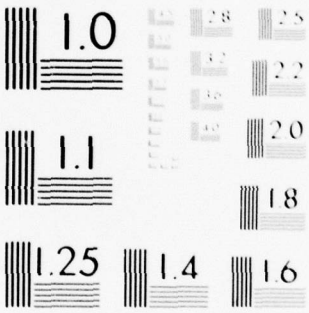

MICROCOPY RESOLUTION TEST CHART
NATIONAL BUREAU OF STANDARDS-1963-A

(2) LEVEL III
A066816

AFFDL-TR-78-194
Part II

AD A071420

TRANSONIC WIND TUNNEL TESTS ON AN OSCILLATING WING WITH EXTERNAL STORES

Part II. The Clean Wing

National Aerospace Laboratory
The Netherlands

DDC
RECEIVED
JUL 19 1979
B

March 1979
TECHNICAL REPORT AFFDL-TR-78-194
Final Report for the Period February 1977 through December 1978

DDC FILE COPY

Approved for Public Release; Distribution Unlimited

AIR FORCE FLIGHT DYNAMICS LABORATORY
AIR FORCE WRIGHT AERONAUTICAL LABORATORIES
AIR FORCE SYSTEMS COMMAND
WRIGHT-PATTERSON AIR FORCE BASE, OHIO 45433

79 07 03 016

NOTICE

When Government drawings, specifications, or other data are used for any purpose other than in connection with a definitely related Government procurement operation, the United States Government thereby incurs no responsibility nor any obligation whatsoever; and the fact that the government may have formulated, furnished, or in any way supplied the said drawings, specifications, or other data, is not to be regarded by implication or otherwise as in any manner licensing the holder or any other person or corporation, or conveying any rights or permission to manufacture, use, or sell any patented invention that may in any way be related thereto.

This report has been reviewed by the Information Office (OI) and is releasable to the National Technical Information Service (NTIS). At NTIS, it will be available to the general public, including foreign nations.

This technical report has been reviewed and is approved for publication.

JAMES D. OLSEN
Principal Scientist
Structural Integrity Branch

NELSON D. WOLF, Acting Chief
Structural Integrity Branch

FOR THE COMMANDER

RALPH L. KUSTER, JR., Col, USAF
Chief, Structures & Dynamics Division

"If your address has changed, if you wish to be removed from our mailing list, or if the addressee is no longer employed by your organization please notify AFFDL/FBE, WPAFB, OH 45433 to help us maintain a current mailing list."

Copies of this report should not be returned unless return is required by security considerations, contractual obligations or notice on a specific document.

AIR FORCE/56780/4 June 1979 — 125

UNCLASSIFIED

SECURITY CLASSIFICATION OF THIS PAGE (When Data Entered)

REPORT DOCUMENTATION PAGE

READ INSTRUCTIONS BEFORE COMPLETING FORM

1. REPORT NUMBER
AFFDL-TR-78-194, ~~Part II~~ PT-2

2. GOVT ACCESSION NO.

3. RECIPIENT'S CATALOG NUMBER

4. TITLE (and Subtitle)
Transonic Wind Tunnel Tests on an Oscillating Wing with External Stores. Part II, The Clean Wing.

5. TYPE OF REPORT & PERIOD COVERED
Final Report,
Feb~~ruary~~ 1977-Dec~~ember~~ 1978

6. PERFORMING ORG. REPORT NUMBER
NLR-TR-78106-U, ~~Part II~~ PT-2

7. AUTHOR(s)
H. Tijdeman, J. W. G. van Nunen, A. N. Kraan, A. J. Persoon, R. Poestkoke, R. Roos, P. Schippers, C. M. Siebert

8. CONTRACT OR GRANT NUMBER(s)
AFOSR ~~Grant~~ 77-3233

9. PERFORMING ORGANIZATION NAME AND ADDRESS
National Aeropsace Laboratory
Anthony Fokkerweg 2
Amsterdam, The Netherlands

10. PROGRAM ELEMENT, PROJECT, TASK AREA & WORK UNIT NUMBERS
PE 61101F, Project 2307
Task 2307N5
Work Unit 2307N503

11. CONTROLLING OFFICE NAME AND ADDRESS
Air Force Flight Dynamics Laboratory
Structures and Dynamics Division
WPAFB, OH 45433

12. REPORT DATE
MARCH 1979

13. NUMBER OF PAGES
120

14. MONITORING AGENCY NAME & ADDRESS (if different from Controlling Office)

15. SECURITY CLASS. (of this report)
Unclassified

15a. DECLASSIFICATION/DOWNGRADING SCHEDULE

16. DISTRIBUTION STATEMENT (of this Report)

DISTRIBUTION STATEMENT A
Approved for public release;
Distribution Unlimited

17. DISTRIBUTION STATEMENT (of the abstract entered in Block 20, if different from Report)

Approved for Public Release; Distribution Unlimited.

18. SUPPLEMENTARY NOTES

19. KEY WORDS (Continue on reverse side if necessary and identify by block number)

Transonic
Flutter
Unsteady Aerodynamics
Experiments
External Stores

20. ABSTRACT (Continue on reverse side if necessary and identify by block number)

A wind-tunnel investigation was carried out on an oscillating model of the F-5 wing with and without an external store (AIM-9J missile). The store was mounted at the wing tip as well as at a pylon underneath the wing. Detailed steady and unsteady pressure distributions were measured over the wing, while on the store aerodynamic loads were obtained. In addition, wind-tunnel wall pressures were recorded.

The tests covered the Mach numbers of 0.6, 0.8, 0.9, 0.95, 1.0, 1.05, 1.1, 1.2 and 1.35 and oscillatory frequencies of 0, 20, and 40 Hz.

DD FORM 1 JAN 73 1473 EDITION OF 1 NOV 65 IS OBSOLETE

UNCLASSIFIED

SECURITY CLASSIFICATION OF THIS PAGE (When Data Entered)

(Cont'd from Block 20)

This report, Part II, gives an analysis of the results for the Clean Wing. A complete set of tabulated data is available on magnetic tape from AFFDL/FBE, WPAFB, OH, USA 45433.

FOREWORD

This report was prepared by the National Aerospace Laboratory (NLR) of Amsterdam, the Netherlands. The sponsors were the Air Force Armament Test Laboratory (AFATL/DLJ) of Eglin Air Force Base, Florida and the Air Force Flight Dynamics Laboratory (AFFDL/FBR and AFFDL/FBE) of Wright-Patterson Air Force Base, Ohio. The sponsorship was performed through AFOSR Grant 77-3233, administered by Captain D. Wilkins of the Air Force Office of Scientific Research (AFOSR/TKN) of Bolling Air Force Base, Washington D.C.

The report consists of four parts. Part I contains the general description; Part II discusses the steady and unsteady aerodynamic tests of the clean F-5 wing; Part III discusses the tests for the wing with tip-mounted stores; and Part IV discusses the tests for the wing with under-wing stores.

The principal investigators were Dr. H. Tijdeman and Mr. J.W.G. van Nunen of NLR. They were assisted by A. N. Kraan, A. J. Persoon, R. Poestkoke, Dr. R. Roos, P. Schippers and C. M. Siebert of NLR.

Within the United States Air Force, this program was initiated by Lovic Thomas of the AFATL. It would not have been possible without the expert assistance of Richard Wallace (Lt Colonel, USAF, Retired), and Lt Colonel Daniel Seger and Major Robert Powell of the European Office of Aerospace Research Development (EOARD).

Accession For
NTIS GRA&I ✓
DDC TAB
Unannounced
Justification
By
Distribution/
Availability Codes
Dist | Avail and/or special
A

CONTENTS

	Page
1 INTRODUCTION	1
2 STEADY RESULTS	2
2.1 General	2
2.2 Steady pressure distributions	2
2.3 Quasi-steady pressure and load distributions	3
3 UNSTEADY RESULTS	5
3.1 Vibration modes	5
3.2 Unsteady pressures	5
3.2.1 General	5
3.2.2 Unsteady pressure distributions	6
3.2.3 Unsteady load distributions	7
3.2.4 Unsteady wall pressures	9
4 CONCLUSIONS	10
5 REFERENCES	11
Appendix II.A: Definitions of steady and unsteady aerodynamic quantities	45
Appendix II.B: Steady pressure distributions	47
Appendix II.C: Unsteady pressure distributions	72

PRECEDING PAGE BLANK

LIST OF FIGURES

FIGURE		PAGE
1a	Dimensions of the Clean Wing Model	13
1b	Model of the Clean Wing Mounted in the NLR High Speed Tunnel (HST)	14
1c	Location of the Pressure Orfices	15
2	Steady and Quasi-Steady Pressure Distribution on the Clean Wing	16
3	Sectional Quasi-Steady Load Distribution	24
4	Quasi-Steady Spanwise Normal Load Distribution	25
5	In-Wind Vibration Modes of the Clean Wing	26
6	Unsteady Pressure Distributions on the Clean Wing	29
7	Panel Distribution Used in Theoretical Calculations	37
8	Sectional Unsteady Normal Load Distribution	38
9	Unsteady Spanwise Normal Load Distributions at 20 Hz	40
10	Unsteady Spanwise Normal Load Distributions at 40 Hz	41
11	Unsteady Spanwise Pitch Moment Distributions at 20 Hz	42
12	Unsteady Spanwise Pitch Moment Distributions at 40 Hz	43
13	Unsteady Pressure Distributions on the Slotted Tunnel Wall Plotted in the Spanwise Direction	44

LIST OF SYMBOLS

a_{mn}	coefficient in the approximation of the vibration modes	
C	chord	(m)
$\bar{C}$	mean geometric chord; $\bar{C} = .4183$	(m)
C_m	pitch moment coefficient	
C_p	pressure coefficient	
C_r	root chord; $C_r = 0.6396$	(m)
C_z	normal force coefficient	
F	frequency of oscillation	(Hz)
K	reduced frequency; $K = \frac{\pi F C_r}{V}$	
M	pitching moment	(Nm)
Ma	free-stream Mach number	
P	free-stream static pressure	(Pa)
P_i	unsteady pressure at model surface	(Pa)
P_{loc}	local static pressure	(Pa)
P_o	stagnation pressure	(Pa)
Q	dynamic pressure	(Pa)
S	semi span; $S = 0.6226$	(m)
V	free-stream velocity	(m/s)
w	modal displacement	(m)
x	coordinate in free-stream direction	(m)
y	coordinate in spanwise direction	(m)
Z	normal force	(N)
α	incidence; positive nose up	(degrees)
θ	amplitude of oscillation in the section of accelerometers 1 and 2; positive nose up	(rad)
ω	angular velocity; $\omega = 2\pi F$	(rad/s)

SUBSCRIPTS

i	referring to unsteady quantities
q	referring to quasi-steady quantities

SUFFICES

+	denotes upper surface
−	denotes lower surface

1 INTRODUCTION

In October 1977 wind-tunnel tests were carried out on an oscillating model of the F-5 wing with and without external store. If present, this external store (AIM-9J missile + launcher) was mounted either at the tip or under the wing.

The aim of this investigation was to determine the unsteady airloads on a representative fighter-type wing in the transonic and low-supersonic speed regimes.

The wing model was oscillated in pitch about a 50 per cent root-chord axis at frequencies varying up to 40 Hz (for dimensions see Fig. 1a). The Mach number ranged between 0.6 and 1.35. Detailed pressure distributions, both steady and unsteady, were measured over the wing, while on the store the total aerodynamic loads were obtained. A description of the experimental set-up and the testprogram is given in Part I of the present report (Ref. 1). The results are published in a data report (Ref. 2), while for easy data handling they are available also on magnetic tape.

To assist in the evaluation of the data reference 1 is supplemented by three additional parts, covering successively the clean wing, the wing with tipstore and the wing with underwing store. Each part contains plots of the steady, and unsteady pressure distributions and gives a brief analysis of some selected results.

The present Part II covers the clean wing configuration, of which some preliminary results were given already in reference 3. Figure 1b shows the clean wing mounted on the side wall of the NLR High Speed Tunnel (HST), while the location of the pressure orifices is given in figure 1c.

First, the steady flow field is discussed, which includes shock positions and quasi-steady pressure distributions. Next the vibration modes of the model during the unsteady tests, are analyzed, followed by a presentation of the unsteady pressure and load distributions. For a few cases a comparison with theoretical results obtained with the Doublet Lattice method is given. Finally, the value of the pressures measured at the wind-tunnel wall is examined.

2 STEADY RESULTS

2.1 General

As part of the wind-tunnel experiment steady pressures were measured at incidences of -0.5, 0 and 0.5 degrees. For the clean wing configuration a listing of the test variables as well as a complete set of plots of the resulting steady pressure distributions in the eight measuring sections is gathered in Appendix II.B.

2.2 Steady pressure distributions

To illustrate the development of the flowfield with Mach number, the steady pressure distributions in sections 2, 5 and 8 for zero incidence are presented on the left-hand side of figures 2a to 2h.[x)] At subsonic conditions (Ma = 0.6, Fig. 2a) the chordwise pressure distributions are characterized by the effects of the droop nose of the wing airfoil. This is reflected in a high suction peak at the leading edge on the lower side of the wing. The influence, however, is felt only in a limited area, since the symmetrical aft part of the airfoil causes the pressure distribution over the last 60 % of the chord to be symmetrical again. In spanwise direction the pressure distribution is very regular.

With increasing Mach number the effect of the droop nose becomes more pronounced, with the suction peaks reaching a maximum around Ma = 0.95. A weak shock wave appears at Ma = 0.9 on the upper surface near the wing tip, between 40 and 50 per cent of the chord (Fig. 2c). At Ma = 0.95 (Fig. 2d) the strength of the shock is increased and its position is changed to about 85 per cent of the local chord. At the same time the shock has grown in spanwise direction. Further, on the lower side of the wing a second shock has developed, slightly ahead of the one on the upper surface. Figure 2d shows also that in section 8 ahead of the shock the pressures on the upper surface keep an elevated level as compared to the lower surface, which probably should be attributed to the flow around the tip.

As the free-stream Mach number becomes supersonic the shock waves on both sides of the wing move towards the trailing edge of the wing and the pressure distribution obtains a supersonic character. The suction peak

---

x) Note that in these figures the first point on the upperside of section 5 has been eliminated, since it showed a faulty measurement.

on the lower side remains present, although it diminishes with further increasing Mach number. In addition, from the root to the tip the leading edge suction region shows a tendency to widen in chordwise direction. This typical three-dimensional effect is caused by the fact that the induced angle of attack reduces the actual local incidence when going more outwards. As a consequence the size of the expansion-recompression region widens as can also be observed form the steady results for a typical section, when the angle of incidence is reduced (see for instance Figs. II.B. 16 to 18 of Appendix II.B.).

2.3 Quasi-steady pressure and load distributions

For the limiting case of zero frequency so-called "quasi-steady" results can be obtained by considering the steady results for small incidences around a certain mid-position. In the present investigation quasi-steady pressure distributions were obtained from the steady distributions for incidences of -0.5 and 0.5 degrees. The definitions are given in Appendix II.A. For the sections 2, 5 and 8 these quasi-steady distributions are presented in the right hand side of figures 2a to 2h. For the purpose of comparison the values on the upperside are plotted with a reversed sign.

When evaluating the quasi-steady distributions it should be realized that as with the steady distributions, the differences between upper and lower side of the wing are caused by the asymmetry of the airfoil and three dimensional effects such as the varying induced angle of attack.

For subsonic Mach numbers the development of the quasi-steady pressure distribution in chordwise direction is very regular, except for Ma = 0.8, where on the lowerside the values near the leading edge have decreased significantly (Fig. 2b). A possible reason for this is a slight shift in the position of the stagnation line along the leading edge of the wing. Although this feature is not important for the interpretation of the pressure distributions, it does influence the integrated quasi-steady normal force and moment coefficients, resulting in a dip in the development of the normal force coefficient with Mach number (see Fig. 3).

For Ma = 0.9 (Fig. 2c) the upperside at section 8 shows a sharp peak obviously caused by the presence of a shock at 40 per cent of the chord. Apparently due to the flow around the tip the lowerside remains shock free at incidences between -0.5 and 0.5 degrees. The sections 5 and 2 do show weak signs of shocks forming on both sides of the wing. The strong expansion around the droop nose causes very large quasi-steady values.

As the Mach number increases to Ma = 0.95 the shock induced peaks grow larger and move backwards, while the differences between upper- and lower-side increase.

At supersonic free stream Mach numbers, the shock induced peaks have moved off the wing, resulting in more smooth quasi-steady distributions, especially on the upperside. On the lowerside, however, new large variations in quasi-steady pressure appear near the leading edge, caused by the typical behaviour of the steady suction peak with incidence. These variations are largest near the tip, where they influence the upperside also, and move backwards with further increasing Mach number. At Ma = 1.35 all strong oscillations have disappeared, with the lowerside keeping an elevated level near the tip.

In figure 3 the development of the quasi-steady sectional loading with Mach number is given for the sections 2, 5 and 8[x]. As mentioned before the first two sections show a dip at Ma = 0.8, which is not according to the development with Mach number found in subsonic linearized theories. In all three sections the load grows to a maximum around Ma = 1.0, and decreases again with further increasing Mach number. Between Ma = 0.95 and Ma = 1.05 in section 5 and to some extent also in section 8 the development is less smooth. It is believed that this behaviour is caused partly by the fact, that with only ten pressure orifices over the chord the integrated value becomes less accurate, due to the peaks caused by the shock and the leading edge suction.

An illustration of the behaviour of the spanwise loading with Mach number is given in figure 4, which presents the spanwise distribution for a subsonic (Ma = 0.6), a transonic (Ma = 0.9) and a supersonic (Ma = 1.35) condition. The tendency to reach a maximum in the transonic range is seen to hold all over the span. Further, at supersonic speeds the maximum has shifted to a more outward section, which is caused by the three dimensional behaviour of the suction peak near the leading edge (see section 2a).

---

[x] For the integration in the sections 3 and 5, the wrong value found on the upperside near the leading edge was replaced by a new value obtained by interpolation between the sections 2, 4 and 6.

3 UNSTEADY RESULTS

3.1 Vibration modes

To monitor the vibration modes of the wing during the tests, the model was equipped with eight accelerometers (for exact locations see figure 1a). The readings of these accelerometers were used to make analytical approximations of the vibration modes for the 20 and 40 Hz testruns. The polynomial expression used for these approximations is:

$$w(x,y) = \sum a_{mn} x^n y^m \quad (m = 0,1,2;\ n = 0,1) \quad .$$

This expression assumes no deformation in chordwise direction and a parabolic deformation in spanwise direction. In using the measured values, the readings of accelerometers 5 and 7 were carefully weighted to ensure a realistic development of the torsion angle along the span. Taking this into account, for all vibration modes, the difference between the analytically approximated displacements and the experimental readings remains within 2.5 per cent of the maximal displacement. Table 1 presents the numerical values of the coefficients a_{mn} for the analyzed vibration modes. The normalization is carried out such that at the wingsection of accelerometer 2 the tangent of the angle of oscillation equals one.

To illustrate the vibrational behaviour of the wing the vibration modes, i.e. the nodal lines, are plotted in figure 5. The plots indicate that both for 20 and 40 Hz the nodal line bends backwards with increasing Mach number up to Ma = 0.95, after which it moves forward again. Also, for all Mach numbers the nodal line at 40 Hz lays ahead of the one at 20 Hz. Further for all cases it was found that the pitch angle remained constant over the span.

3.2 Unsteady pressures

3.2.1 General

Also the unsteady pressure distributions for the clean wing configuration (tabulated in reference 2), have been plotted. These plots together with a list of the relevant test variables are given in Appendix II.C. For better comparison the values on the upperside are shown with a reversed sign.

3.2.2 Unsteady pressure distributions

The development of the measured unsteady pressures on the wing with respect to Mach number and frequency is shown in a set of plots selected from Appendix II.C. For frequencies of 20 and 40 Hz, they present the unsteady pressure distributions in the sections 2, 5 and 8 for a subsonic (Ma = 0.6), a transonic (Ma = 0.9) and a supersonic (Ma = 1.35) Mach number[x]. For the subsonic case these plots are supplemented with a theoretical result obtained with the Doublet Lattice method (Ref. 4). This method computes the jump in unsteady pressure across a lifting surface. However, in figure 6 the measured unsteady pressures are presented separately for both sides of the wing. As a consequence the theoretical line in the figures 6a and 6b represents the pressure jump divided by two. The panel distribution used in these calculations is given in figure 7.

A first impression from figure 6 is that in section 2 on the upperside the data obtained with the tubes and the Kulites are in perfect agreement, also with a shock present. This indicates that the experimentally determined transfer functions of the tube system, which were obtained as average values from a large number of readings (see reference 1), indeed give a correct calibration.

When considering the unsteady pressure distribution for Ma = 0.6 (Figs. 6a and 6b) it is clear that the behaviour over the wing is very regular except in section 8. In this section a bulge occurs in the distribution on the upperside. This bulge occurs for all test frequencies (see also Appendix II.C), but is not visible in the quasi-steady distribution for Ma = 0.6 (Fig. 2a). An explanation for this bulge is not readily available, especially since at Ma = 0.8 (Figs. II.C 5 and 6) it is not present any longer.

The comparison with theoretical results for both 20 and 40 Hz shows a very good agreement between theory and experiment except of course in section 8. Further, it indicates that the development with frequency is very regular, showing the same trend as the theoretical predictions.

At Ma = 0.9 the shock induced peaks, already found in the quasi-steady distributions (Fig. 2c), are present also in the unsteady distributions and they intensify with increasing frequency. At 20 Hz (Fig. 6c) the effects of a shock show up only in sections 5 and 8 on the upper

---

[x] Note that in section 5 the first point on the upperside has been estimated, since it was faulty.

surface, while in section 2 on both sides and in section 5 on the lower-side high-subsonic bulges have appeared. Apparently these bulges are caused by a coalescence of very weak shocklets, which extend from the end of the shock near section 5 towards the root and move upstream over a considerable part of the chord. At higher oscillation frequencies these shocklets do not move as much and converge into a weak but more stable shocklet thus changing the bulges into sharper peaks. This development is clear in the distributions for a frequency of 40 Hz (Fig. 6d).

As expected, when the Mach number is increased to Ma = 0.95, the shock induced peaks in all sections move backwards to about 80 % of the chord (Figs. 6e and 6f). Comparison between the quasi-steady (Fig. 2d) and unsteady pressure distributions show that the differences between upper- and lowerside are less for the latter. However, in section 8 the differences attributed to the flow around the tip remain clearly visible in the unsteady cases. As the frequency increases the behaviour of the shock induced peaks indicate an increased phase lag with respect to the oscillatory motion.

For Ma = 1.35 figures 6g and 6h show a very regular unsteady pressure distribution which only on the lower surface of the wing somewhat deviates from a typical supersonic character. There the effect of the suction peak near the leading edge, which has a tendency to broaden near the tip, is clearly visible. The behaviour with frequency is obscured by the low level of the imaginary part of the pressure distribution.

3.2.3 Unsteady load distributions

The behaviour of the unsteady normal loading[x)] in the sections 2, 5 and 8 as a function of Mach number is presented in figure 8 for frequencies of 20 and 40 Hz. Comparison with figure 3 shows the expected similarity between the quasi-steady normal force coefficient and the real part of the unsteady normal force coefficient. The general trend is that the Re C_{zi} reaches a peak near Ma = 1.0 followed by a decrease with further increasing Mach number, while the Im C_{zi} changes sign in the transonic range. Notice that in figure 8 section 2 shows the already described (chapter 2b) dip at Ma = 0.8.

---

x) For the integration of the unsteady pressure distributions in sections 3 and 5 the zero value, wrongly measured on the upperside near the leading edge, was replaced by a new value obtained by spanwise interpolation between sections 2, 4 and 6.

It is not known whether the sharp peak at Ma = 1.0 in section 8 does show up also in the quasi-steady results, since no steady measurements were made at that Mach number. Some of the irregular behaviour, especially in section 5, may be caused by a lack of resolution in the measured unsteady pressure distribution to fully account for the effect of the moving shock.

As can be expected the differences between 20 and 40 Hz are found mainly in the imaginary part of the unsteady load distribution: the Im C_{zi} is doubled in the subsonic and transonic range. Above Ma = 1.2 this difference is not quite clear due to the almost zero level of the imaginary part of the unsteady pressure distributions (Figs. 6e and 6f). In the real part of C_{zi} the irregularities seem to increase somewhat.

The figures 9 through 12 show the normal load and pitching moment distributions over the span for the Mach numbers 0.6, 0.9 and 1.35 and frequencies of 20 and 40 Hz. In addition for Ma = 0.6 the theoretical distribution obtained with the Doublet Lattice method is given.

For Ma = 0.6 the load and moment distributions are more or less classical except that the difference found normally between theory and experiment (theory slightly higher, see for example Ref. 5) seems to become abnormally large for the real part at the outer half of the wing. The reason for this is twofold. Firstly, considering the unsteady pressure distributions (i.e. Fig. II.C.2) it can be seen that on the lower side at 10 % of the chord the sections 5 through 8 do exhibit an unexpected large negative peak which affects significantly the integrated force and moment values. The second reason is the unusual bulge in the unsteady pressures on the upperside in section 8. These irregularities do not occur in the imaginary pressure distribution, which explains the much better agreement between theory and experiment for the imaginary force and moment distributions. The effect of the frequency enters mainly as a doubling of the imaginary force and moment when the oscillation frequency is increased from 20 to 40 Hz.

As shown already in figure 8 for some individual sections, the real part of the normal force tends to increase with Mach number, while the imaginary part reduces and eventually switches sign over part of the span. This is illustrated clearly in the figures 9 and 11. The behaviour of the real part is similar to that found for the quasi-steady distribution except for the unexpected dip in section 5, which shows up in the imaginary force distribution as well as in the moment distributions. From the data it is not fully clear whether this dip, or perhaps the bulge near the tip,

is due to inaccuracy in the integration process or has a physical cause. It is suspected that at least a part of it is caused by insufficient resolution necessary to integrate over the peaks generated by the moving shock.

The real part of the moment distribution at Ma = 0.9 varies from nose down near the root to nose up near the tip. For the latter region this means that the real normal force acts at about 10 per cent of the local chord. At the same time the imaginary moment distribution has almost doubled with respect to the subsonic values.

At supersonic speed (Ma = 1.35) the maximum of the real part of the normal force is located more towards the tip. As explained already in section 2b, this is due to the influence of the induced angle of attack on the behaviour of the leading edge suction peak. The imaginary part has become fully negative at this Mach number. The moment distributions have changed drastically with respect to the ones found for Ma = 0.9. Now, for both frequencies, Re C_{mi} shows a relatively constant level over the span, while Im C_{mi} varies around the zero level again. As indicated already for the unsteady pressure distributions, the effect of the frequency is minimal for this Mach number.

3.2.4 Unsteady wall pressures

During the wind-tunnel tests unsteady pressures were measured in a mesh of 75 pressure points at the slotted top wall of the wind-tunnel test section (for exact locations see reference 1). These measurements were meant to provide the analysts with a set of data that could be used to model the tunnel wall in theoretical calculations. However, before the tests it was realized already that measuring such unsteady pressures induced by the oscillating model would be questionable. Clearly, for a slotted wall one suffers from a certain level of unsteadiness created by flow in and out of the slots. Therefore, the interpretation of any data taken in such a way may be very difficult and the use as explained above not very realistic.

Nevertheless, to get some insight into the level and the usefulness of the present data a limited analysis is performed. The unsteady pressures, as measured in the direction across the slats above the oscillating clean wing are plotted in figure 13 for Ma = 0.6, 0.9 and 1.35 and frequencies of 20 and 40 Hz. This figure shows that for Ma = 0.6 and 0.9 the unsteady pressures behave very jumpy when going from slat to slat.

The maximum level is of the same order as measured on the aft part of the oscillating wing. Further, increasing the frequency from 20 to 40 Hz does not produce a very systematic change in the measured data.

For the supersonic Mach number 1.35 the measurements show a nominally zero level on the two outer slats indicating a low upstream disturbance level at this speed. However, near the corner of the tunnel over the first slat, which is separated form the side wall by a slot, the disturbance level is appreciable. Again no coherent behaviour with frequency is found.

From this limited analysis it can be concluded that although a certain level of unsteady pressures was measured on the tunnel wall, their magnitude depends very much on the position of the orifice with respect to the slots and that it is difficult to relate these pressures to the oscillatory motion of the wing. Therefore an attempt to use these data as input in a theoretical analysis does not look promising.

4 CONCLUSIONS

A wind-tunnel investigation was carried out on a harmonically oscillating model of the F-5 wing with and without an external store. As part of the test program steady as well as unsteady pressure distributions were measured on the clean wing configuration. In the present report a limited analysis of the clean wing results has been given. This analysis concerns:

- the development of the steady flow field with Mach number
- the behaviour of the quasi-steady pressure and load distributions, which brought to light some typical features resulting from the shock and leading edge suction peak
- the description in terms of polynomials of the in-wind vibration modes for 20 an 40 Hz
- the development of the unsteady pressures and loads with frequency, showing that for Ma = 0.6 and 0.9 a normal behaviour with frequency occurs, while for Ma = 1.35 such a behaviour is not very clear
- the comparison between measured unsteady pressure distributions for Ma = 0.6 and theoretical results obtained with the Doublet Lattice method, showing a good agreement
- an evaluation of the unsteady pressures measured on the slotted tunnel wall, indicating that these do not seem useful as input for theoretical calculation methods.

5 REFERENCES

1 Tijdeman H. et al. — Transonic Wind-tunnel Tests on an Oscillating Wing with External Store. Part I : General Description. NLR TR 78106 U (1978).

2 — Results of Transonic Wind-tunnel Measurements on an Oscillating Wing with External Store. NLR TR 78030 U (1978).

3 — Some Results of Unsteady Pressure Measurements on a Model of an Oscillating Wing with Stores (Clean Wing Configuration). NLR Memo AE-78-007 (1978).

4 Roos R. and Zwaan R.J. — Calculation of Instationary Pressure Distributions and Generalized Forces with the Doublet Lattice Method. NLR TR 72037 U (1972).

5 Roos R. Bennekers B. and Zwaan R.J. — Calculation of Unsteady Subsonic Flow about Harmonically Oscillating Wing/Body Configurations. J. of Aircraft, Vol 14, No. 5, pp 447-454, 1977.

6 — AGARD Manual on Aeroelasticity Vol.VI (1968).

TABLE 1

Coefficients a_{mn} for the approximation of the in-wind vibration modes of the clean wing at oscillation frequencies of 20 and 40 Hz.

Run	Ma	F (Hz)	K	a_{00}	a_{01}	a_{10}	a_{11}	a_{20}	a_{21}
382	0.6	20	.199	-0.330	1.001	0.002	-0.013	-0.052	0.067
383	0.6	40	.399	-0.312	0.954	-0.148	0.532	0.339	-0.602
367	0.8	20	.153	-0.332	1.001	-0.023	-0.012	-0.080	0.048
368	0.8	40	.307	-0.310	0.952	-0.244	0.578	0.434	-0.853
369	0.9	20	.137	-0.339	1.016	0.041	-0.210	-0.269	0.456
370	0.9	40	.275	-0.329	0.977	-0.088	0.244	-0.077	-0.091
160	0.95	20	.132	-0.354	1.016	0.093	-0.185	-0.351	0.266
161	0.95	40	.264	-0.348	1.023	0.165	-0.362	-0.711	1.264
375	1.00	20	.125	-0.346	1.018	0.073	-0.221	-0.332	0.355
376	1.00	40	.250	-0.334	0.985	-0.039	0.144	-0.122	0.057
165	1.05	20	.122	-0.354	1.029	0.134	-0.360	-0.468	0.669
166	1.05	40	.243	-0.333	0.986	-0.050	0.139	-0.103	0.029
172	1.10	20	.116	-0.349	1.019	0.076	-0.231	-0.315	0.346
372	1.10	40	.231	-0.329	0.972	-0.118	0.317	0.056	-0.343
187	1.20	20	.109	-0.345	1.013	0.074	-0.155	-0.225	0.219
188	1.20	40	.218	-0.331	0.983	-0.001	0.173	-0.075	0.036
192	1.35	20	.100	-0.343	1.009	0.072	-0.110	-0.194	0.142
193	1.35	40	.198	-0.328	0.979	-0.016	0.228	-0.001	-0.111

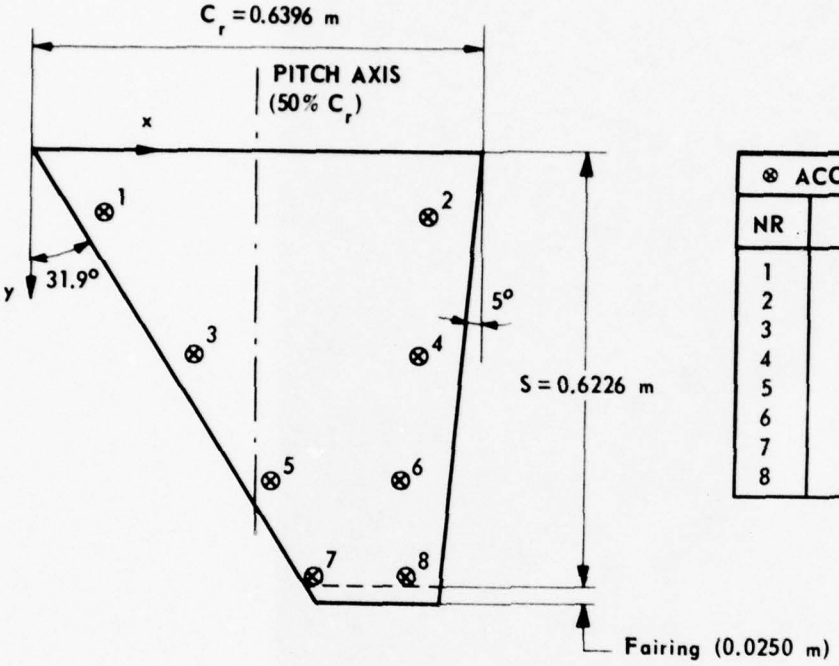

⊗ ACCELEROMETERS		
NR	x (m)	y (m)
1	0.1087	0.0957
2	0.5648	0.0977
3	0.2309	0.2971
4	0.5475	0.2991
5	0.3422	0.4772
6	0.5270	0.4772
7	0.4070	0.6176
8	0.5390	0.6176

Fig. 1a Dimensions of the wing model

Fig. 1b Model of the clean wing mounted in the NLR High Speed Tunnel (HST)

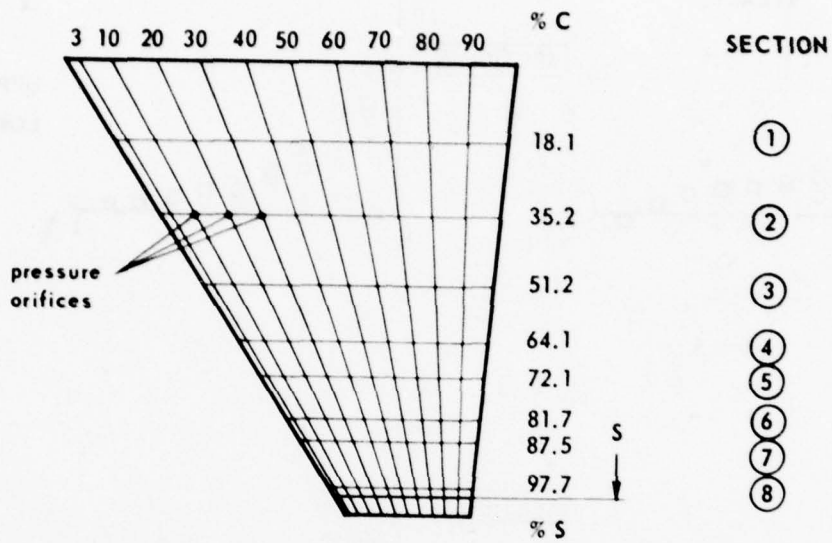

Fig. 1c Location of the pressure orifices

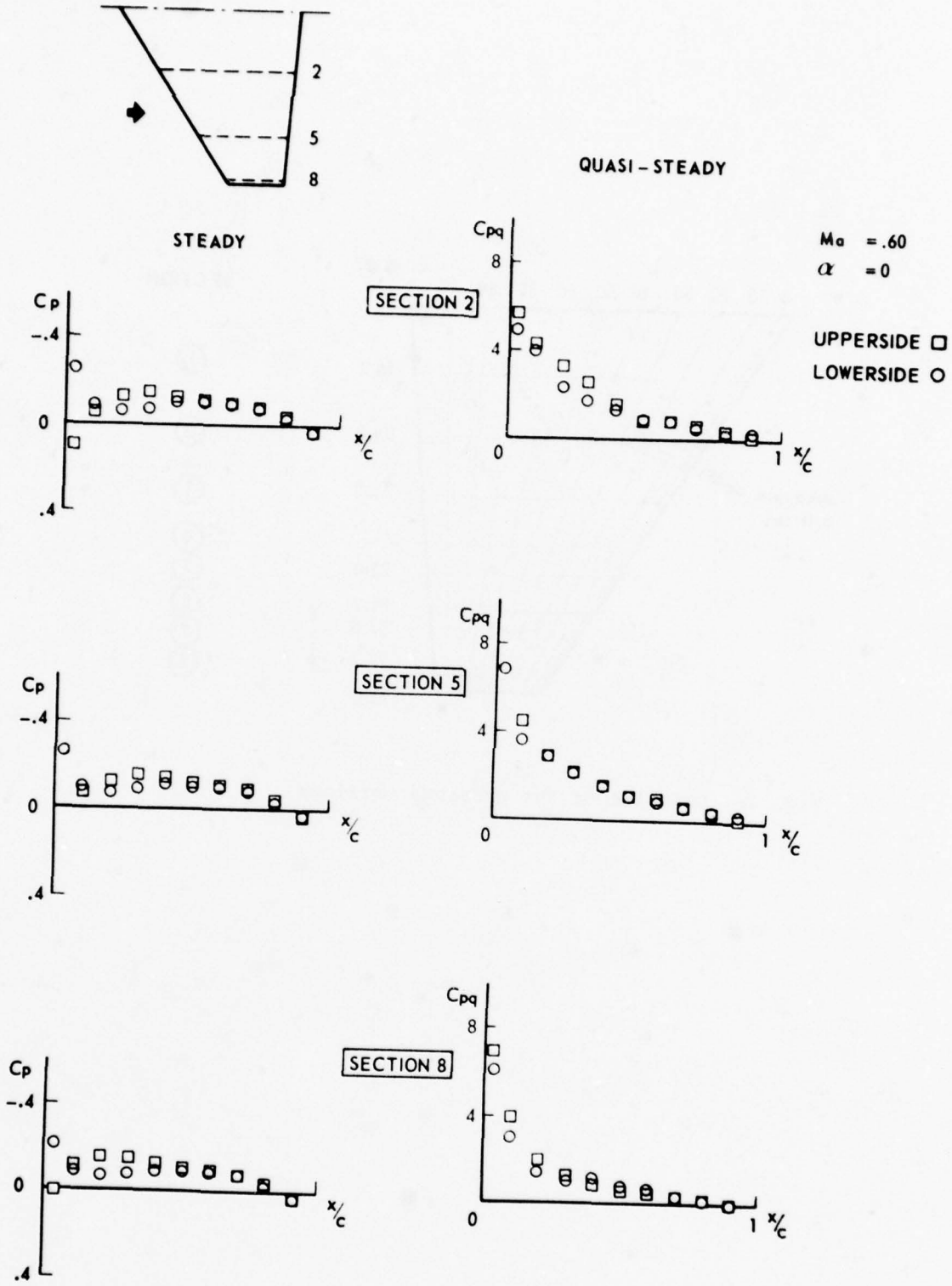

Fig. 2a Steady and quasi-steady pressure distributions on the clean wing

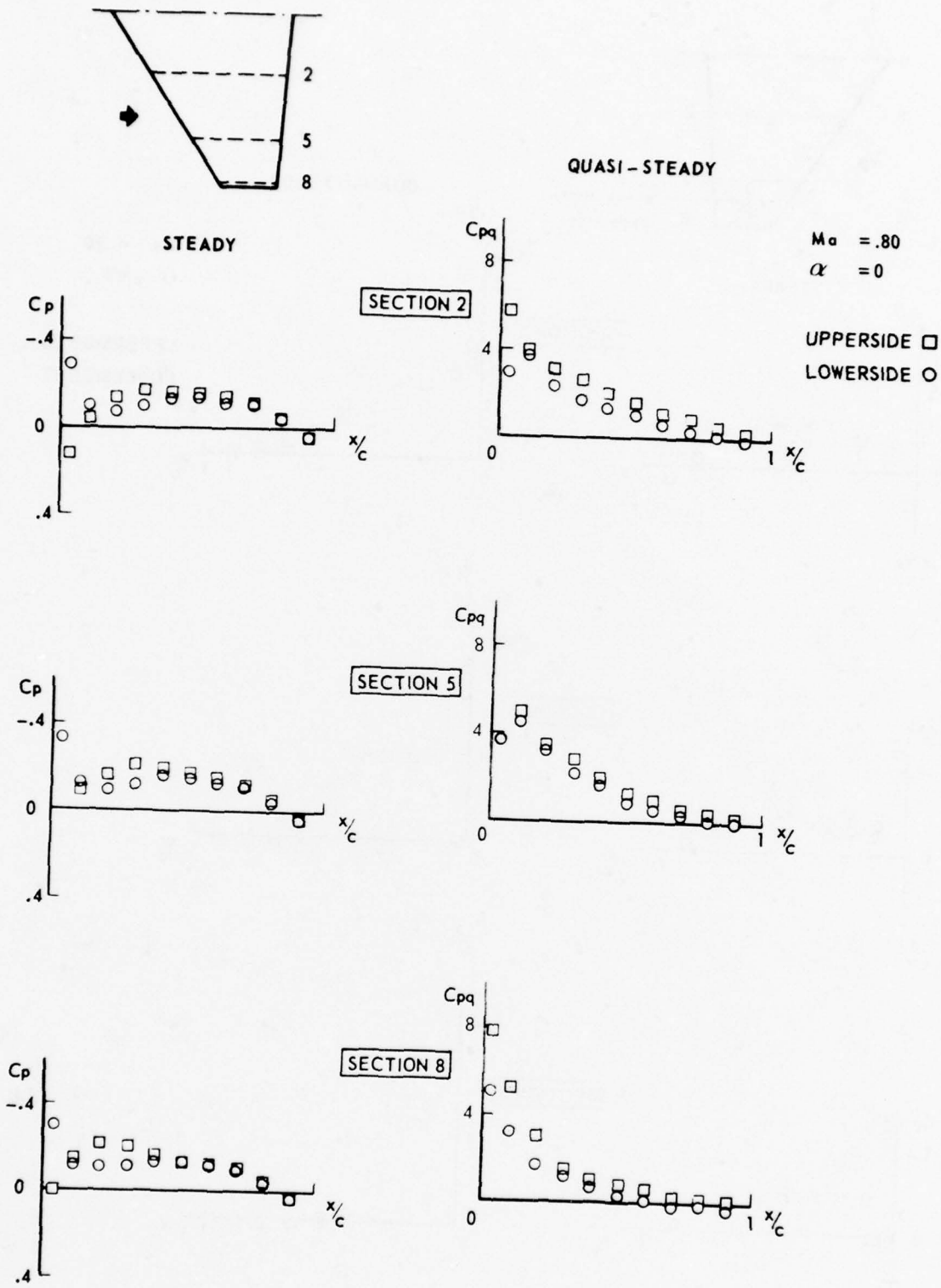

Fig. 2b Steady and quasi-steady pressure distributions on the clean wing

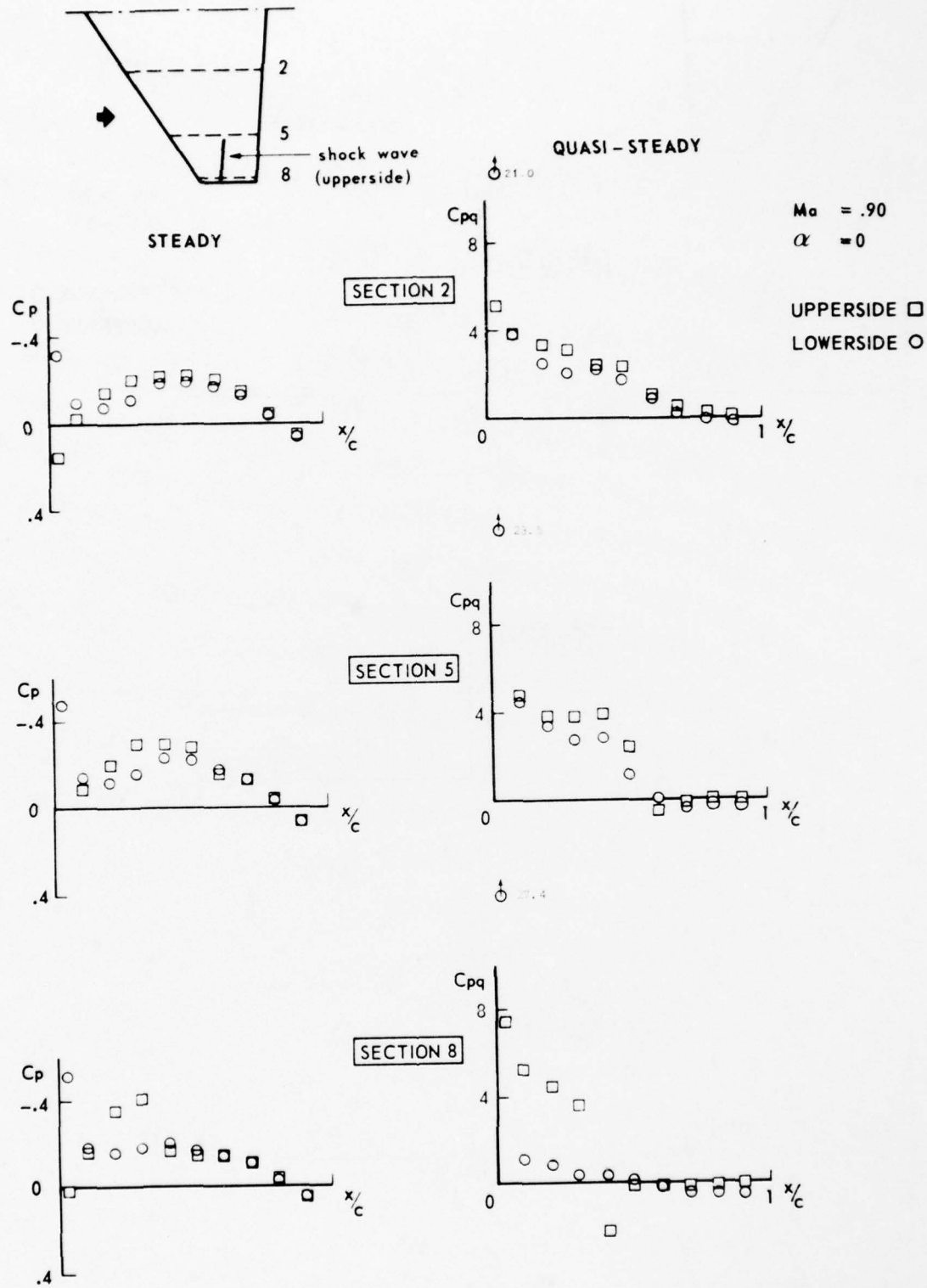

Fig. 2c Steady and quasi-steady pressure distributions on the clean wing

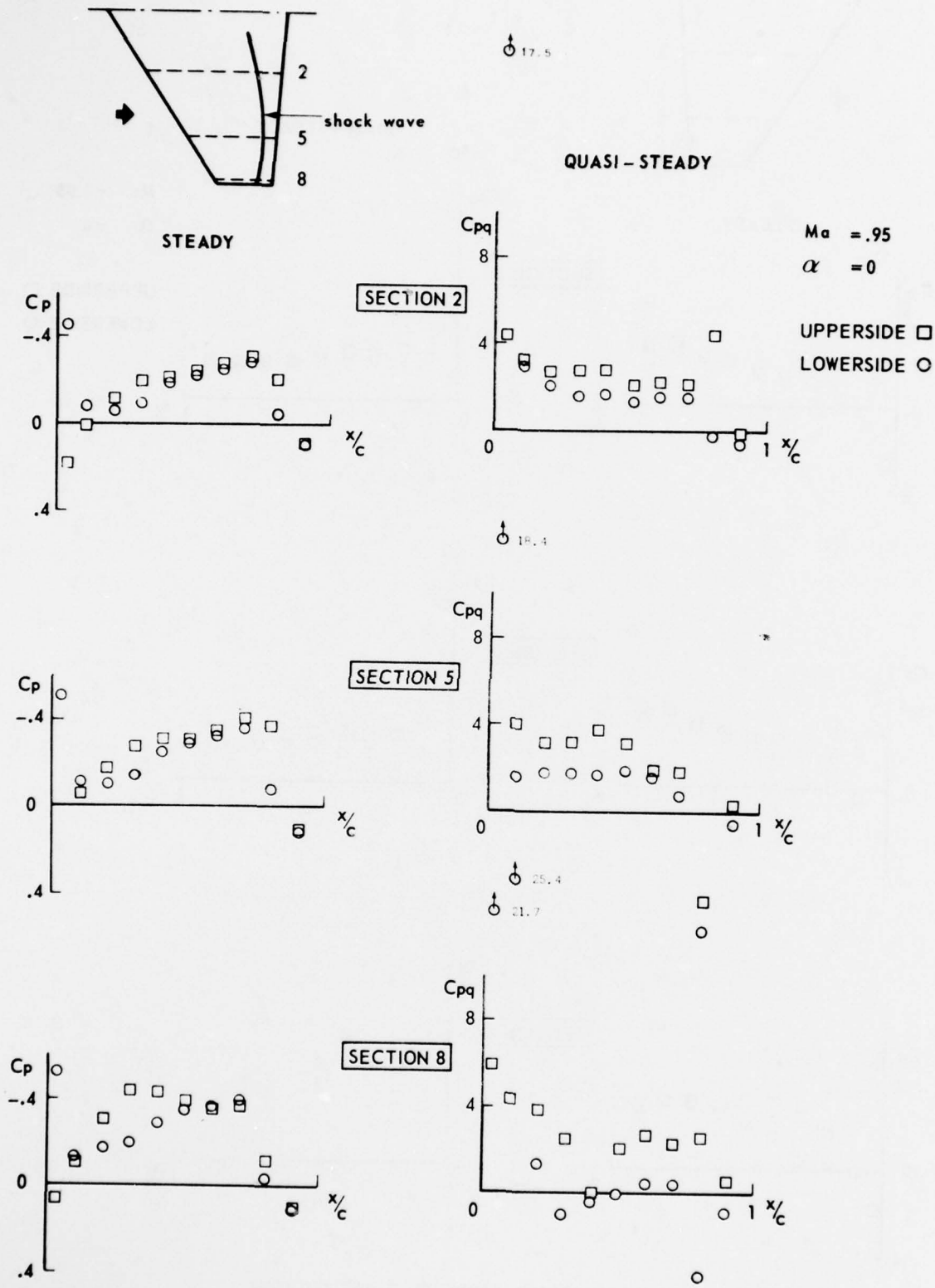

Fig. 2d Steady and quasi-steady pressure distributions on the clean wing

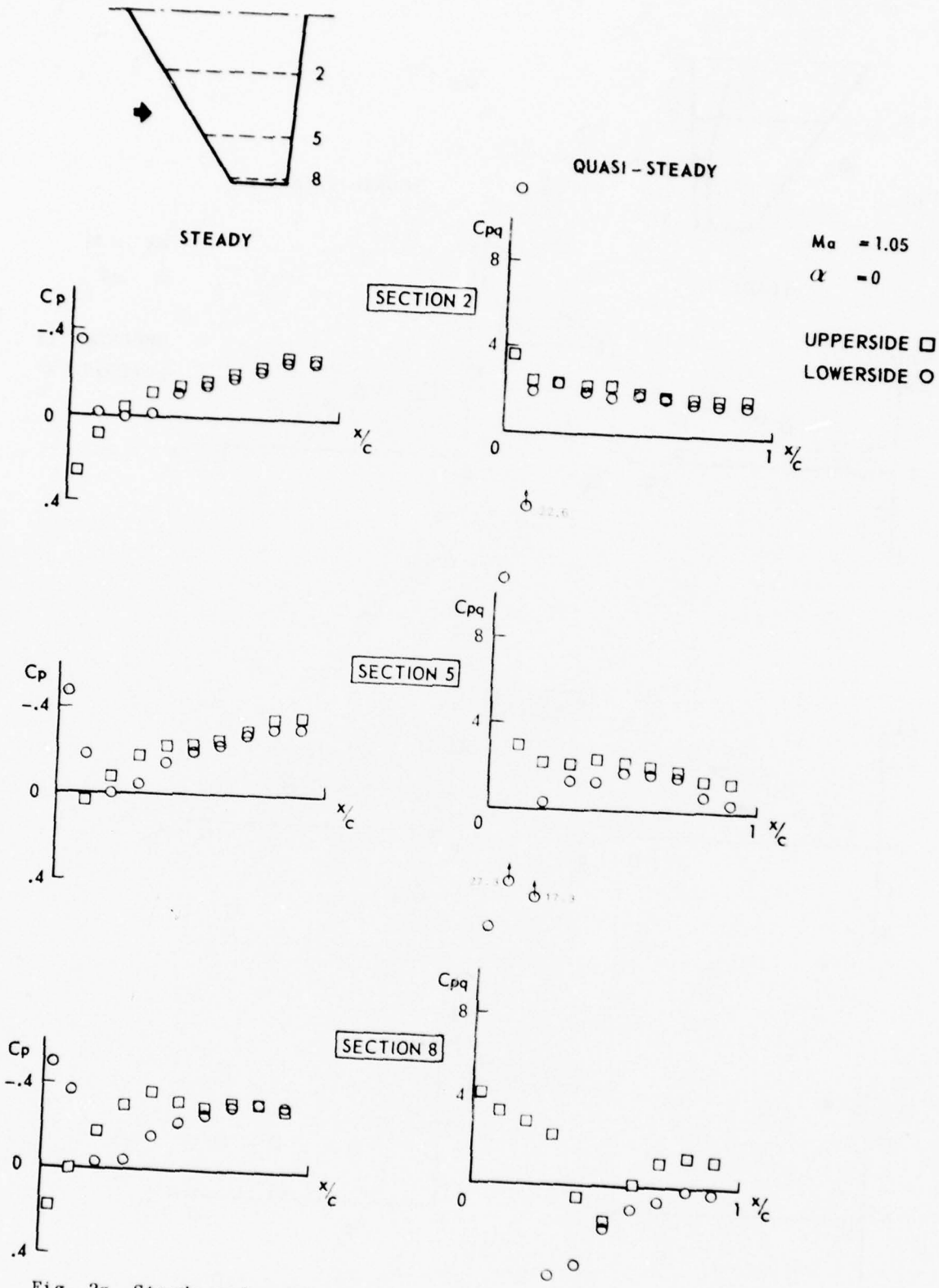

Fig. 2e Steady and quasi-steady pressure distributions on the clean wing

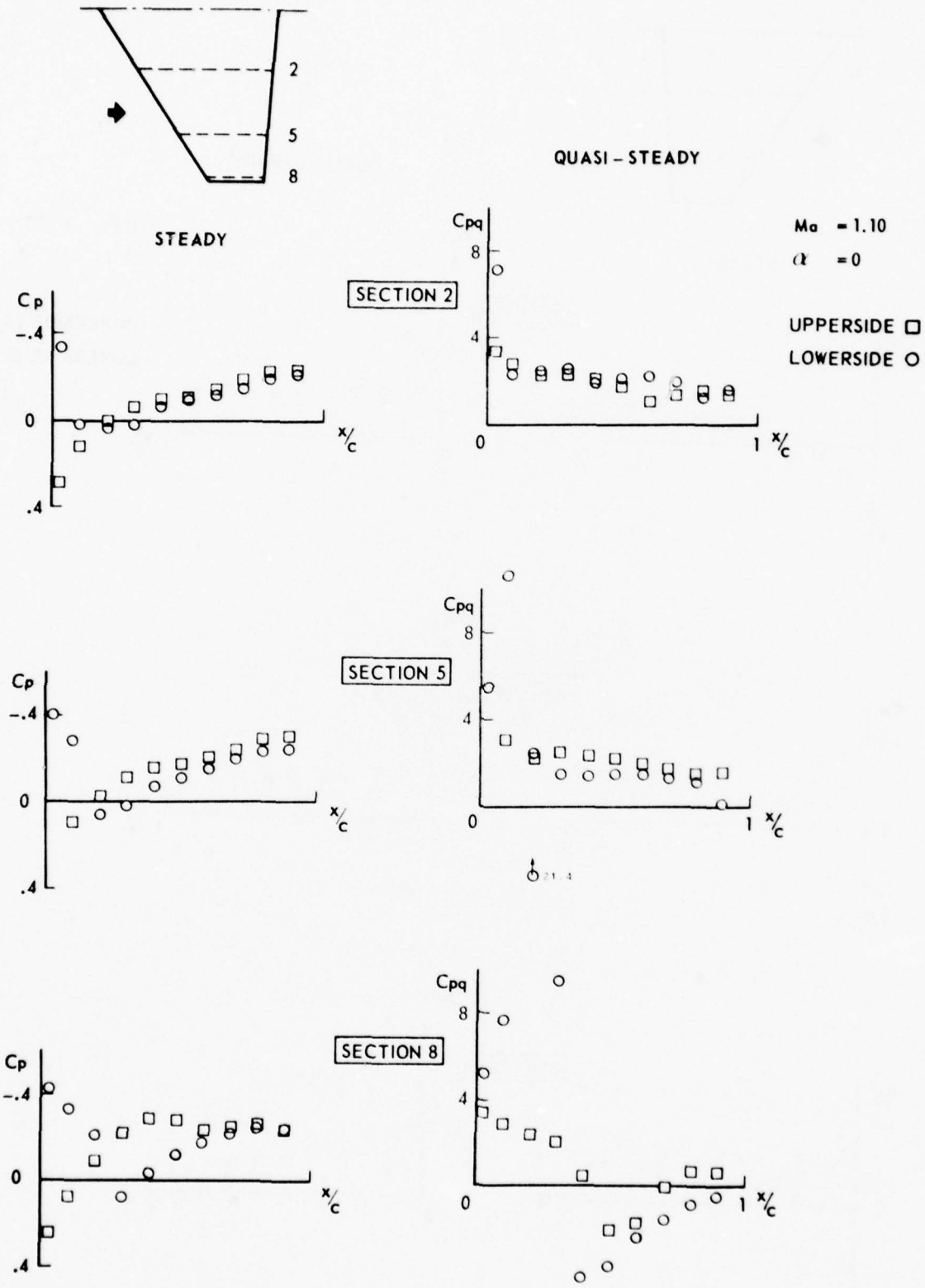

Fig. 2f Steady and quasi-steady pressure distributions on the clean wing

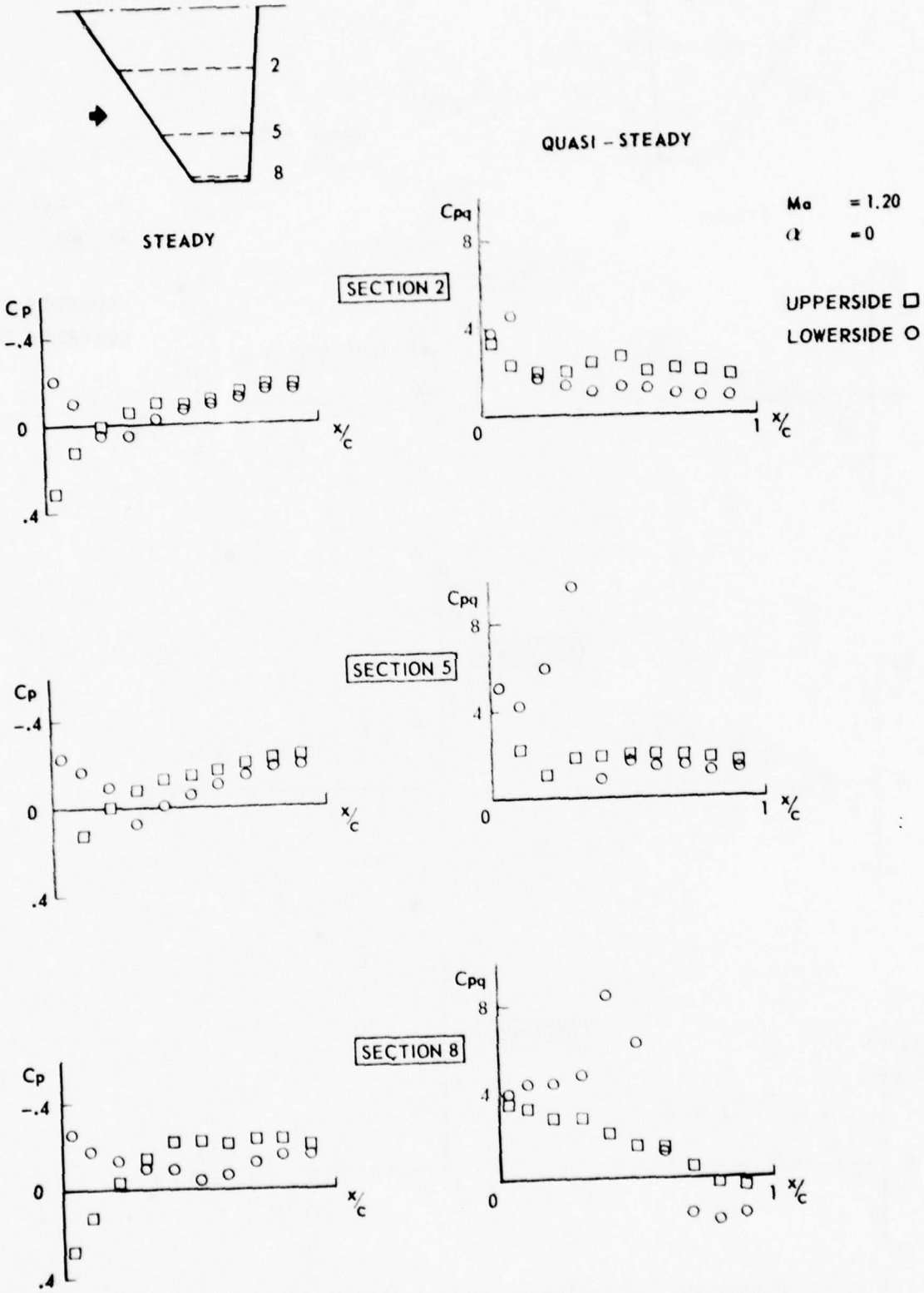

Fig. 2g Steady and quasi-steady pressure distributions on the clean wing

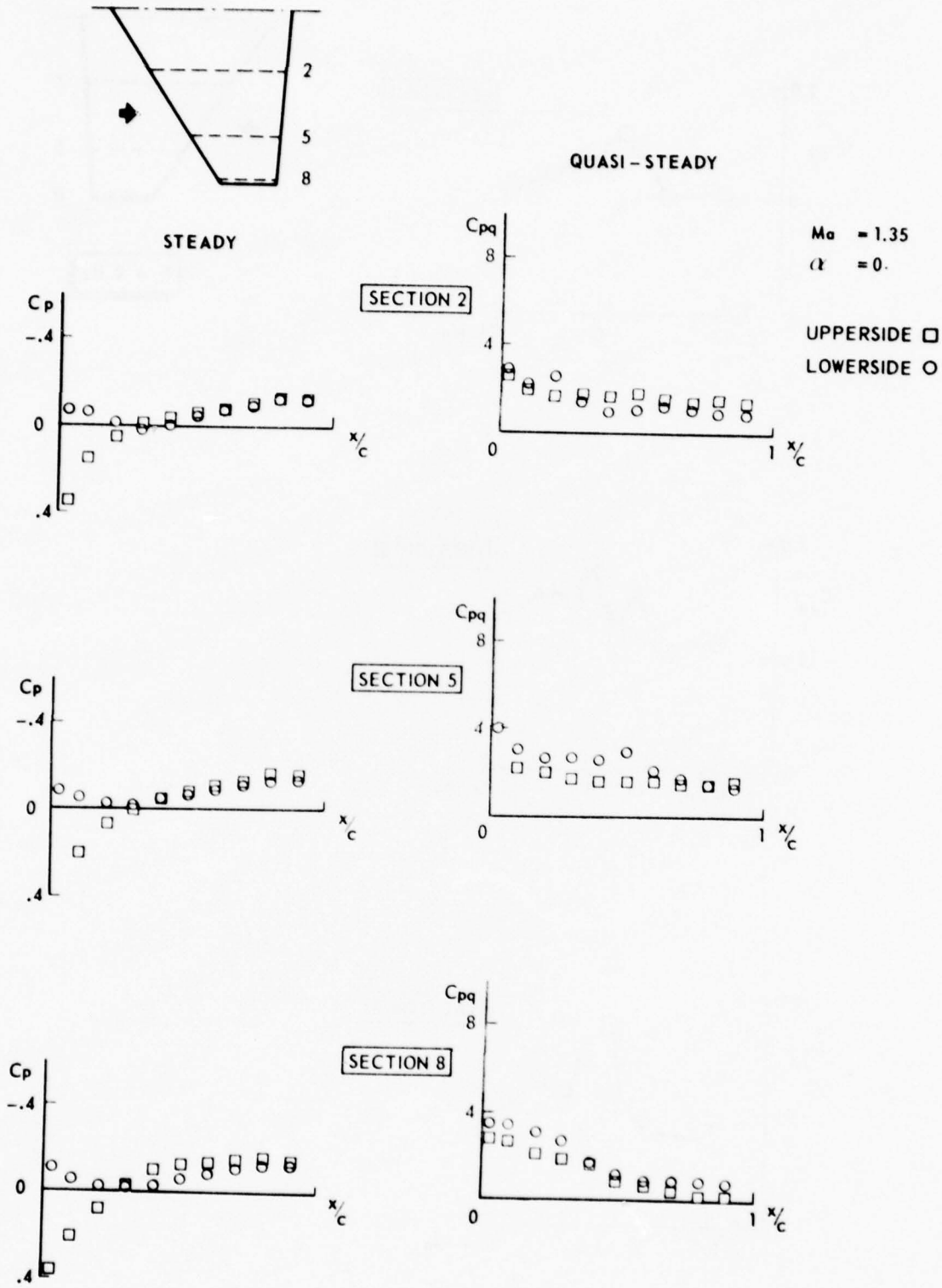

Fig. 2h Steady and quasi-steady pressure distributions on the clean wing

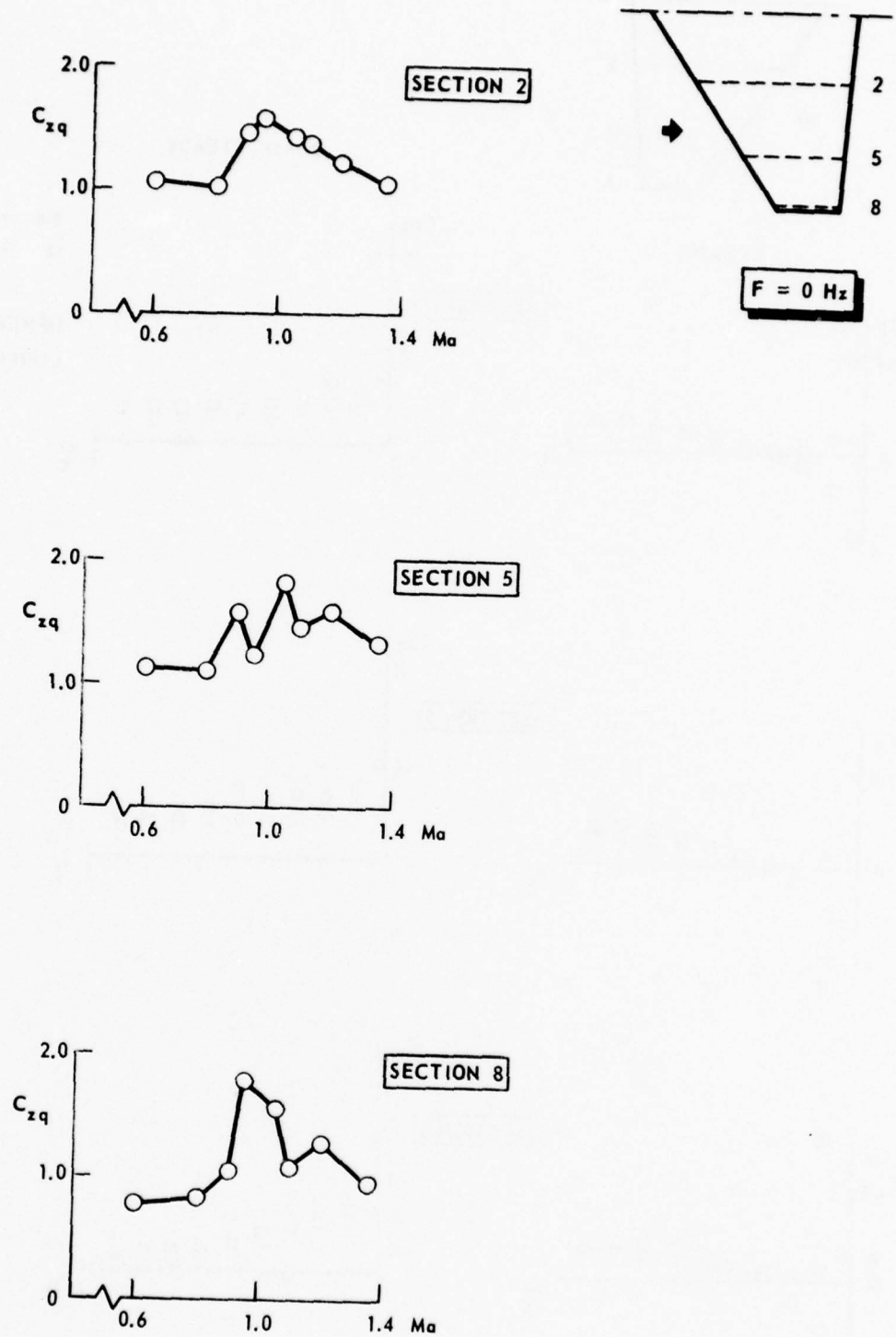

Fig. 3 Sectional quasi-steady normal load distribution

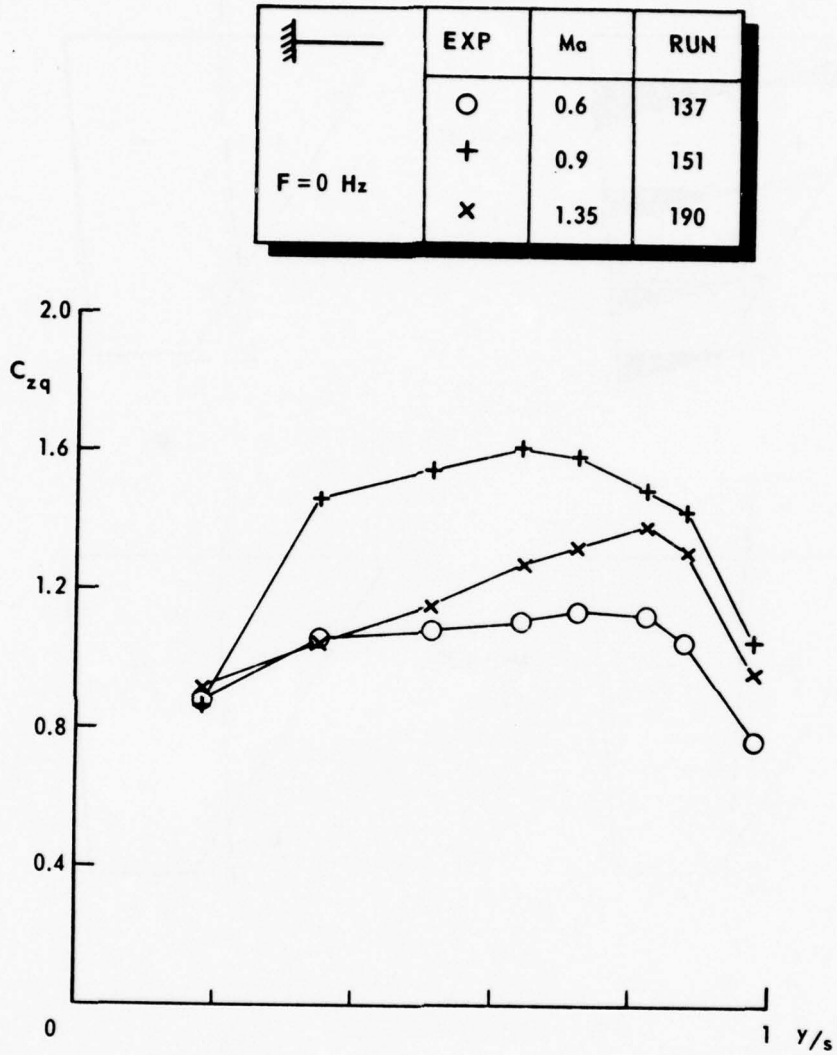

Fig. 4 Quasi-steady spanwise normal load distribution

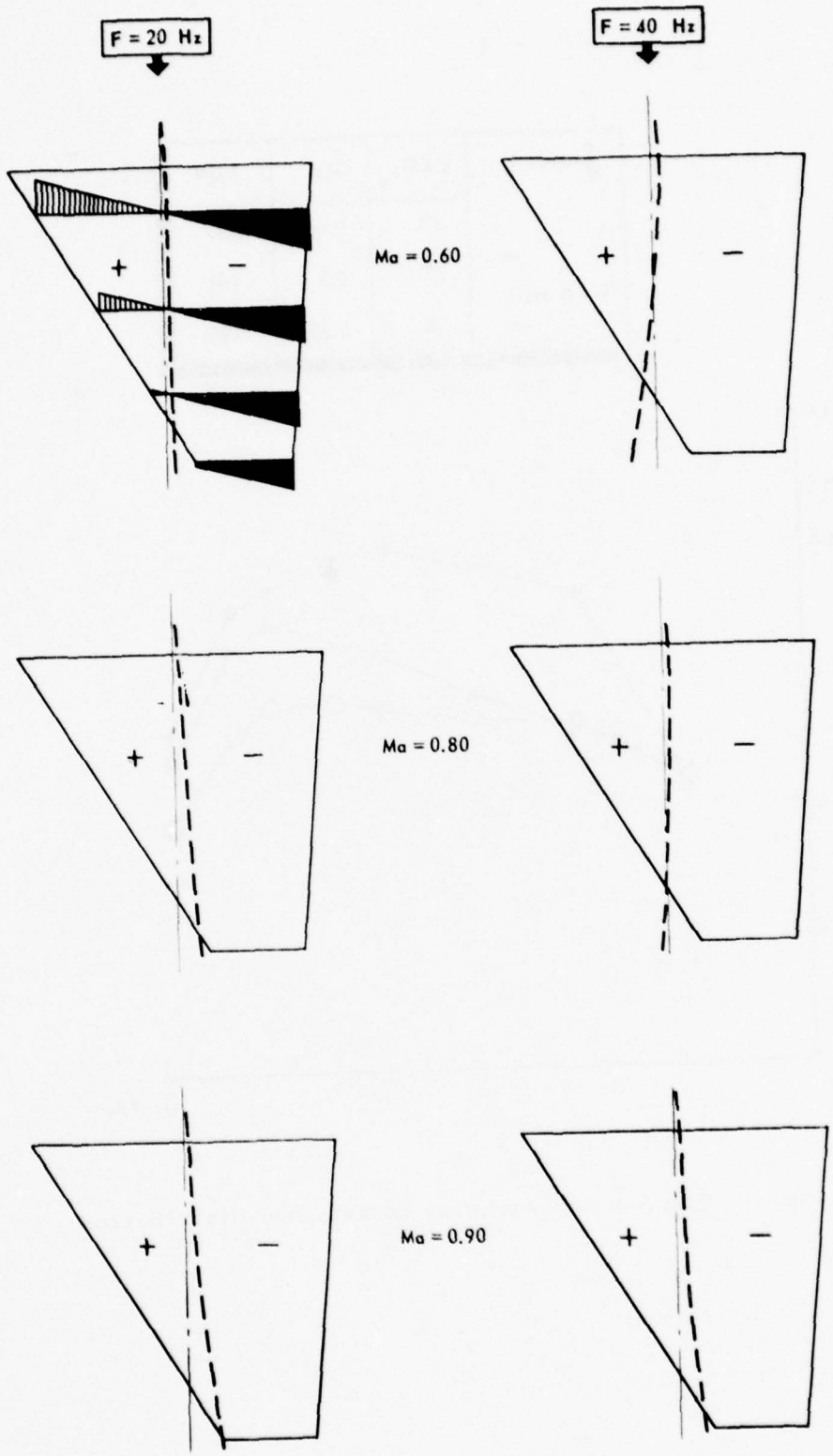

Fig. 5a In-wind vibration modes of the clean wing

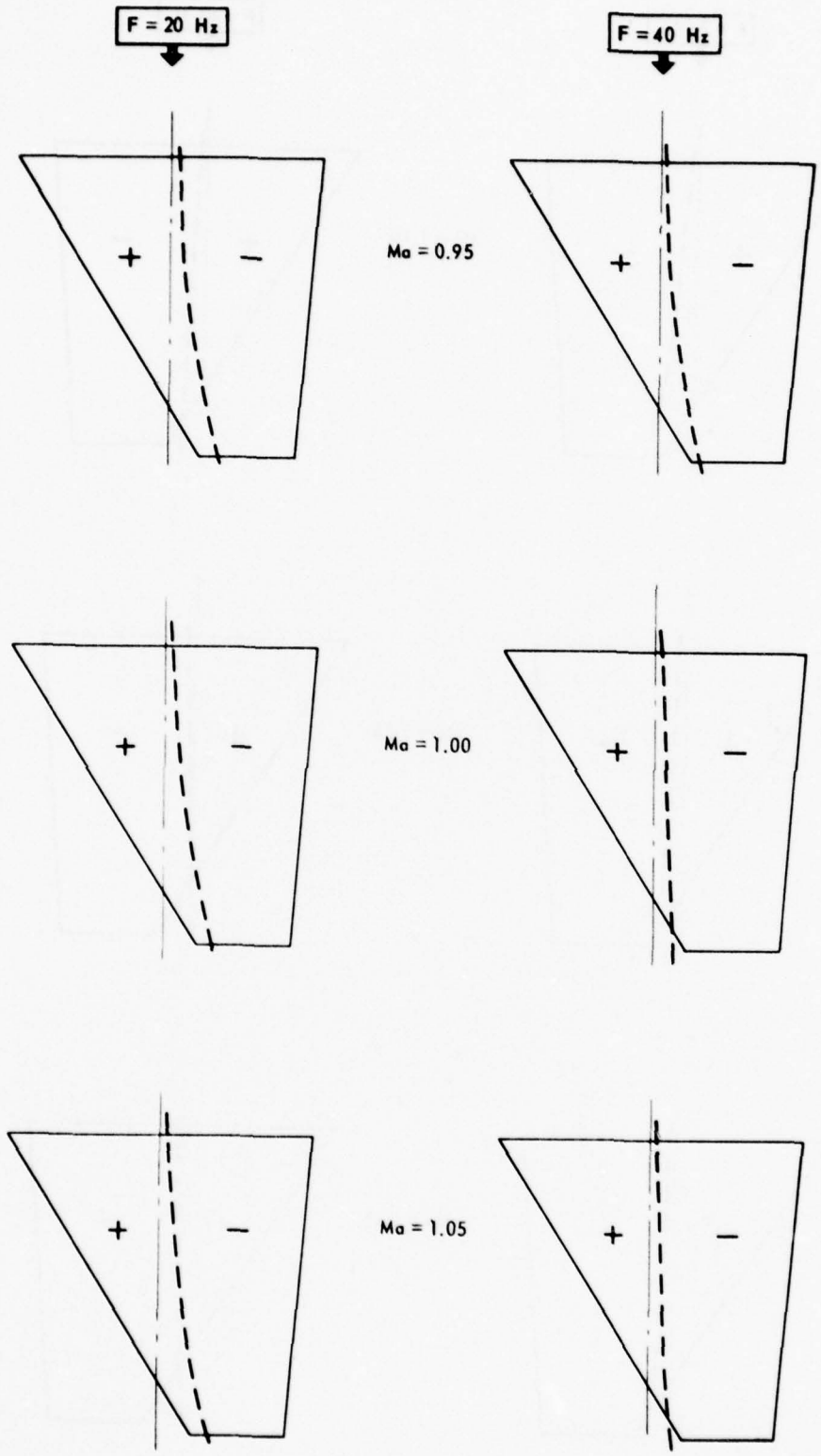

Fig. 5b In-wind vibration modes of the clean wing

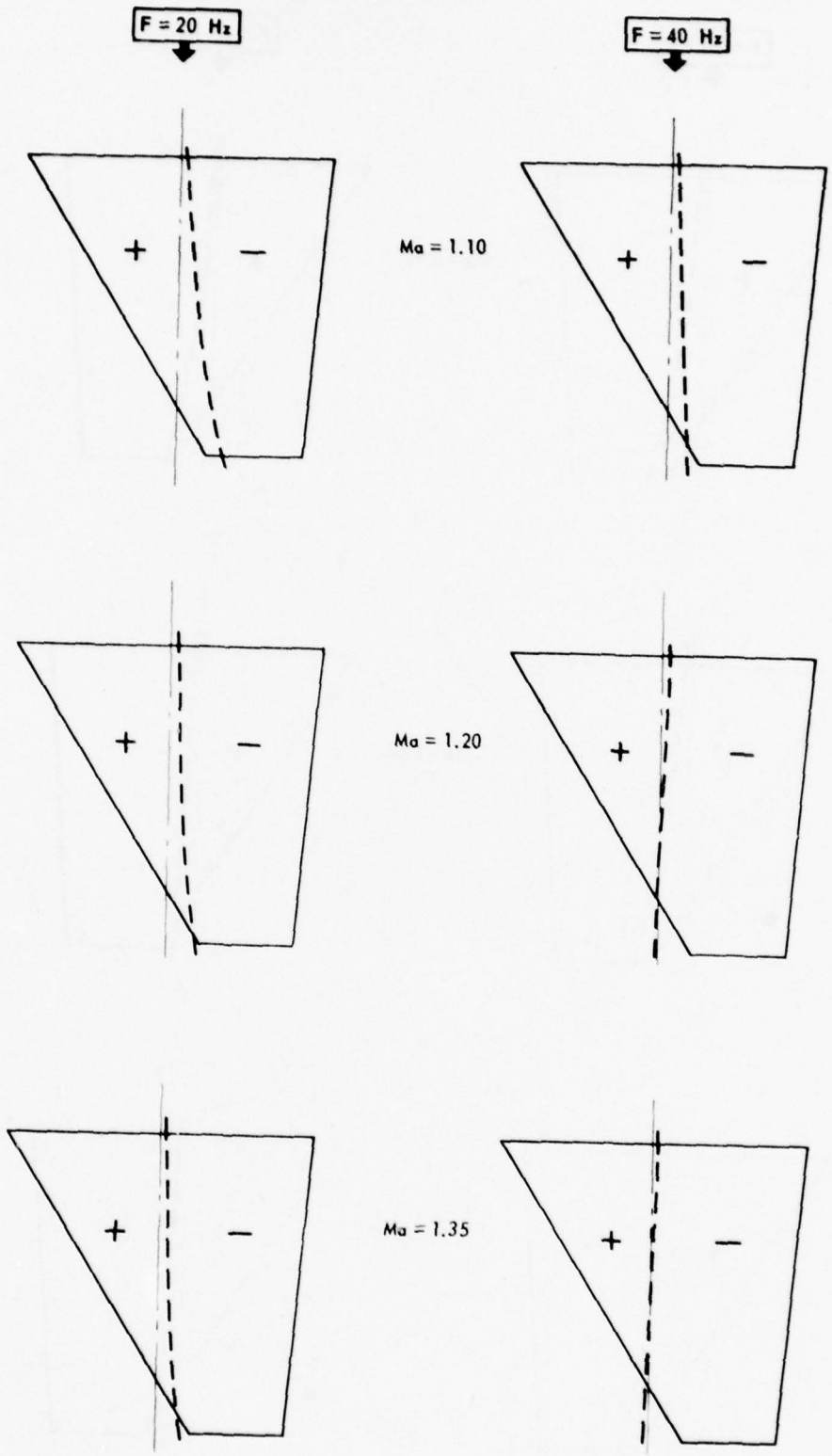

Fig. 5c In-wind vibration modes of the clean wing

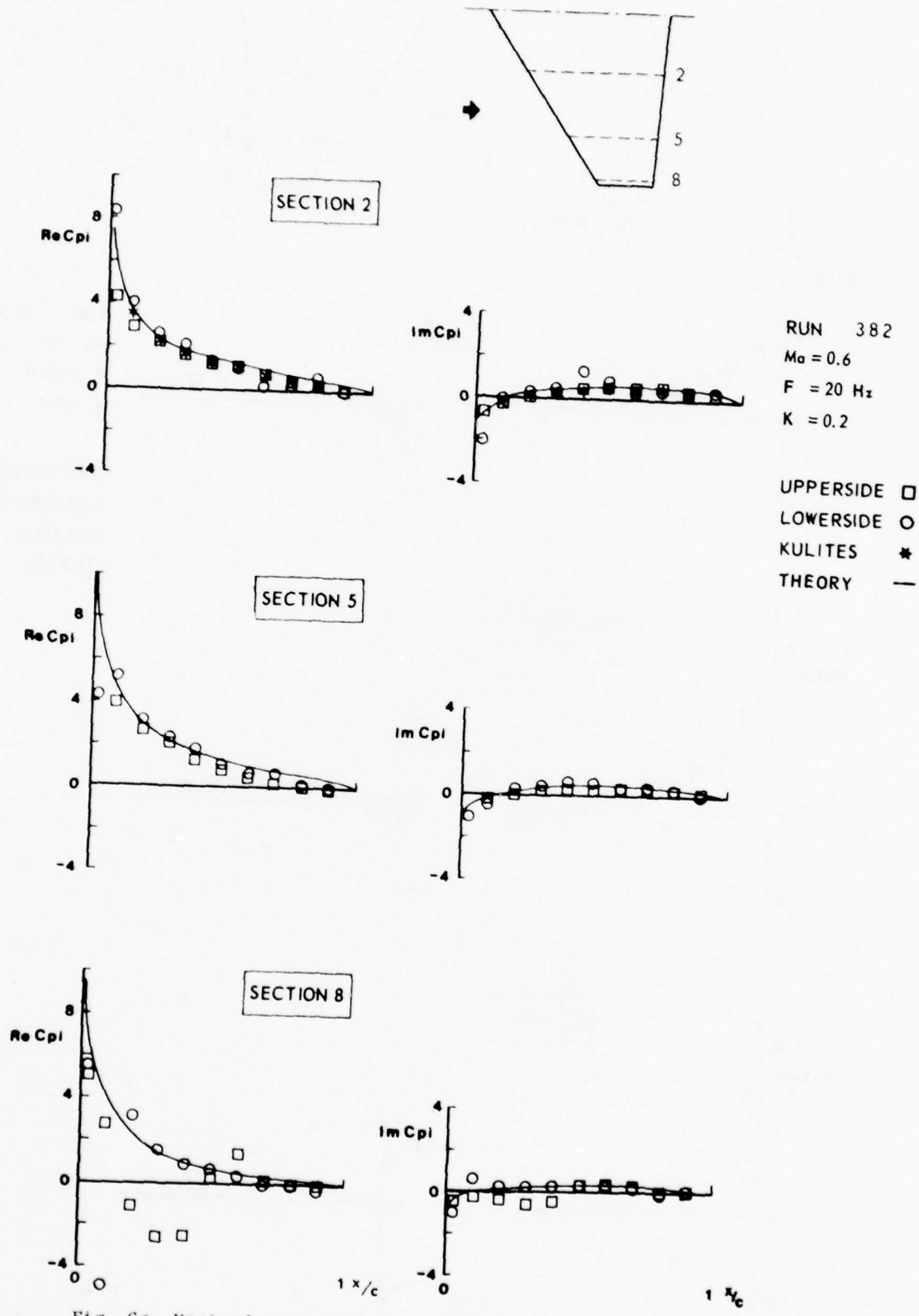

Fig. 6a Unsteady pressure distributions on the clean wing

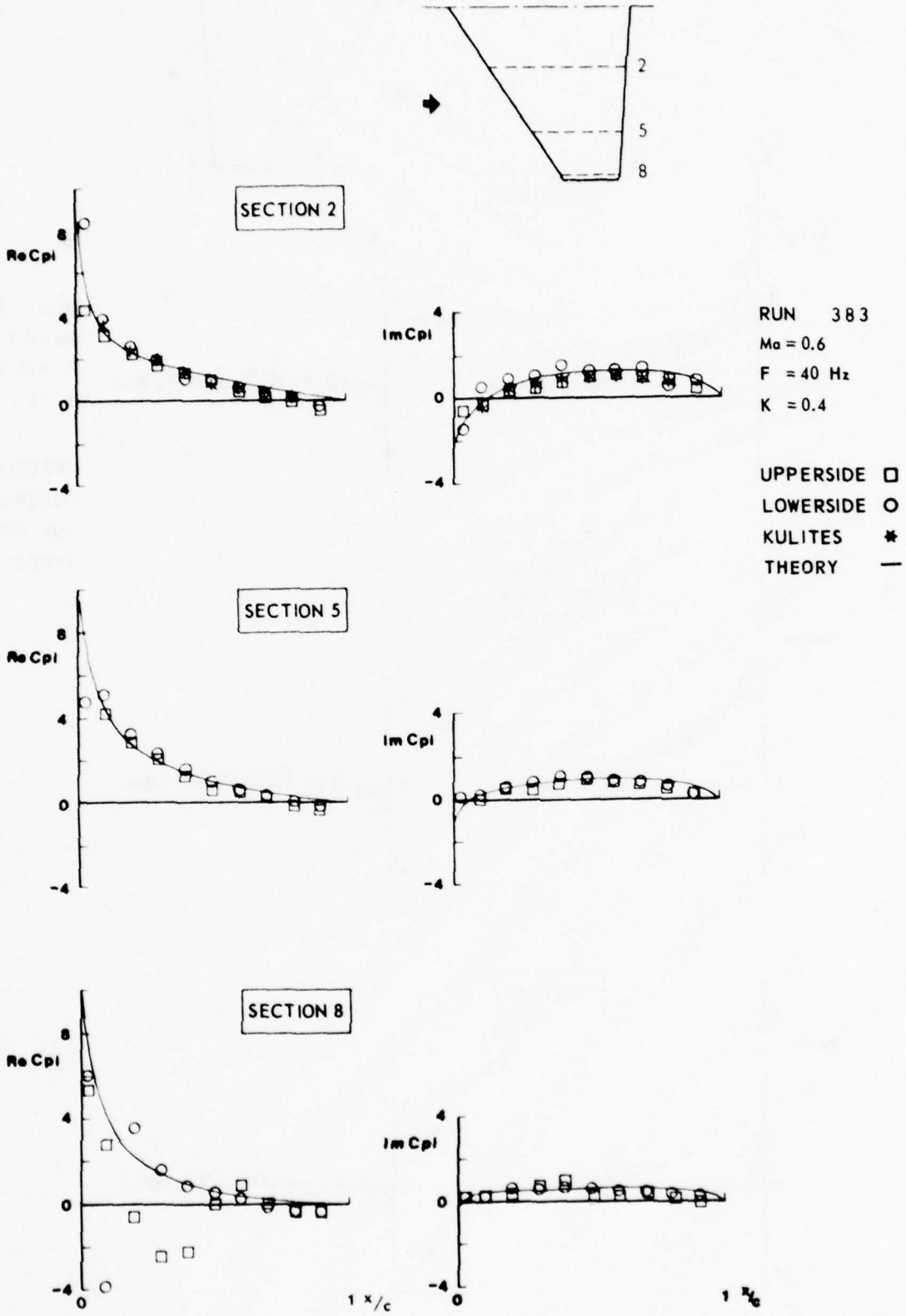

Fig. 6b Unsteady pressure distributions on the clean wing

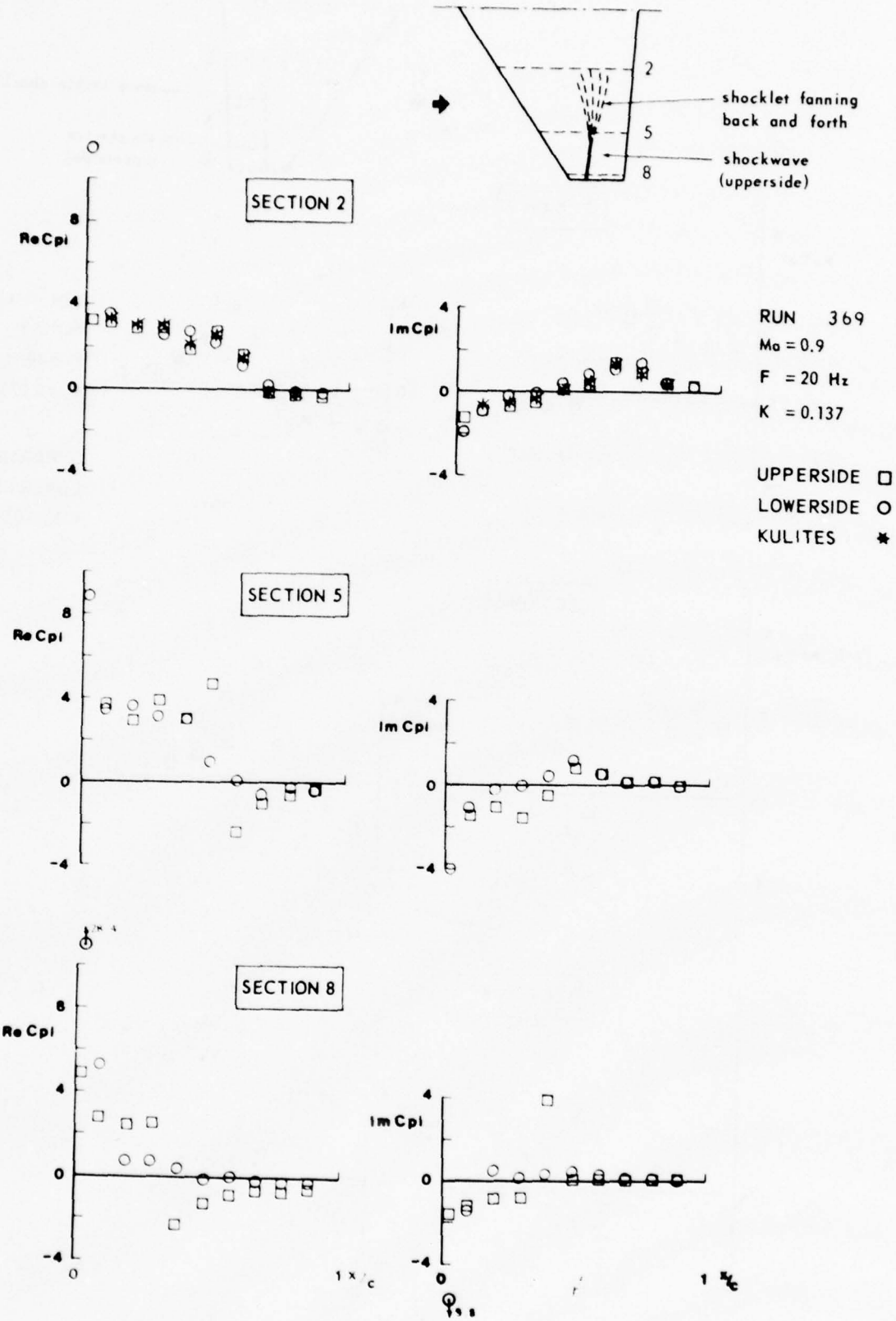

Fig. 6c Unsteady pressure distributions on the clean wing

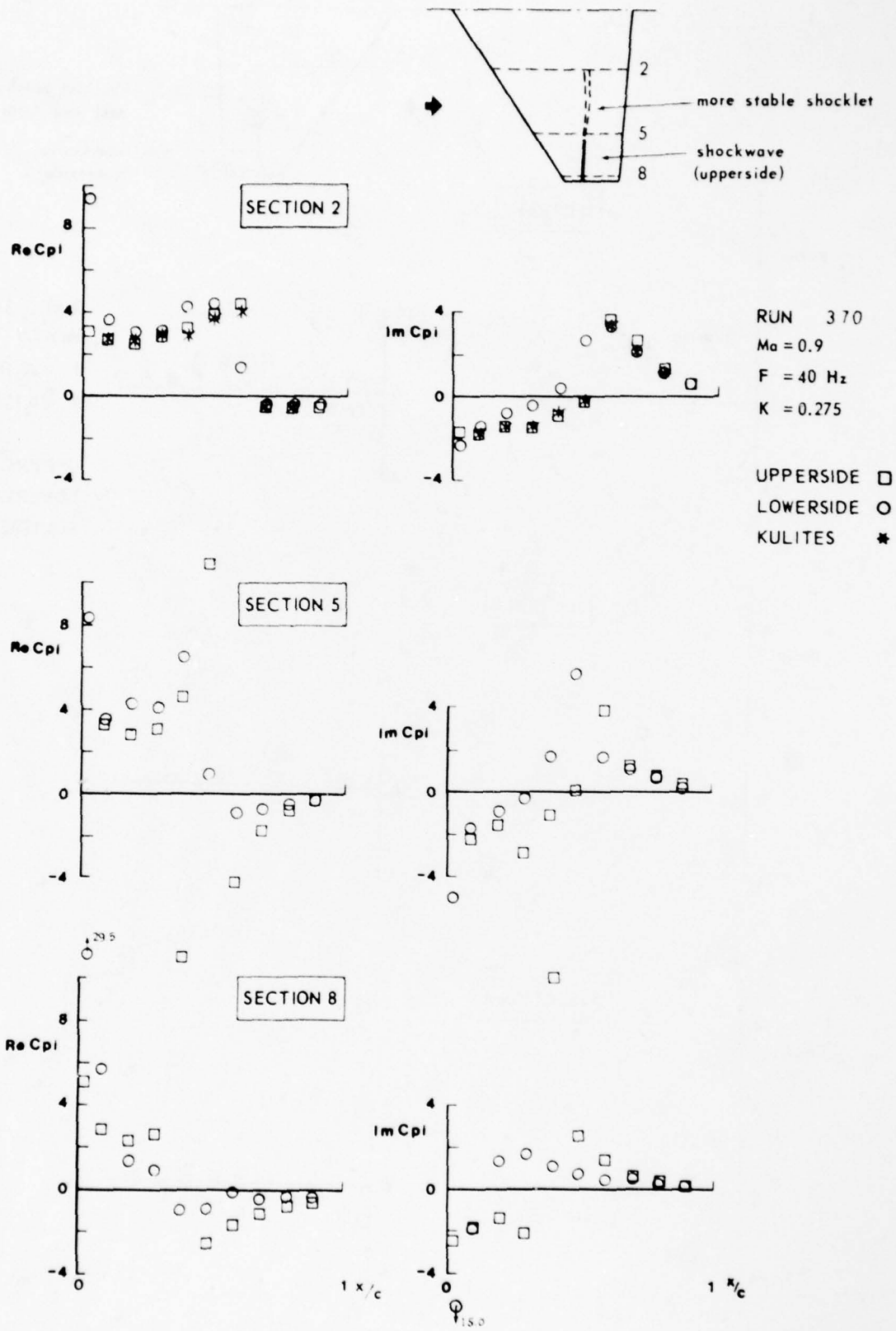

Fig. 6d Unsteady pressure distributions on the clean wing

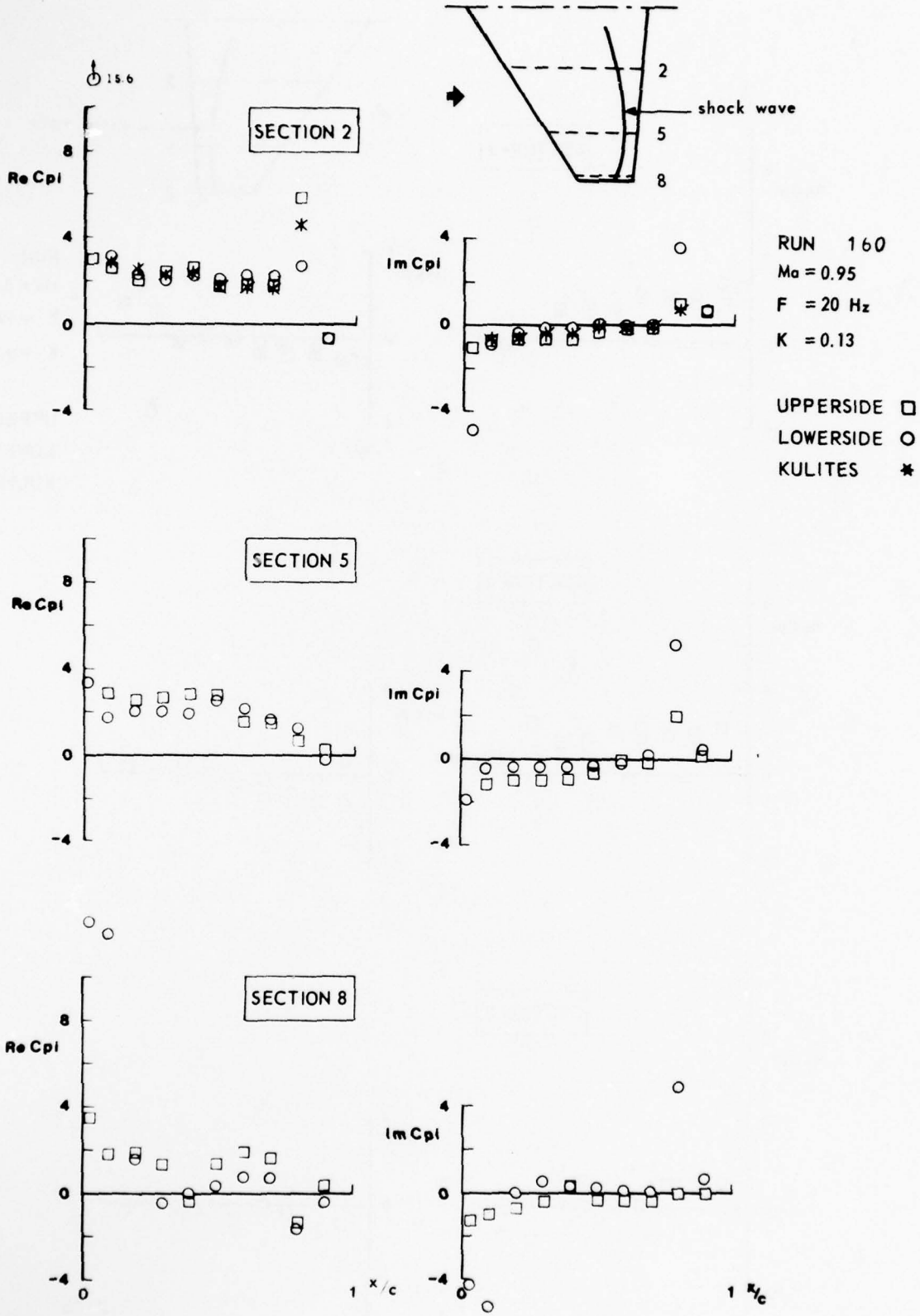

Fig. 6e Unsteady pressure distributions on the clean wing

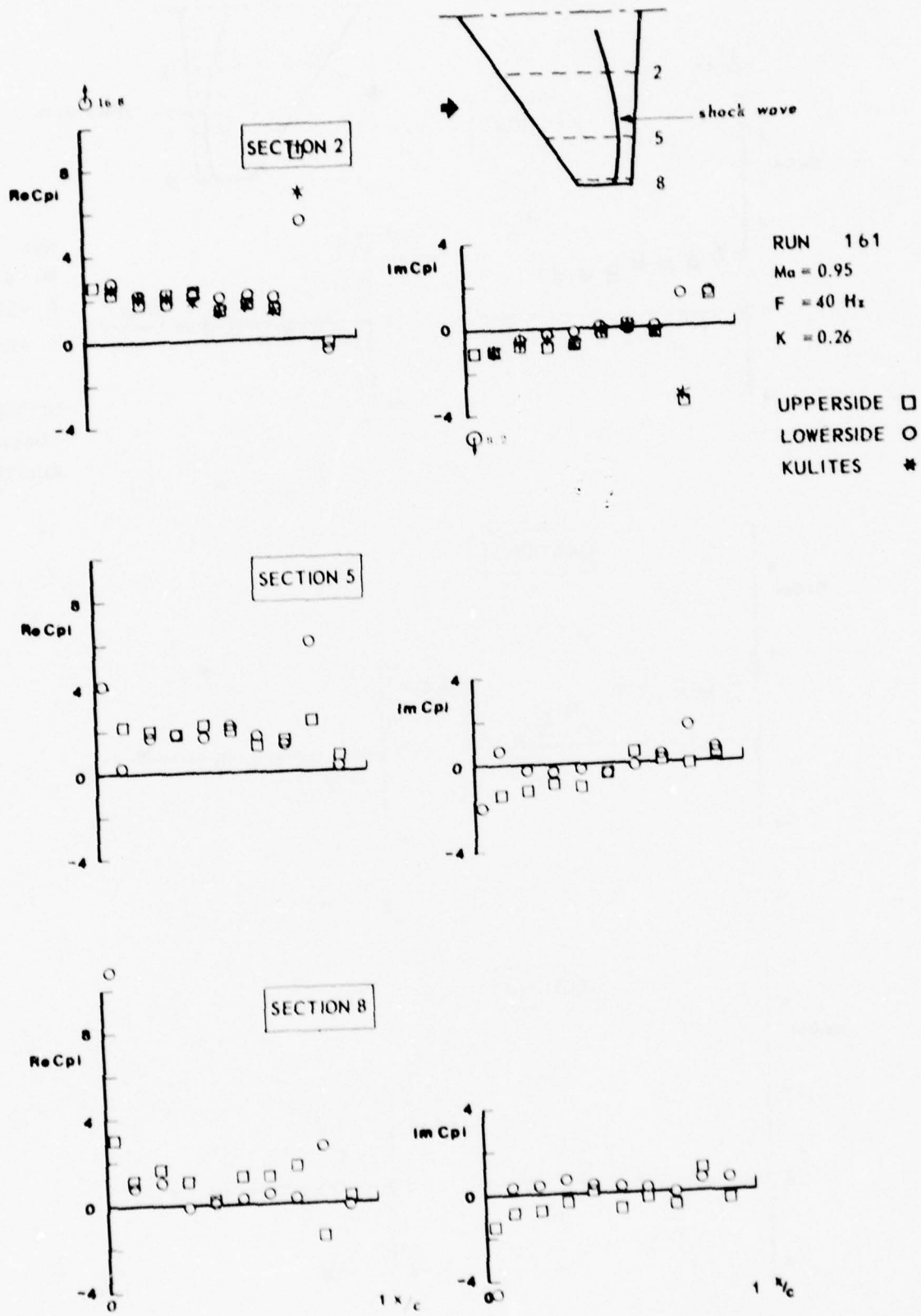

Fig. 6f Unsteady pressure distributions on the clean wing

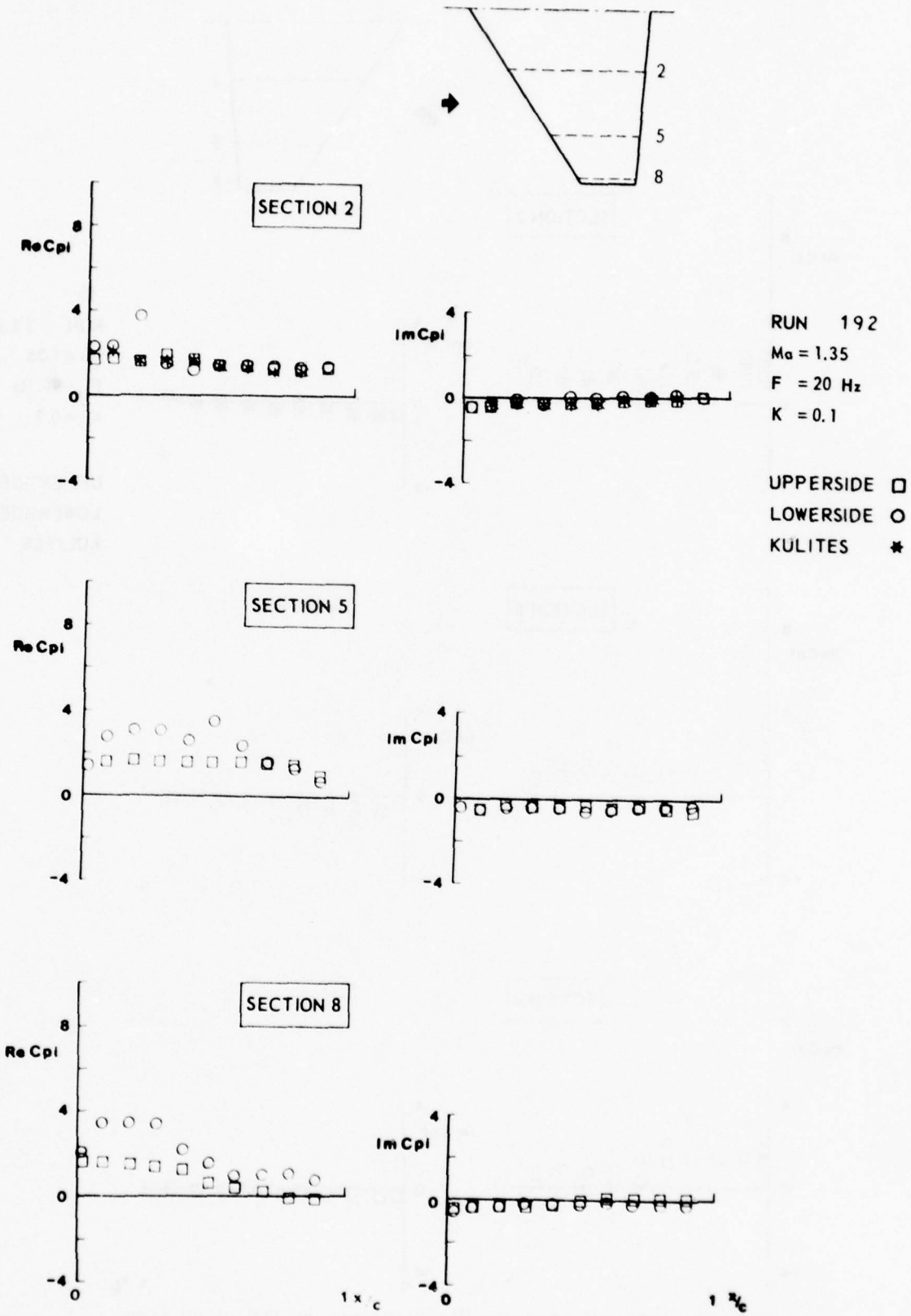

Fig. 6g Unsteady pressure distributions on the clean wing

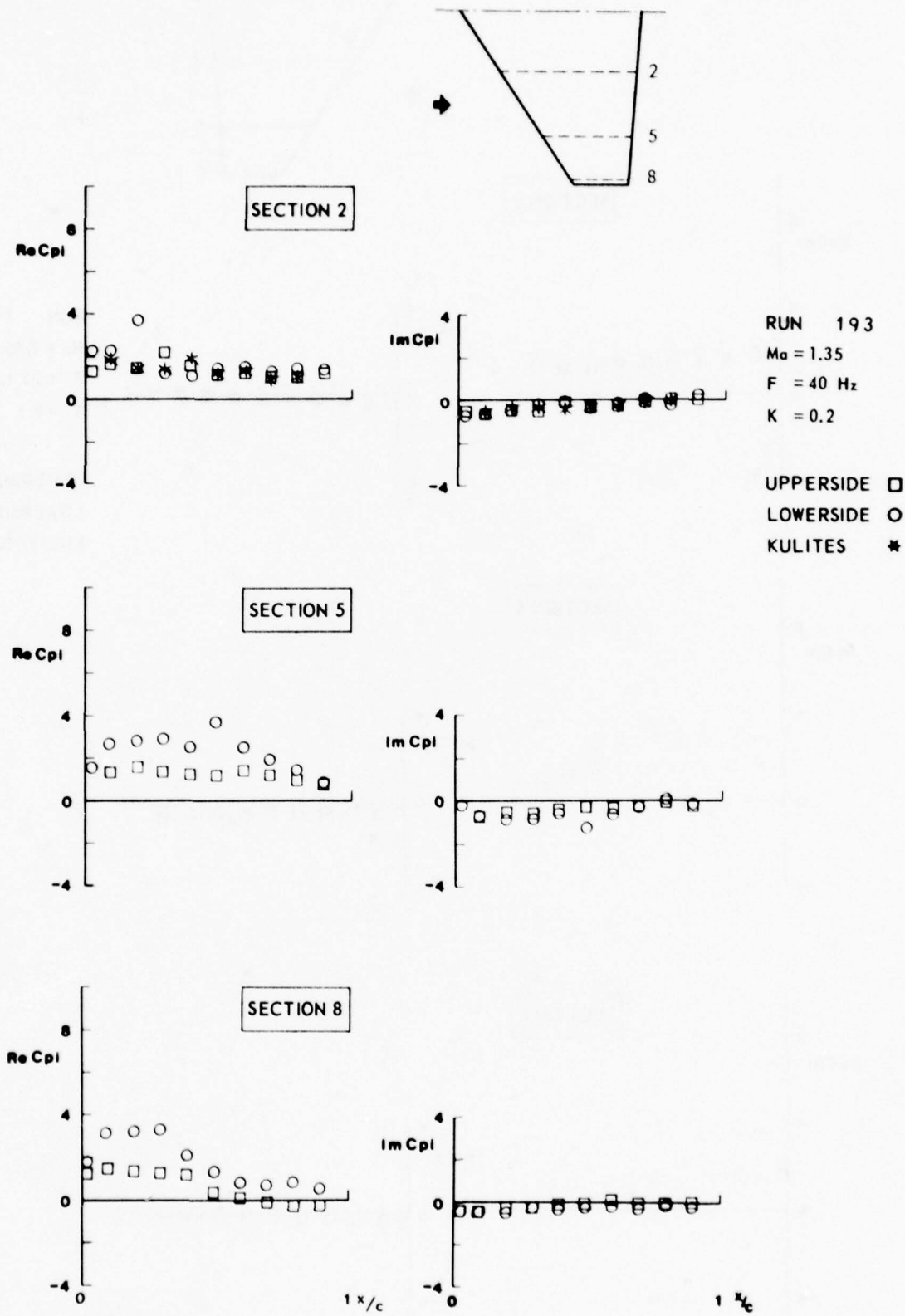

Fig. 6h Unsteady pressure distributions on the clean wing

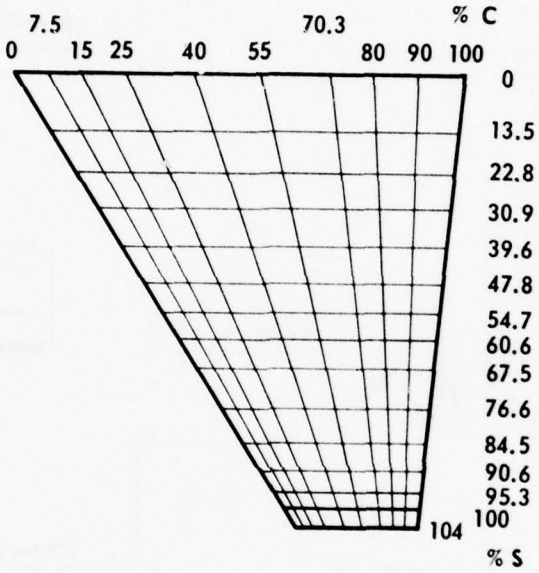

Fig. 7 Panel distribution used in theoretical calculations

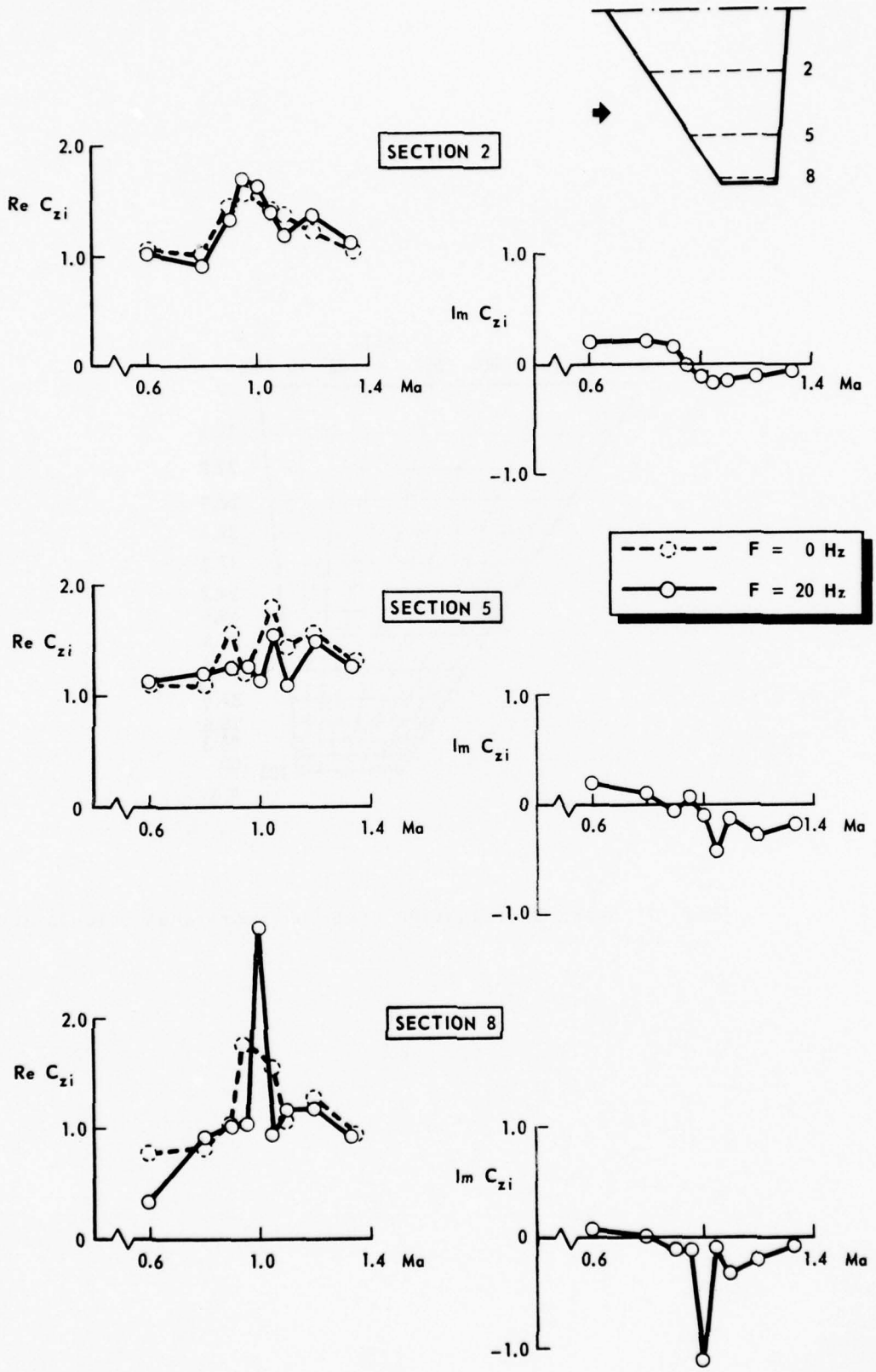

Fig. 8a Sectional unsteady normal load distribution

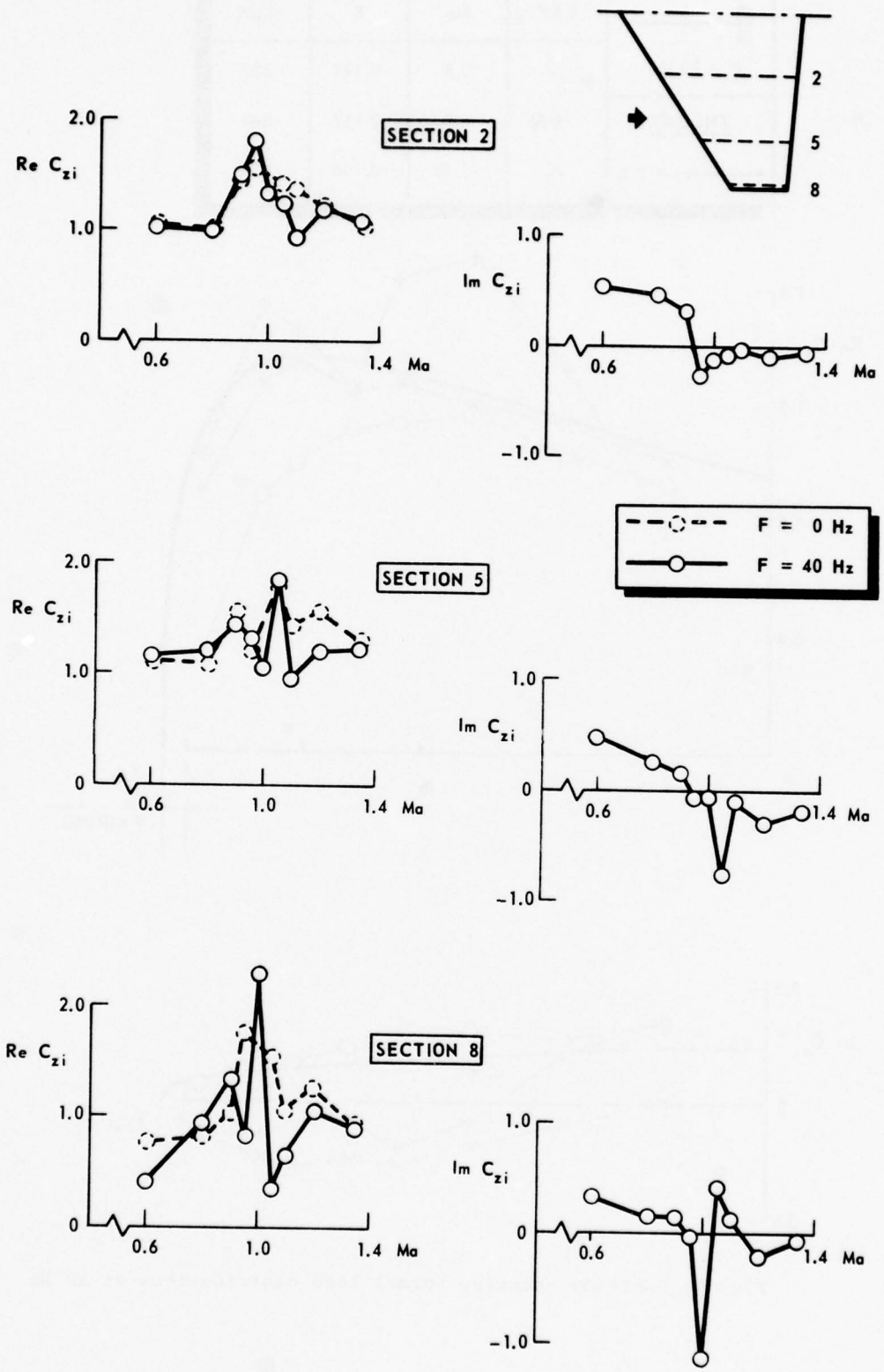

Fig. 8b Sectional unsteady normal load distribution

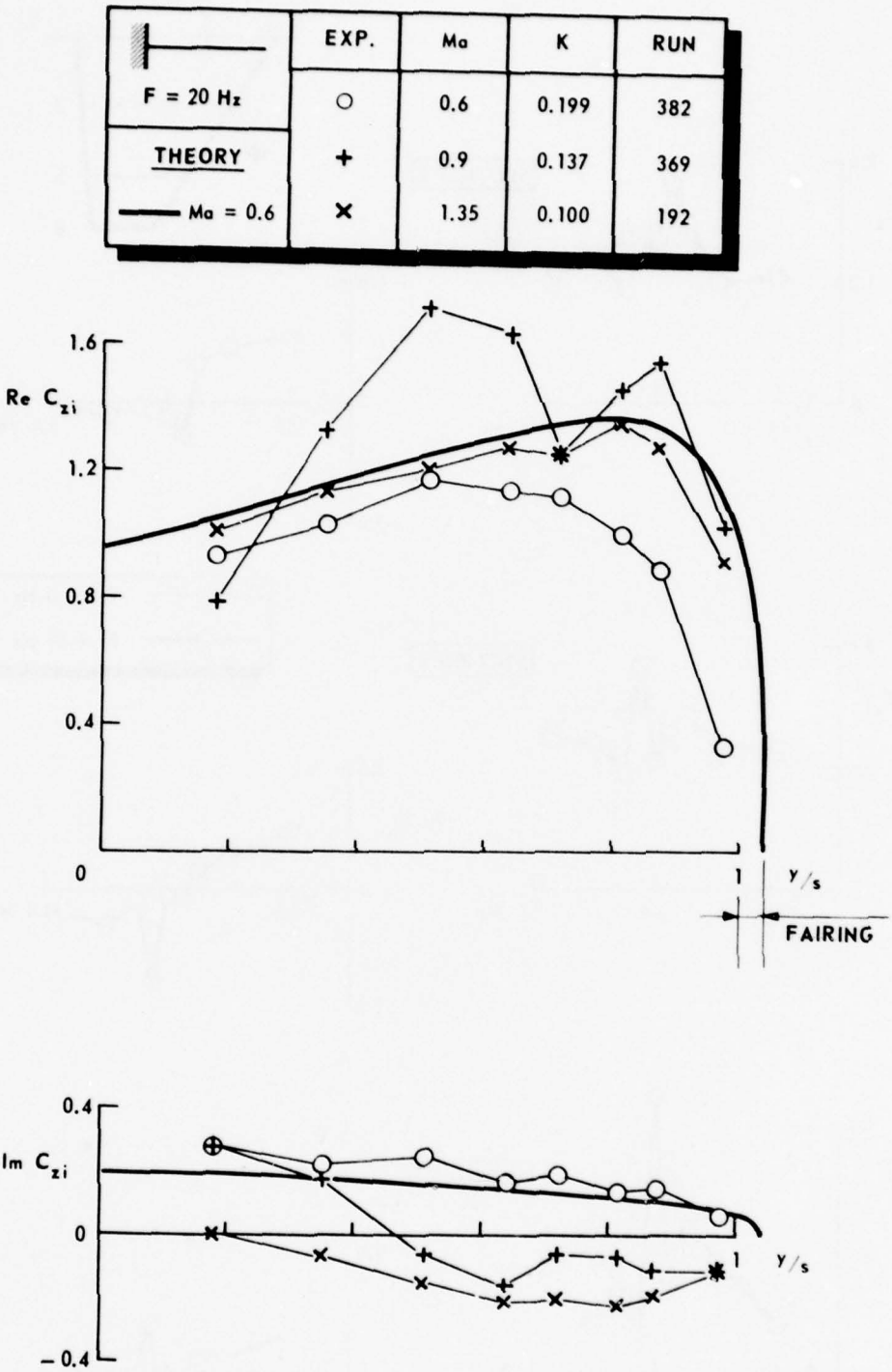

Fig. 9 Unsteady spanwise normal load distributions at 20 Hz

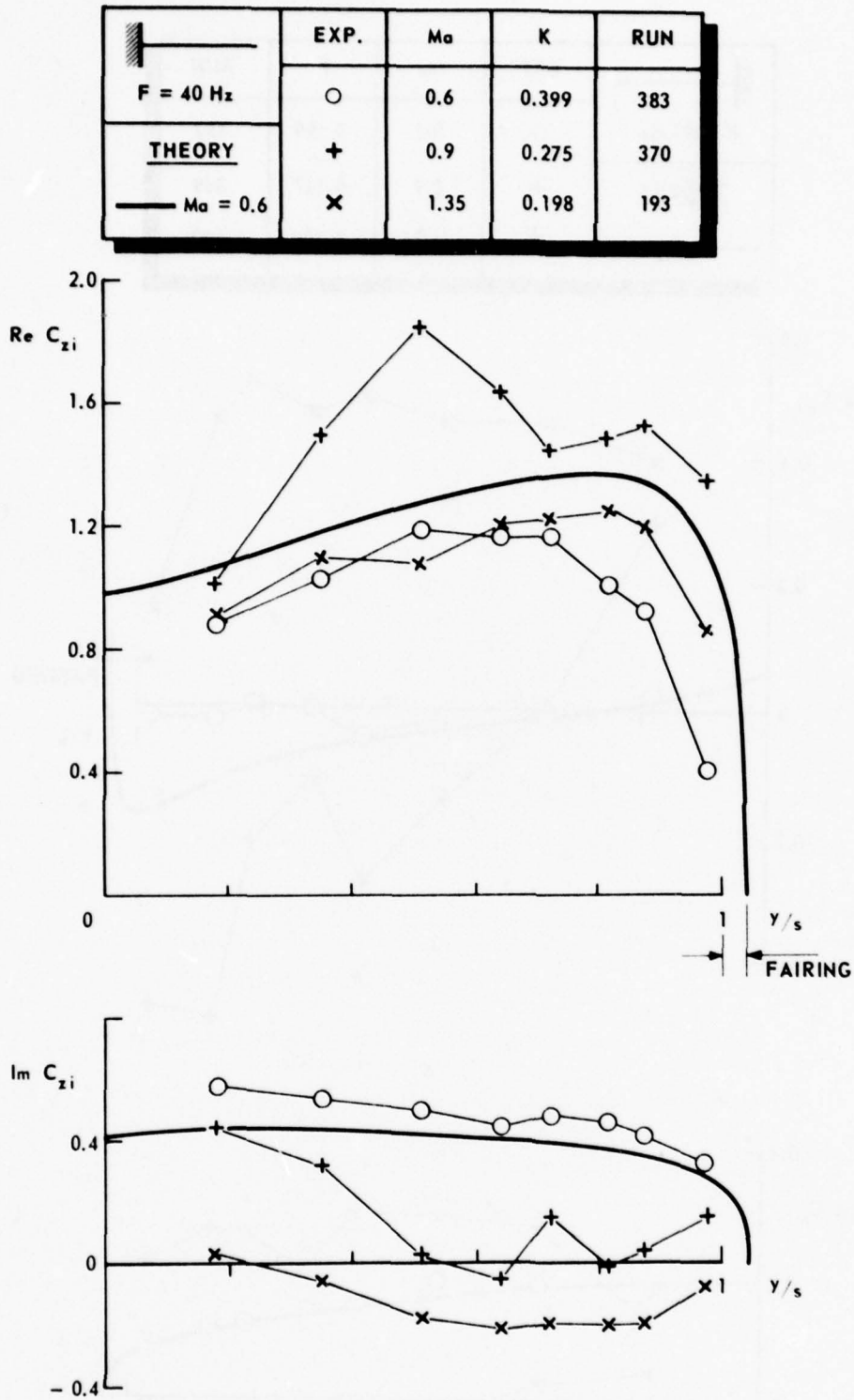

Fig. 10 Unsteady spanwise normal load distributions at 40 Hz

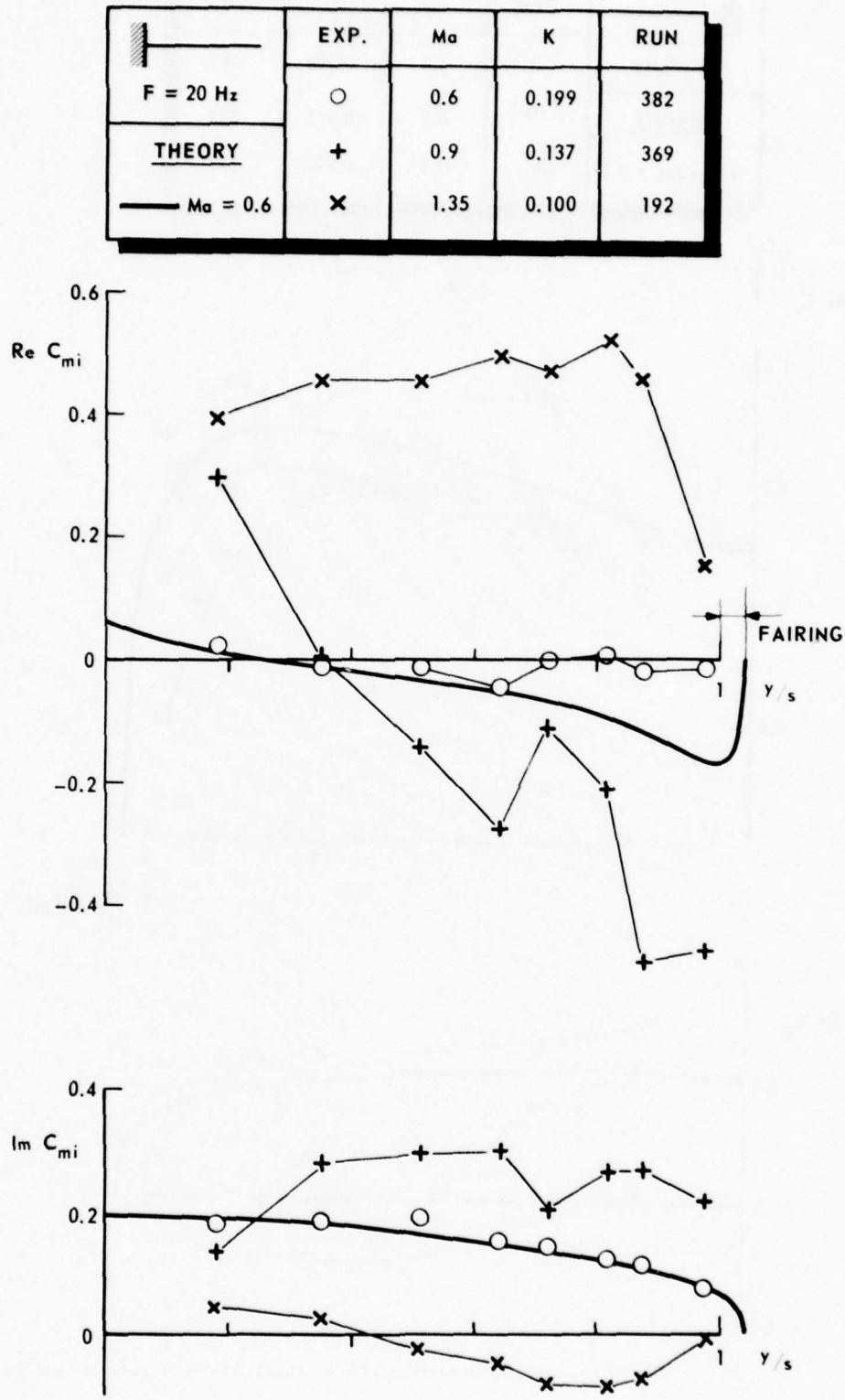

Fig. 11 Unsteady spanwise pitch moment distributions at 20 Hz

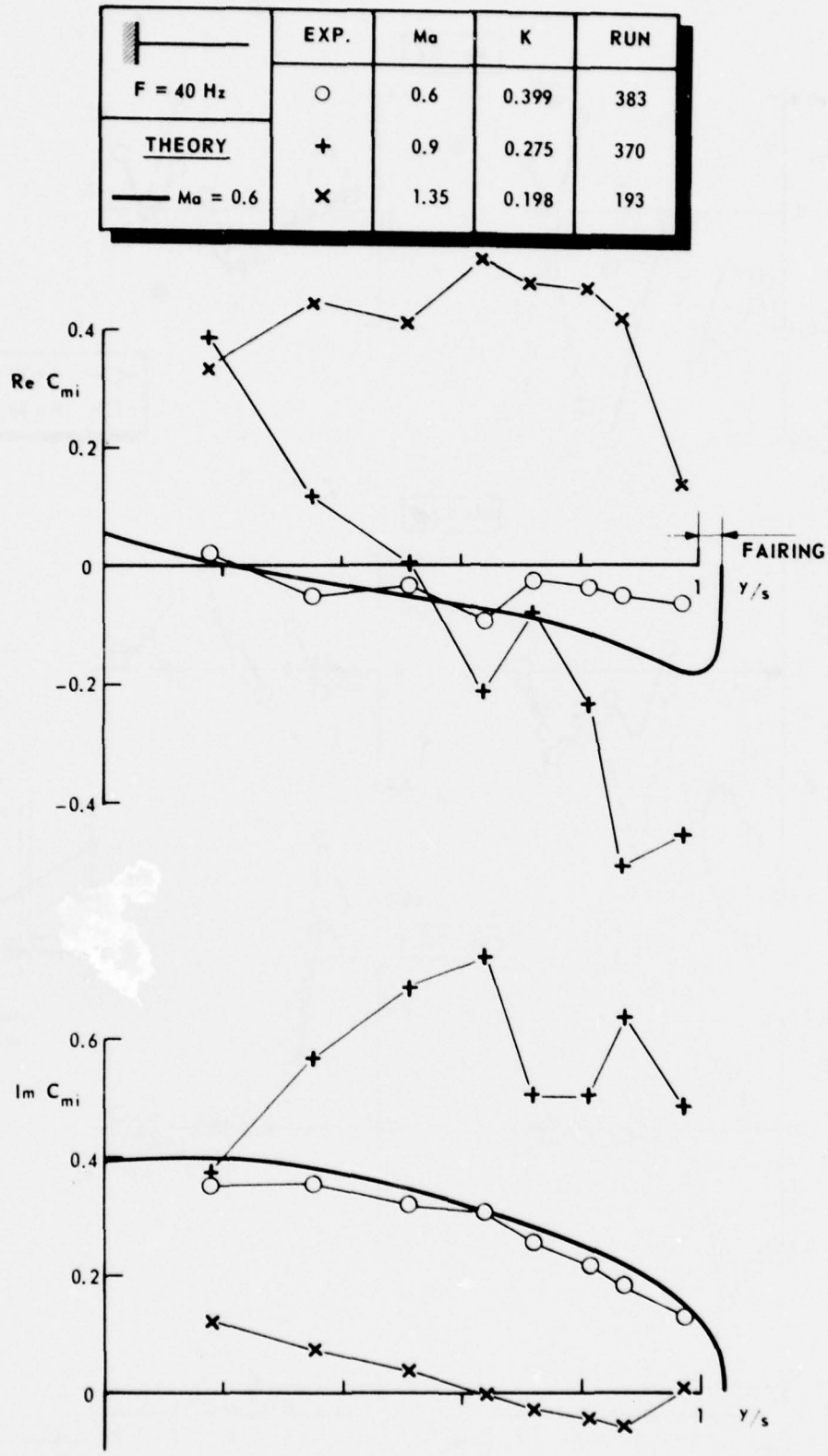

Fig. 12 Unsteady spanwise pitch moment distributions at 40 Hz

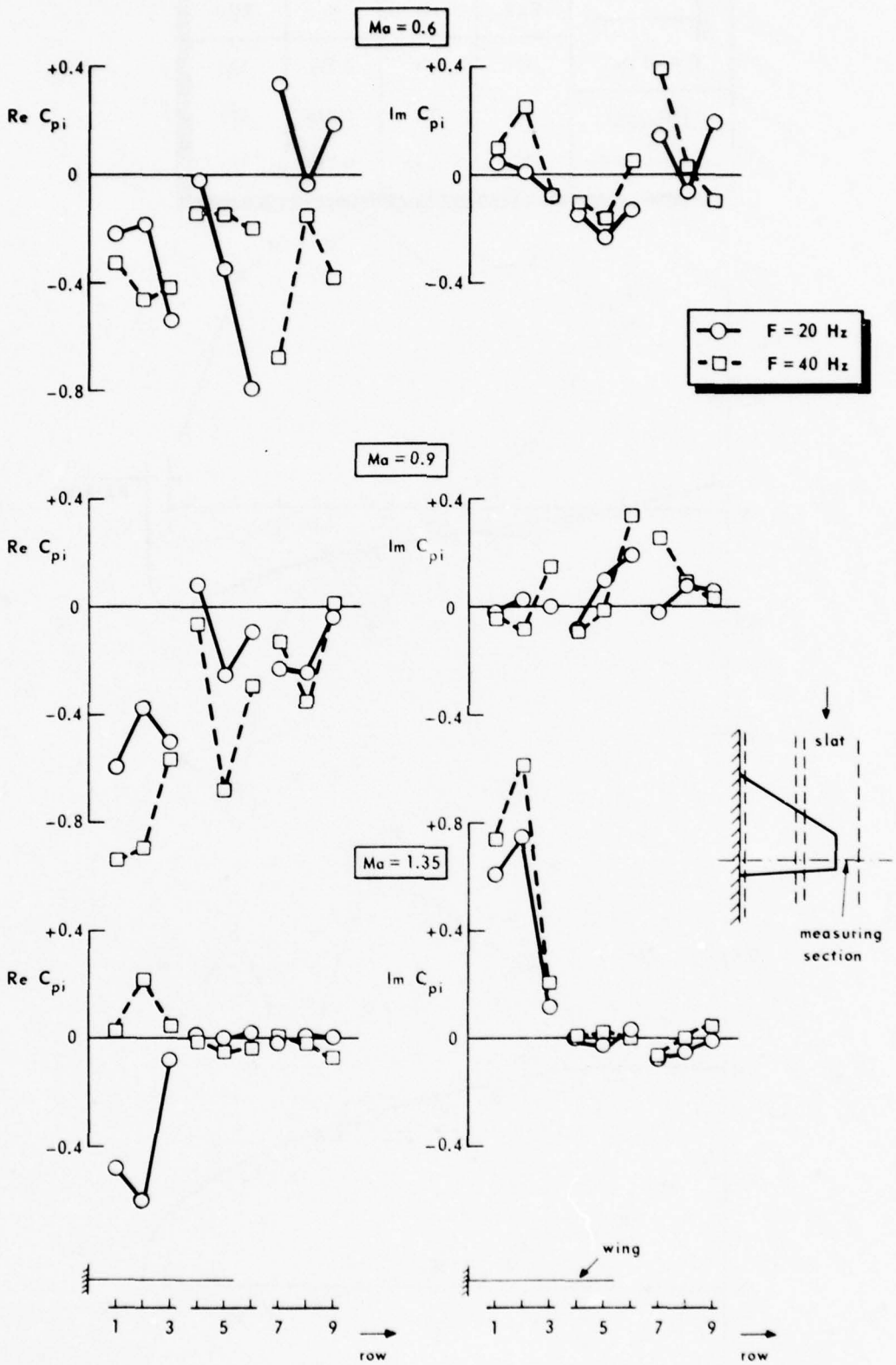

Fig. 13 Unsteady pressure distributions on the slotted tunnel wall plotted in spanwise direction (x = 1.0 m)

APPENDIX II.A

Definitions of steady and unsteady aerodynamic quantities*)

Steady

Pressure coefficient C_p :

$$C_p = (P_{loc} - P)/Q \quad .$$

Sectional normal force :

$$Z = C_z QC \; ; \; C_z = - \int_0^1 (C_{p+} - C_{p-}) \, d(x/C) \quad .$$

Sectional pitching moment about quarter chord point (positive nose down) :

$$M = C_m QC^2 \; ; \; C_m = - \int_0^1 (C_{p+} - C_{p-}) \, (x/C - 0.25) \, d(x/C) \quad .$$

Quasi-steady at zero incidence ($\omega = 0$; $\alpha_o = 0$)

Pressure coefficient C_{pq} :

$$C_{pq} = \Delta C_p / \Delta\alpha = \frac{C_p(\alpha_o + \Delta\alpha_1) - C_p(\alpha_o - \Delta\alpha_2)}{\Delta\alpha_1 + \Delta\alpha_2} \quad .$$

Sectional normal force :

$$Z_q = \pi QCC_{zq}\Theta e^{i\omega t} \; ; \; C_{zq} = \frac{1}{\pi} \Delta C_z / \Delta\alpha = \frac{1}{\pi} \frac{C_z(\alpha_o + \Delta\alpha_1) - C_z(\alpha_o - \Delta\alpha_2)}{\Delta\alpha_1 + \Delta\alpha_2} \quad .$$

Sectional pitching moment (positive nose down) :

$$M_q = \frac{\pi}{2} QCC_{mq}\Theta e^{i\omega t} \; ; \; C_{mq} = \frac{2}{\pi} \Delta C_m / \Delta\alpha = \frac{2}{\pi} \frac{C_m(\alpha_o + \Delta\alpha_1) - C_m(\alpha_o - \Delta\alpha_2)}{\Delta\alpha_1 + \Delta\alpha_2} \quad .$$

---

*) The definitions for the unsteady aerodynamic quantities are according to the AGARD manual on Aeroelasticity Vol. VI (Ref. 6).

Unsteady

Pressure coefficient C_{pi} :

$$C_{pi} = ReC_{pi} + iImC_{pi} = P_i/Q\Theta \quad .$$

Sectional normal force :

$$Z_i = \pi QCC_{zi}\Theta e^{i\omega t} \; ; \; C_{zi} = ReC_{zi} + iImC_{zi} = -\frac{1}{\pi}\int_0^1 (C_{pi+} - C_{pi-})\, d(x/C) \quad .$$

Sectional pitching moment about quarter chord point (positive nose down) :

$$M_i = \frac{\pi}{2} QC^2 C_{mi}\Theta e^{i\omega t} \; ;$$

$$C_{mi} = ReC_{mi} + iImC_{mi} = -\frac{2}{\pi}\int_0^1 (C_{pi+} - C_{pi-})\,(x/C - 0.25)\, d(x/C) \quad .$$

APPENDIX II.B

Steady Pressure Distributions

Clean Wing (Conf. 0)

Run	Nominal Ma	Nominal α (degrees)	Nominal $P_o \times 10^{-5}$ (Pa)	Fig. No.
136	0.6	-0.5	1.0	II.B. 1
137		0		2
138		+0.5		3
145	0.8	-0.5		II.B. 4
146		0		5
147		+0.5		6
150	0.9	-0.5		II.B. 7
151		0		8
152		+0.5		9
157	0.95	-0.5		II.B.10
158		0		11
159		+0.5		12
162	1.05	-0.5		II.B.13
163		0		14
164		+0.5		15
167	1.10	-0.5		II.B.16
168		0		17
169		+0.5	1.0	18
184	1.20	-0.5	0.7	II.B.19
185		0		20
186		+0.5		21
189	1.35	-0.5		II.B.22
190		0		23
191		+0.5	0.7	24

(Note that in sections 3 and 5 the first point on the upperside, showing a zero value, is a faulty pressure point, which should not be considered in any evaluation).

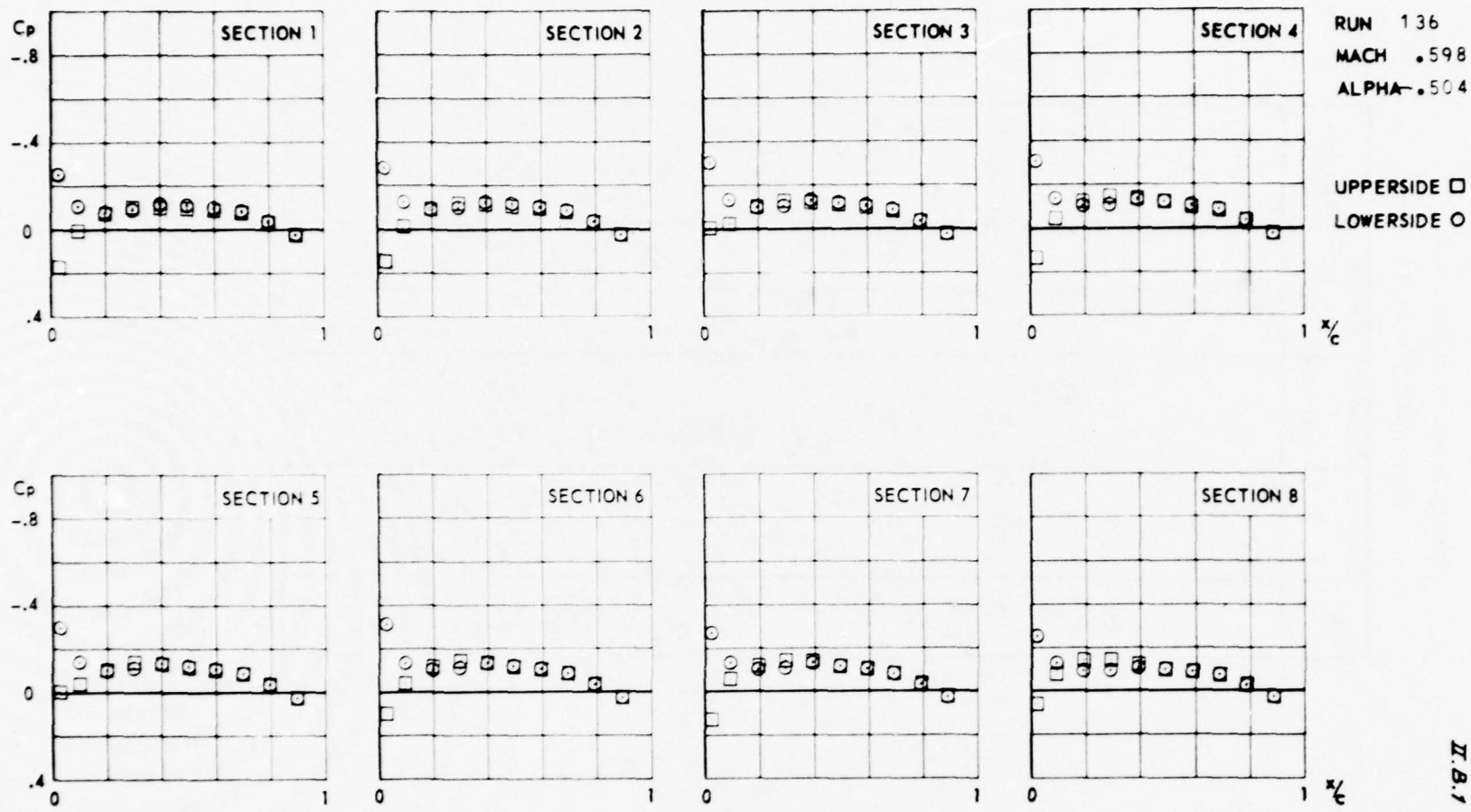

CONF.0 (CLEAN WING)

FIG. II.B.1

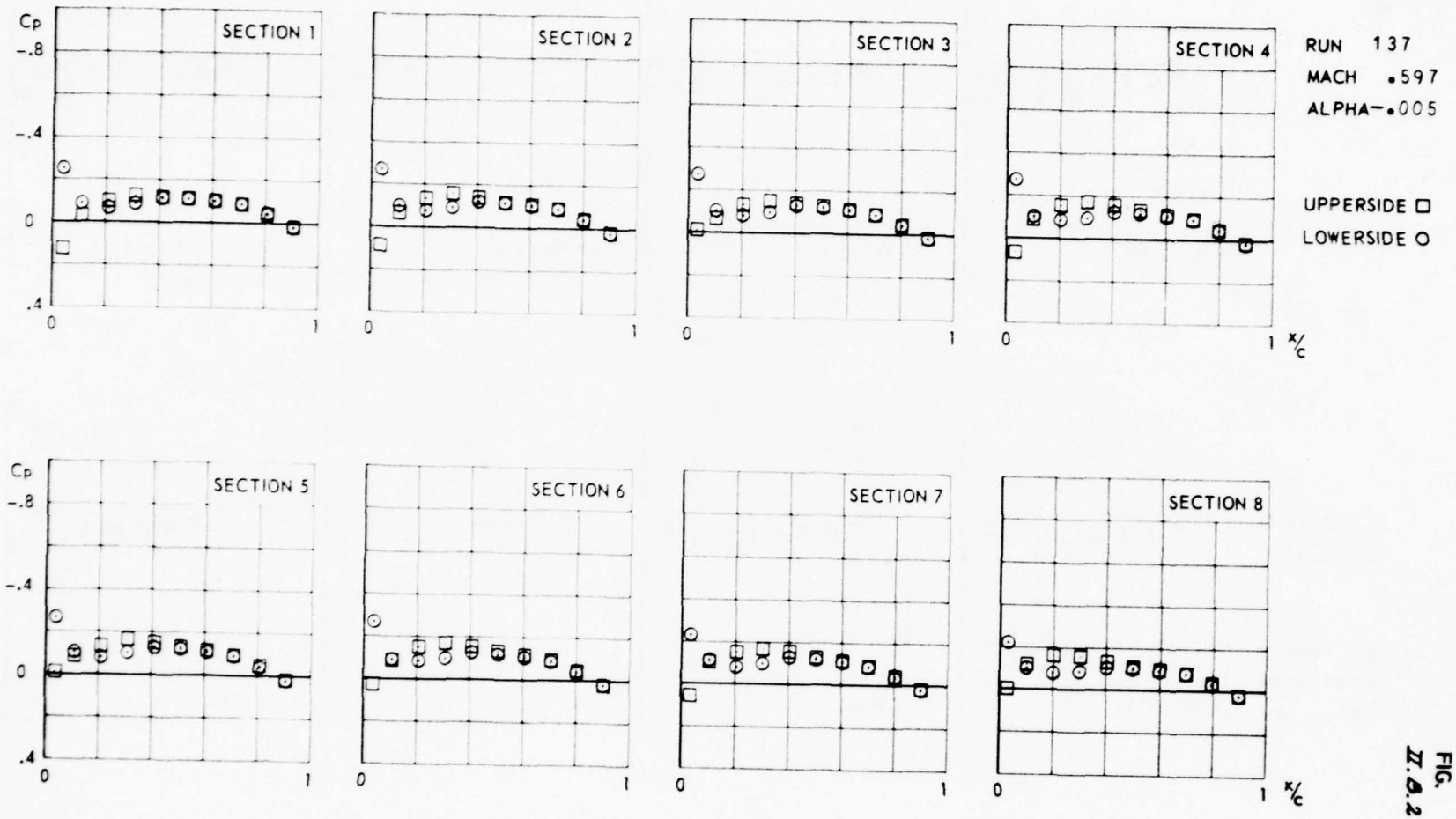

CONF.0 (CLEAN WING)

FIG. II.B.2

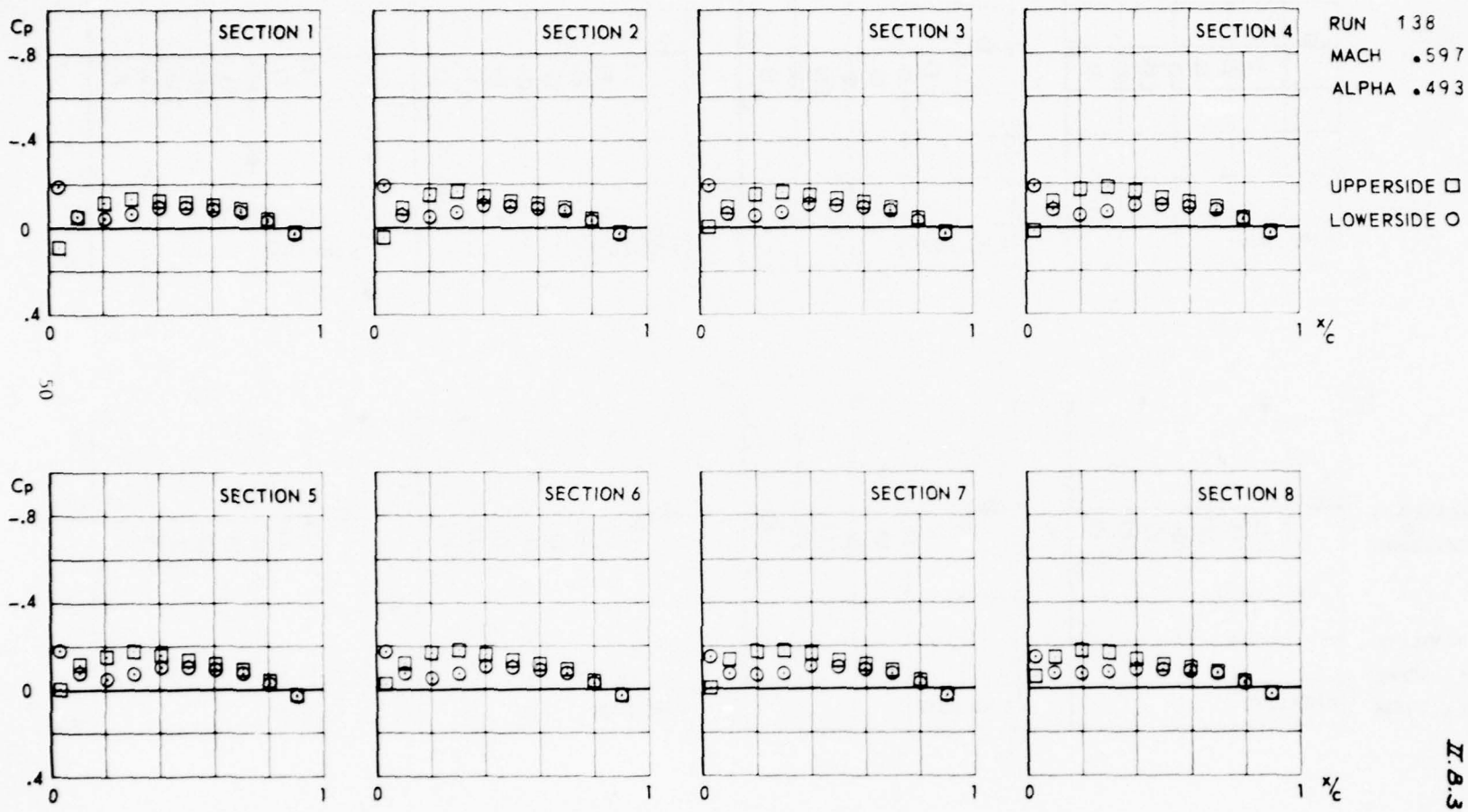

CONF.0 (CLEAN WING)

FIG. II.B.3

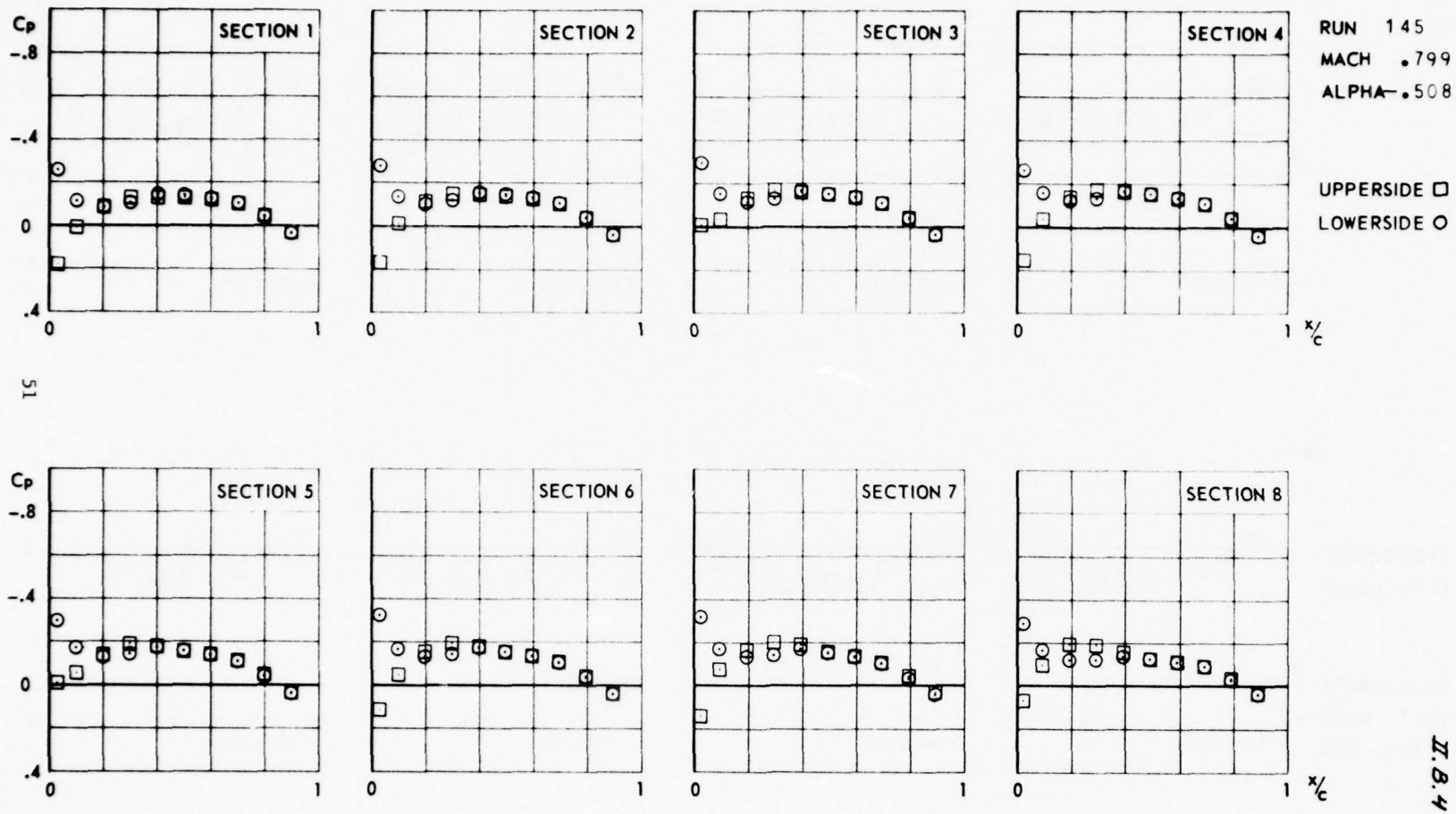

CONF.0 (CLEAN WING)

FIG. II.B.4

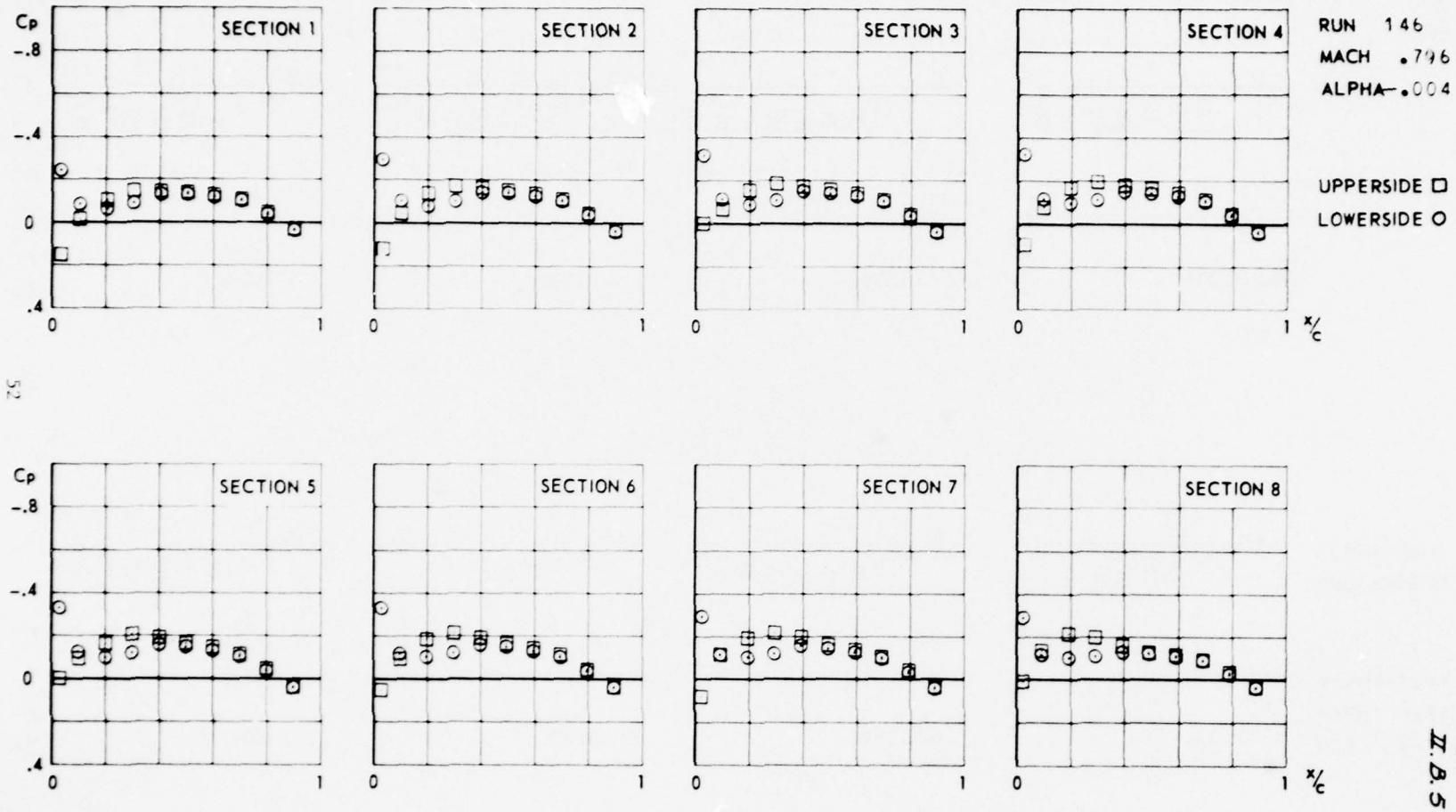

CONF.0 (CLEAN WING)

FIG. II.B.5

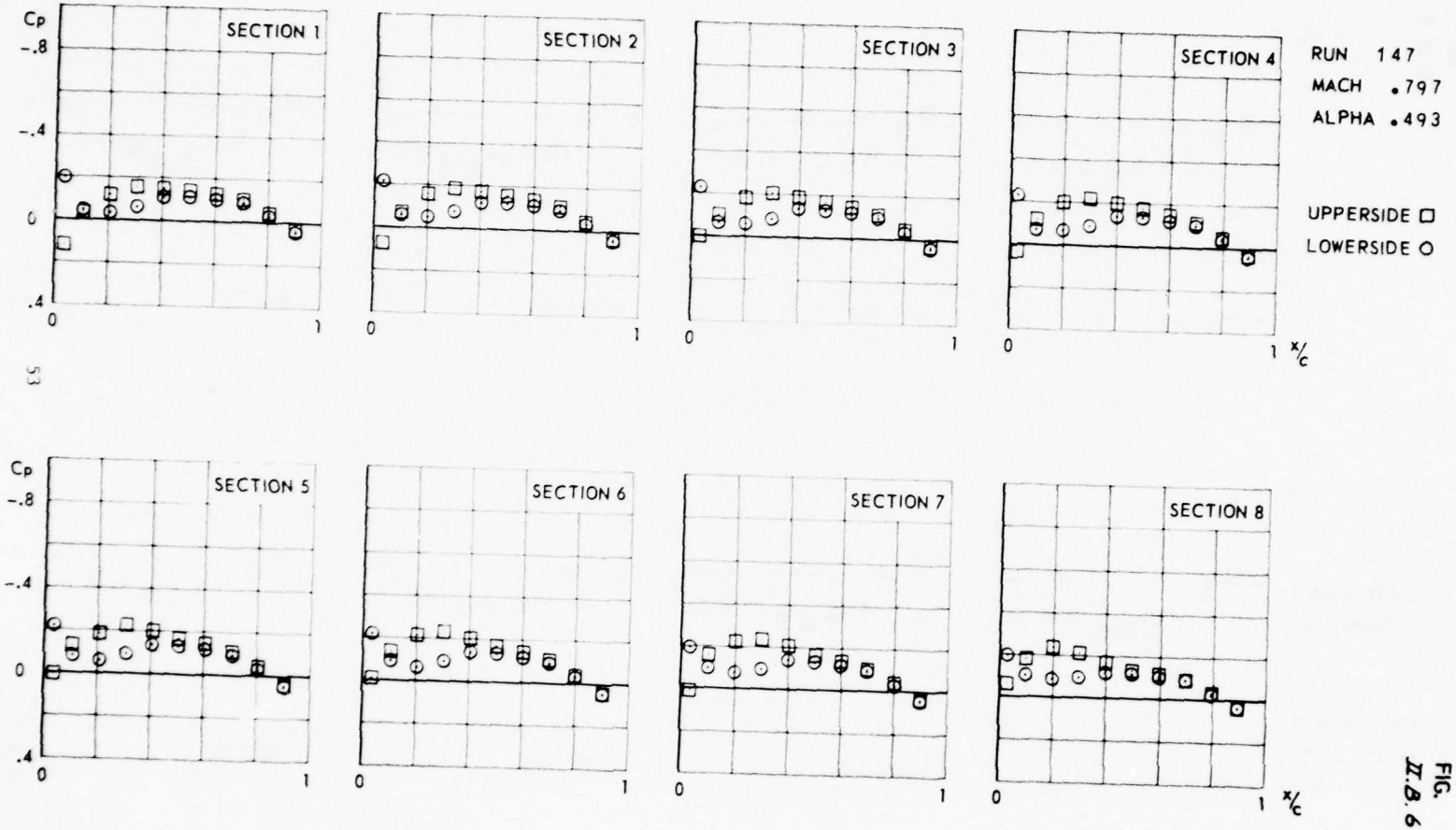

CONF.0 (CLEAN WING)

FIG. II.B.6

FIG.

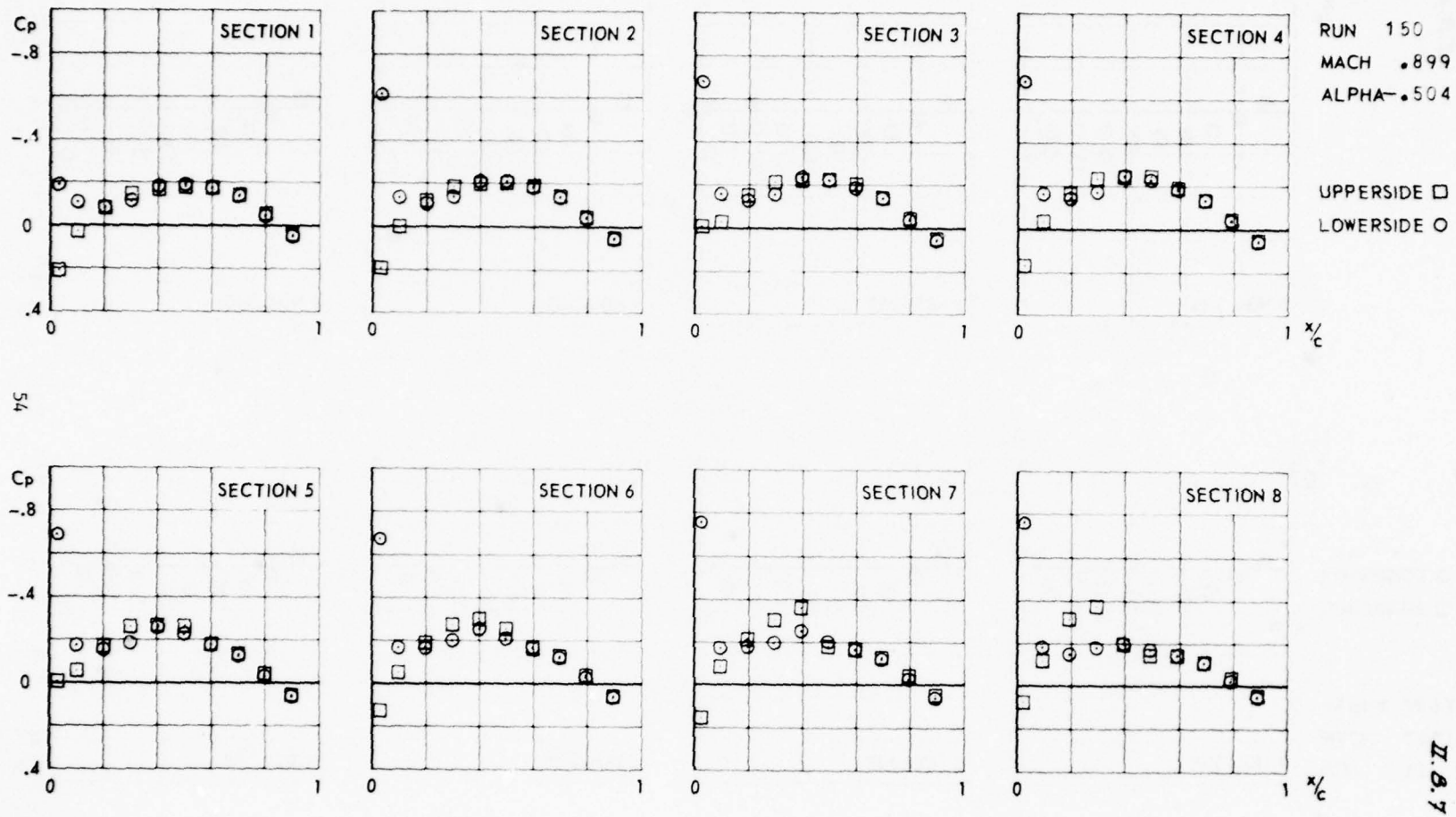

CONF.0 (CLEAN WING)

FIG. II.8.7

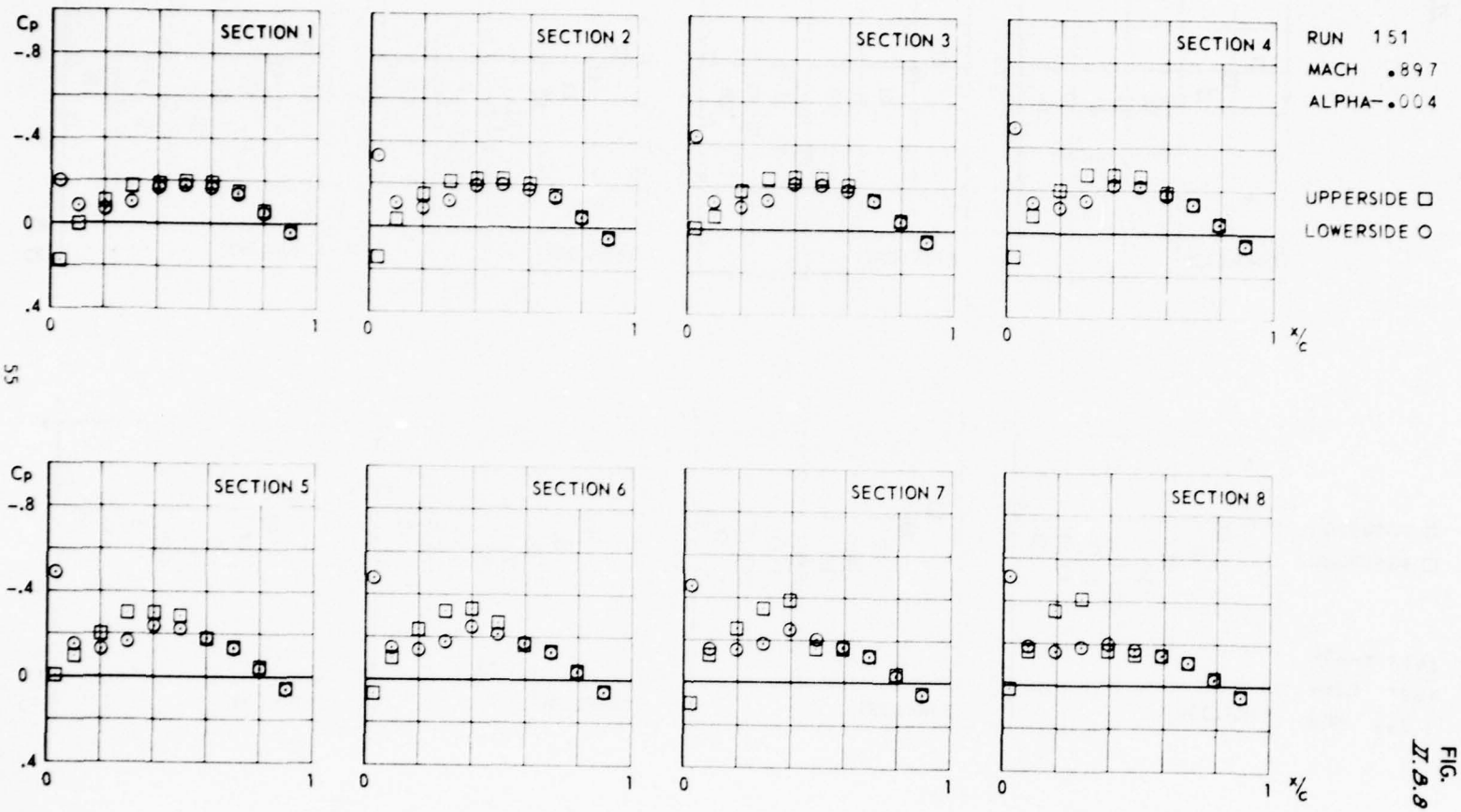

CONF.0 (CLEAN WING)

FIG. 17.8.8

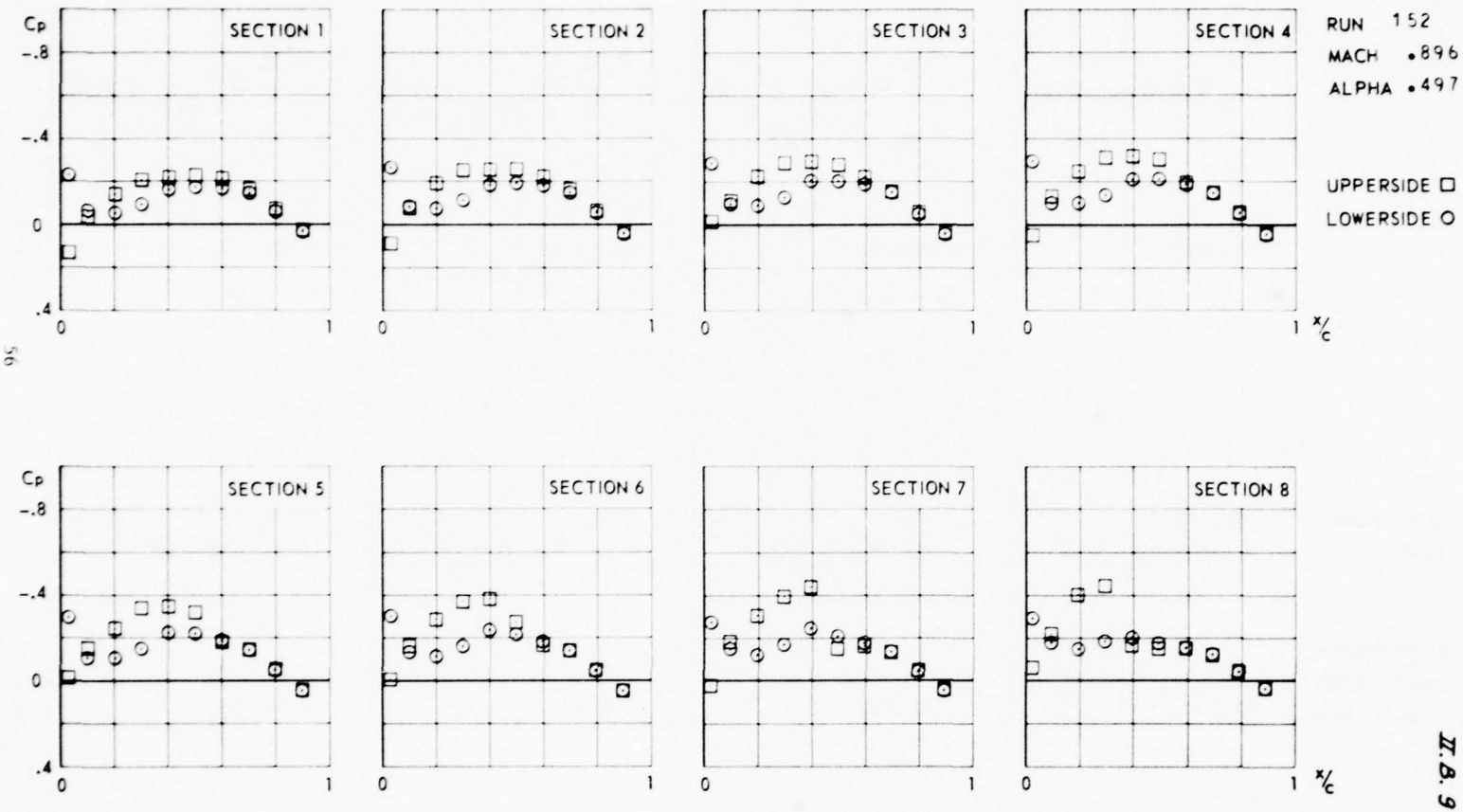

CONF.0 (CLEAN WING)

FIG. II.B.9

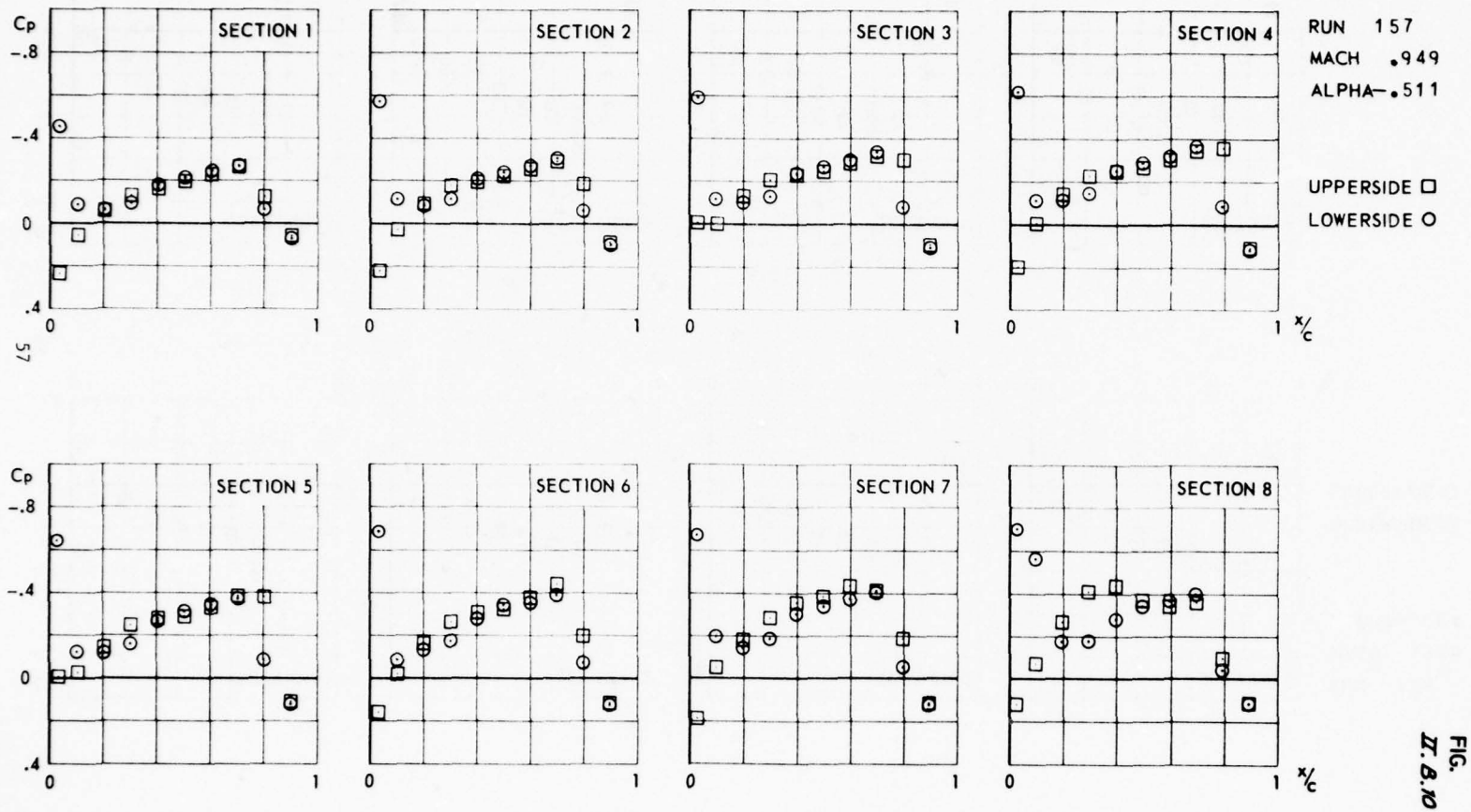

CONF.0 (CLEAN WING)

FIG. II.B.10

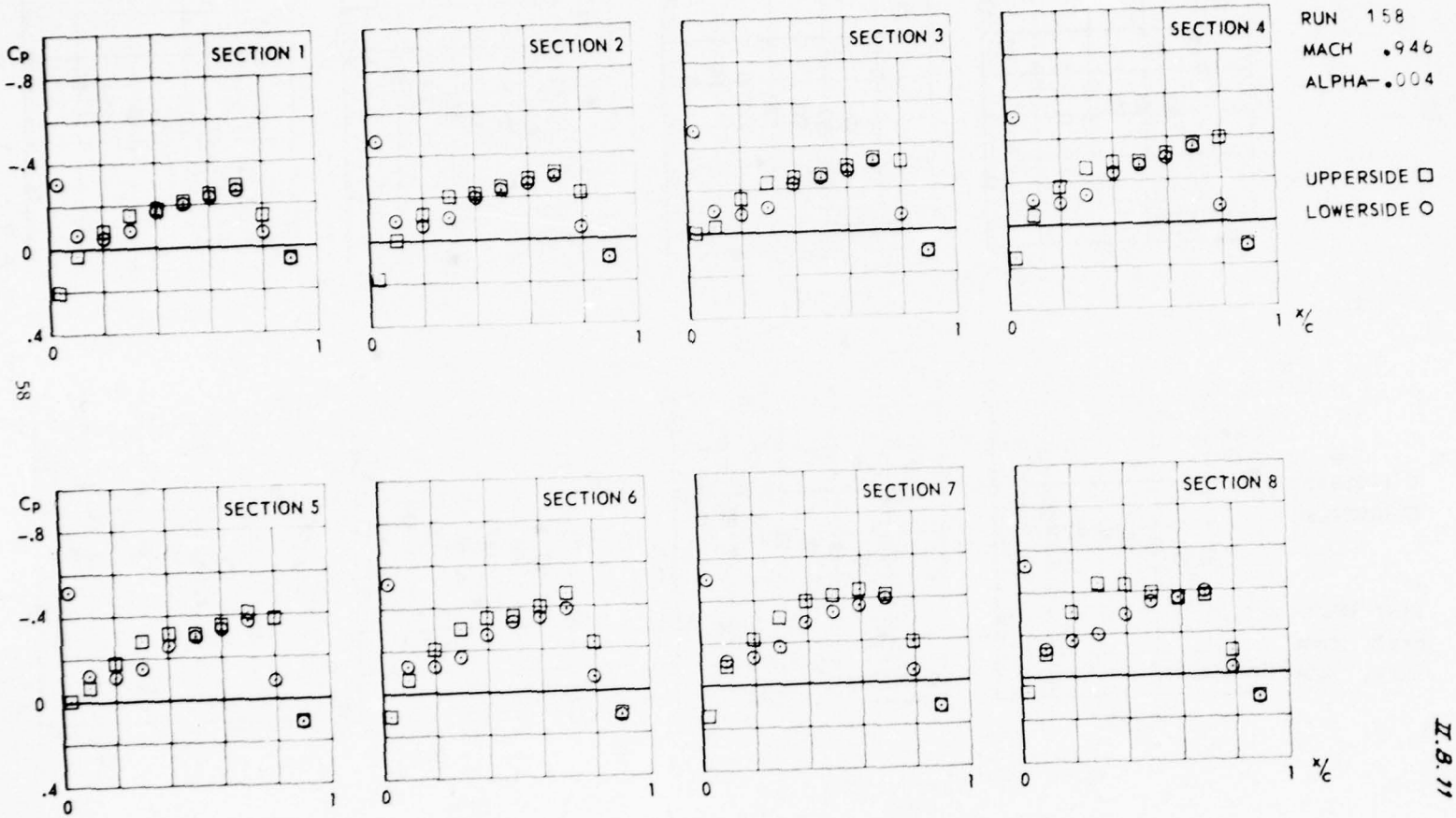

CONF.0 (CLEAN WING)

FIG. II.B.11

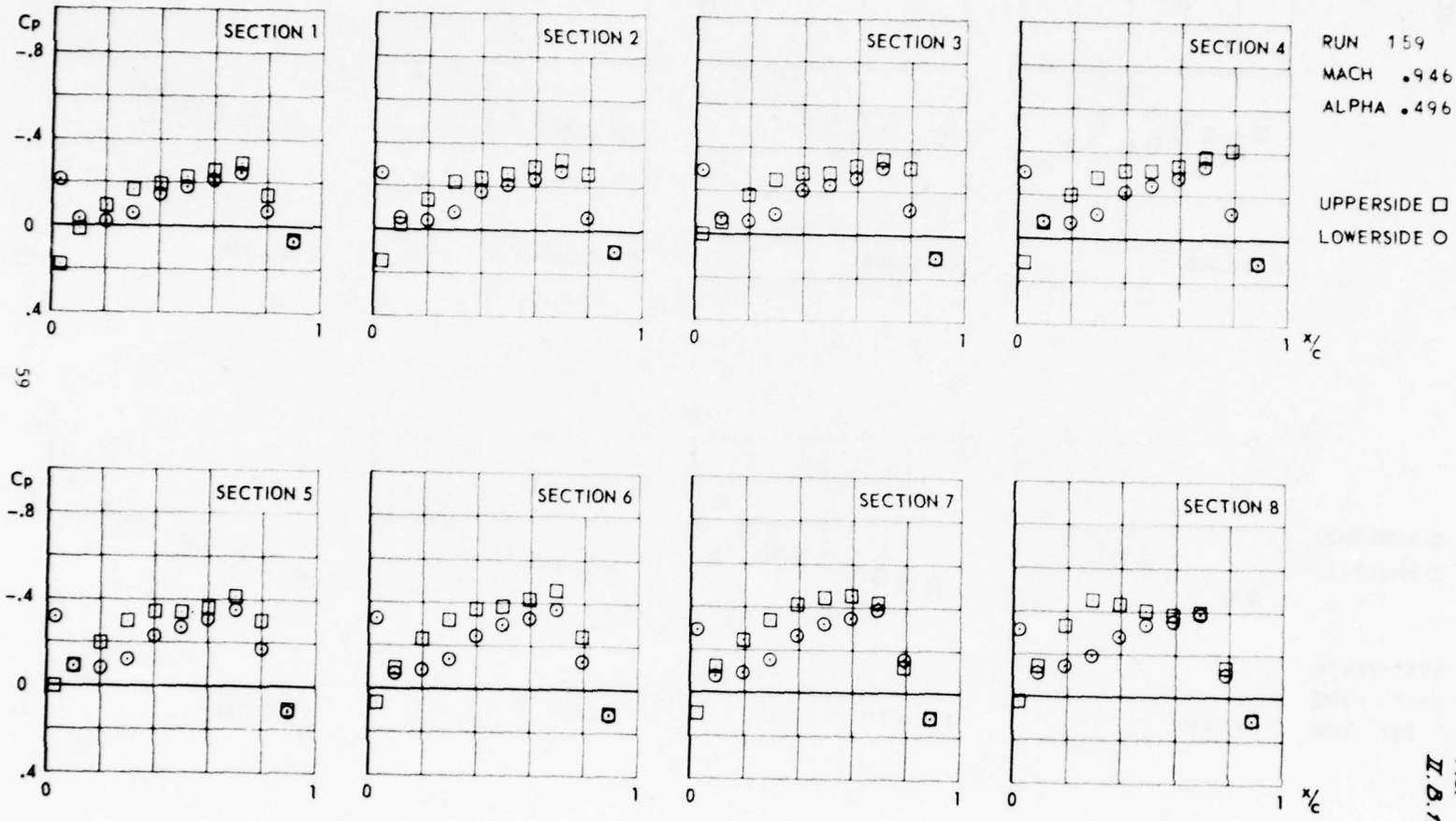

CONF.0 (CLEAN WING)

FIG. II.B.12

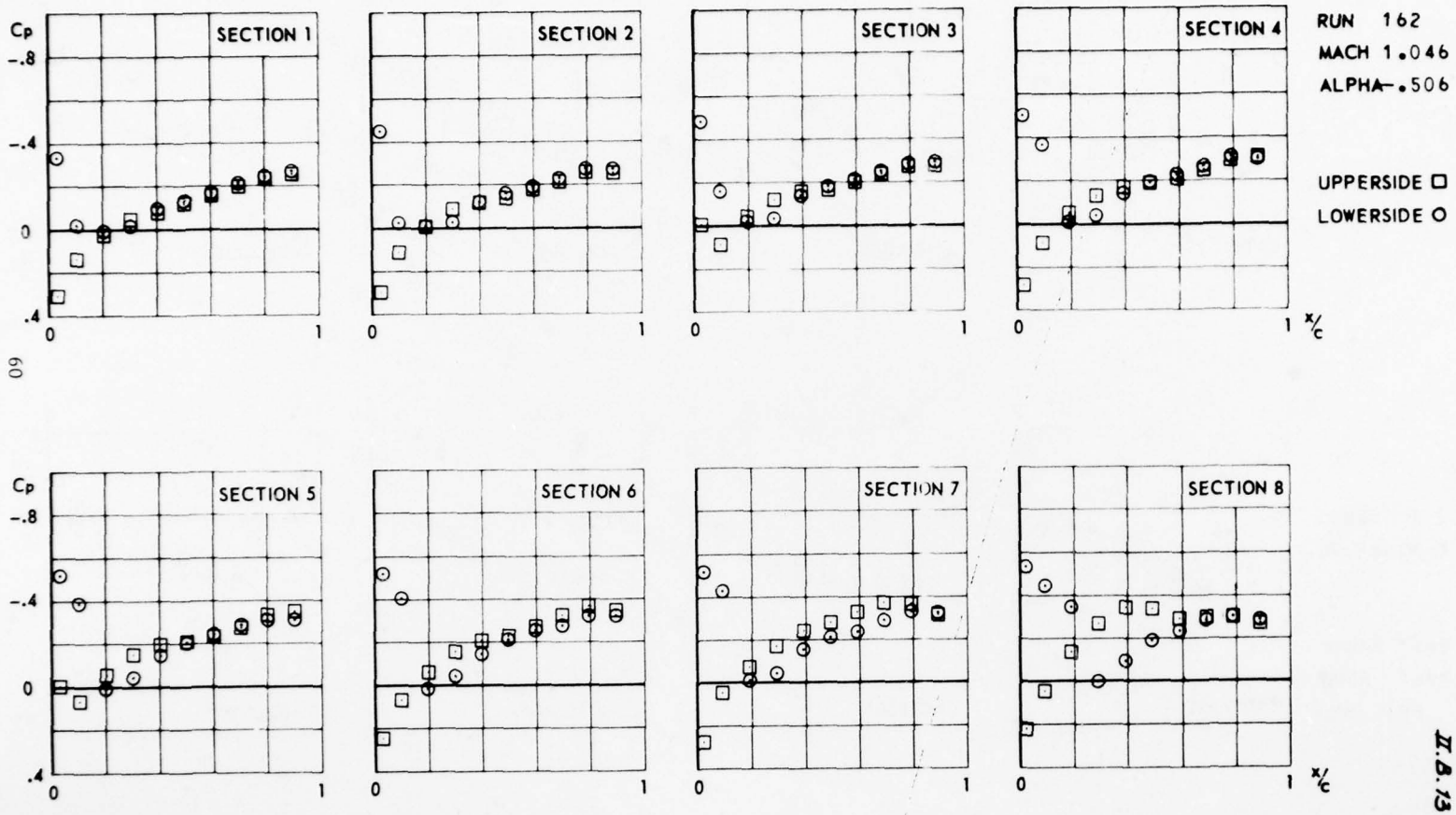

CONF.0 (CLEAN WING)

FIG. II.B.13

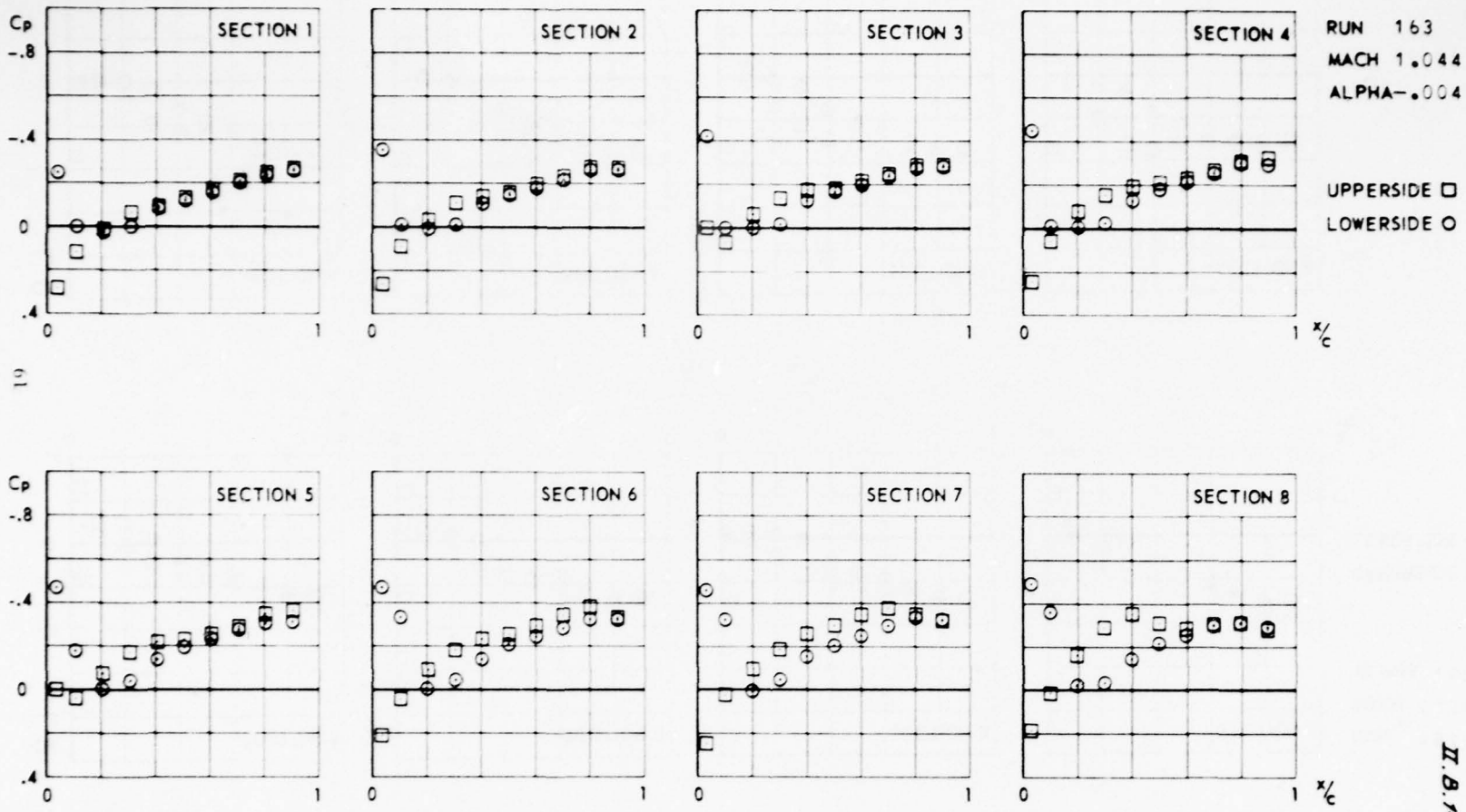

CONF.0 (CLEAN WING)

FIG. II.B.14

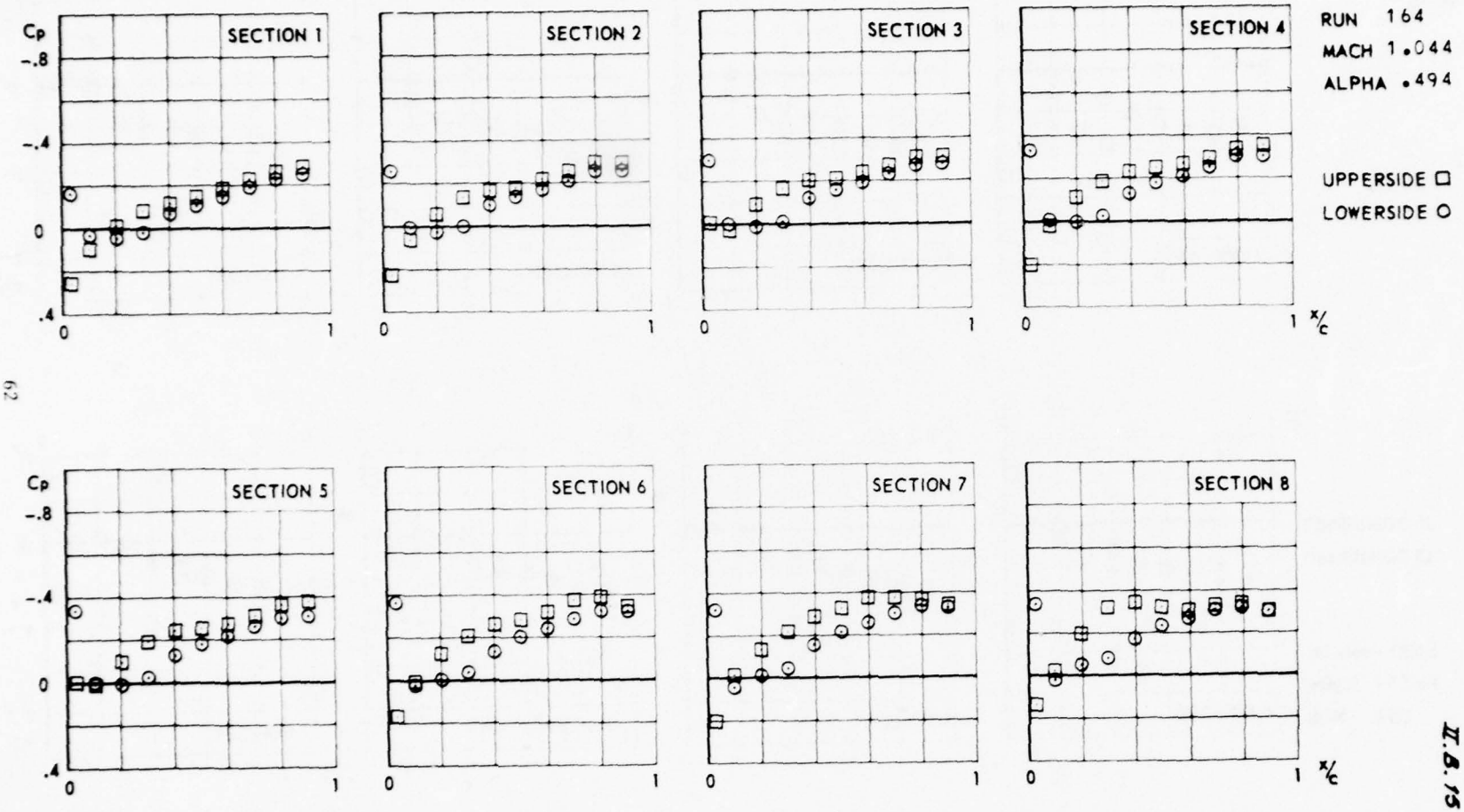

CONF.0 (CLEAN WING)

FIG. II.B.15

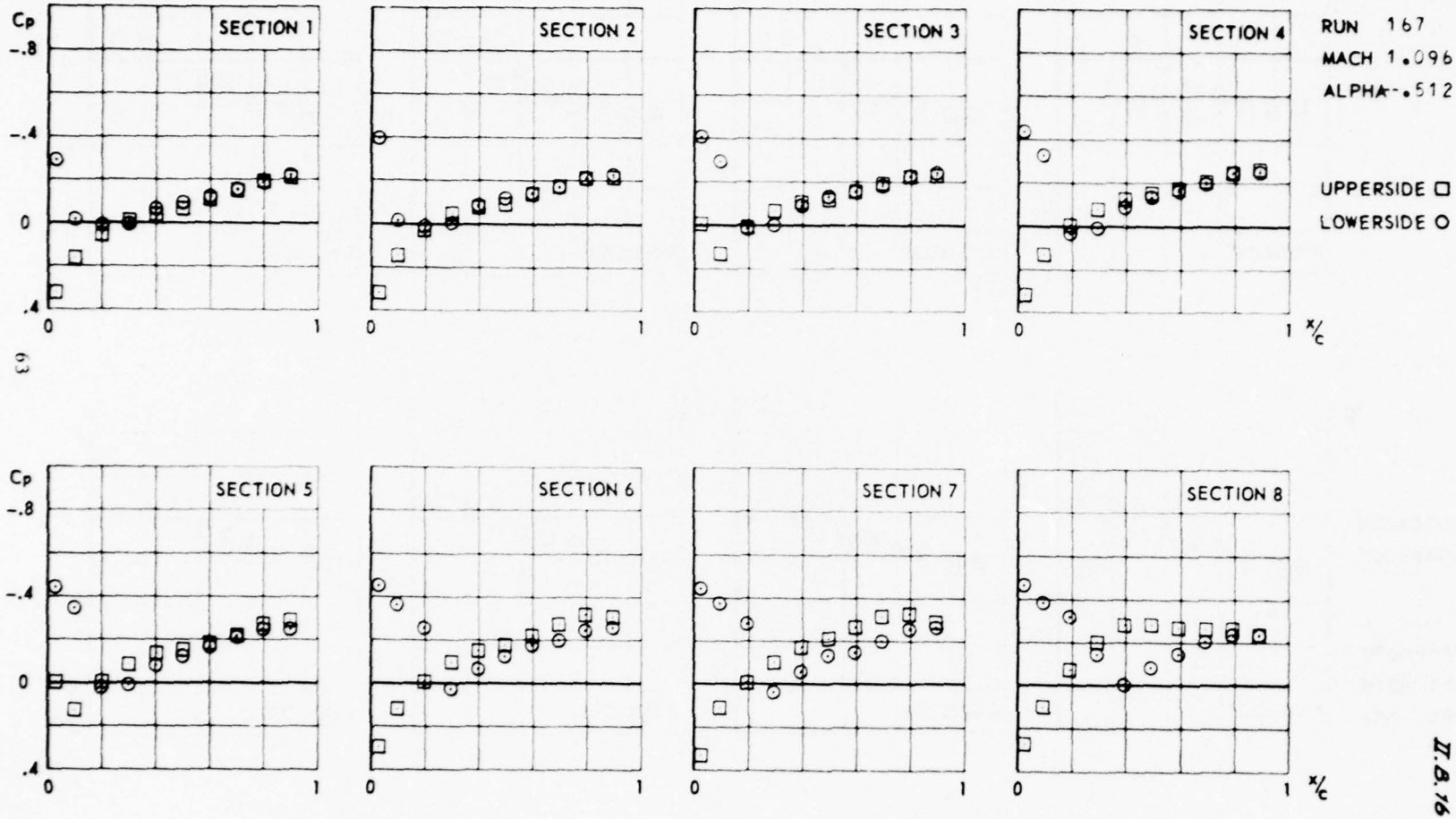

CONF.0 (CLEAN WING)

FIG. II.B.16

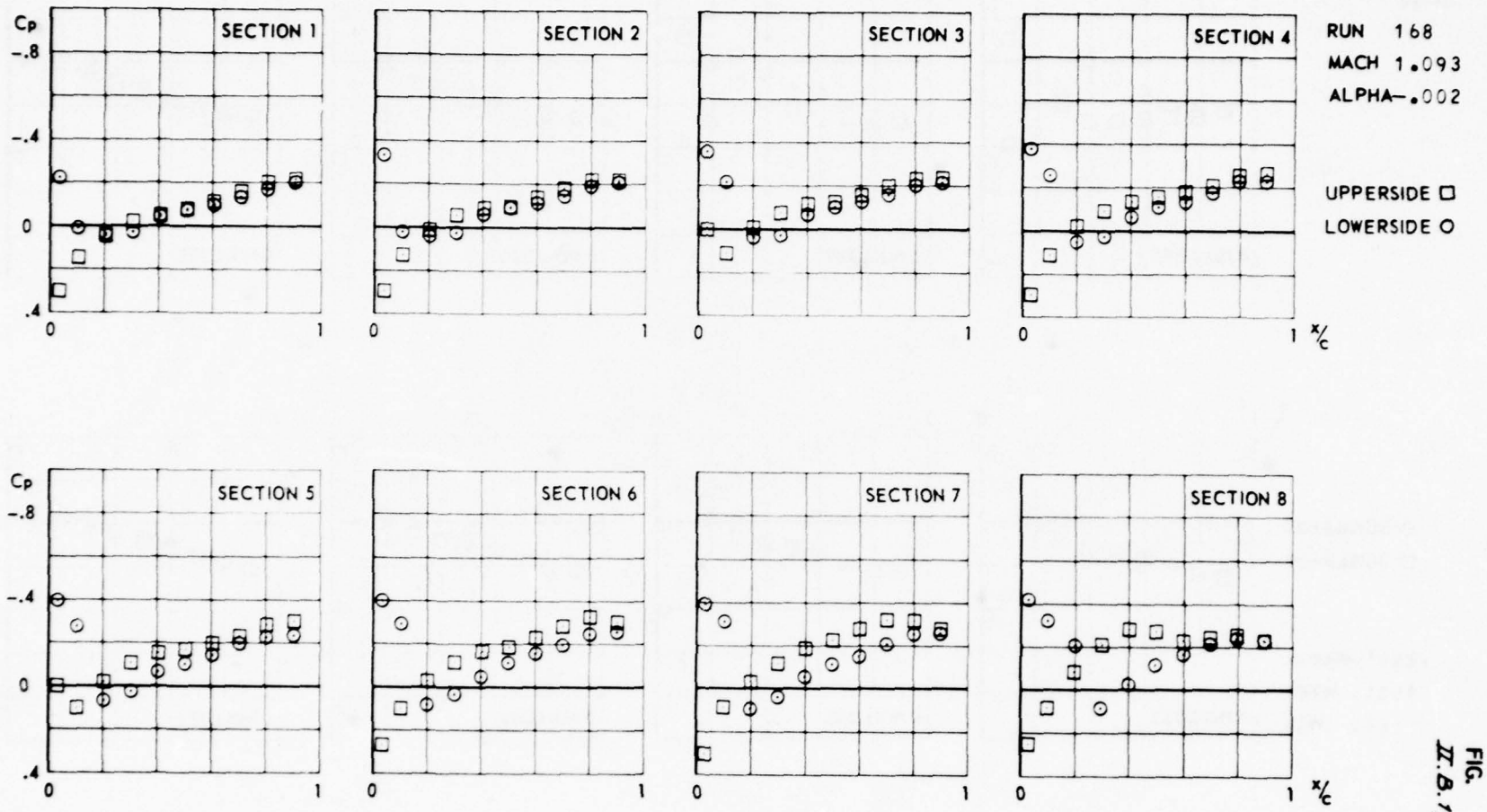

CONF.0 (CLEAN WING)

FIG. II.B.17

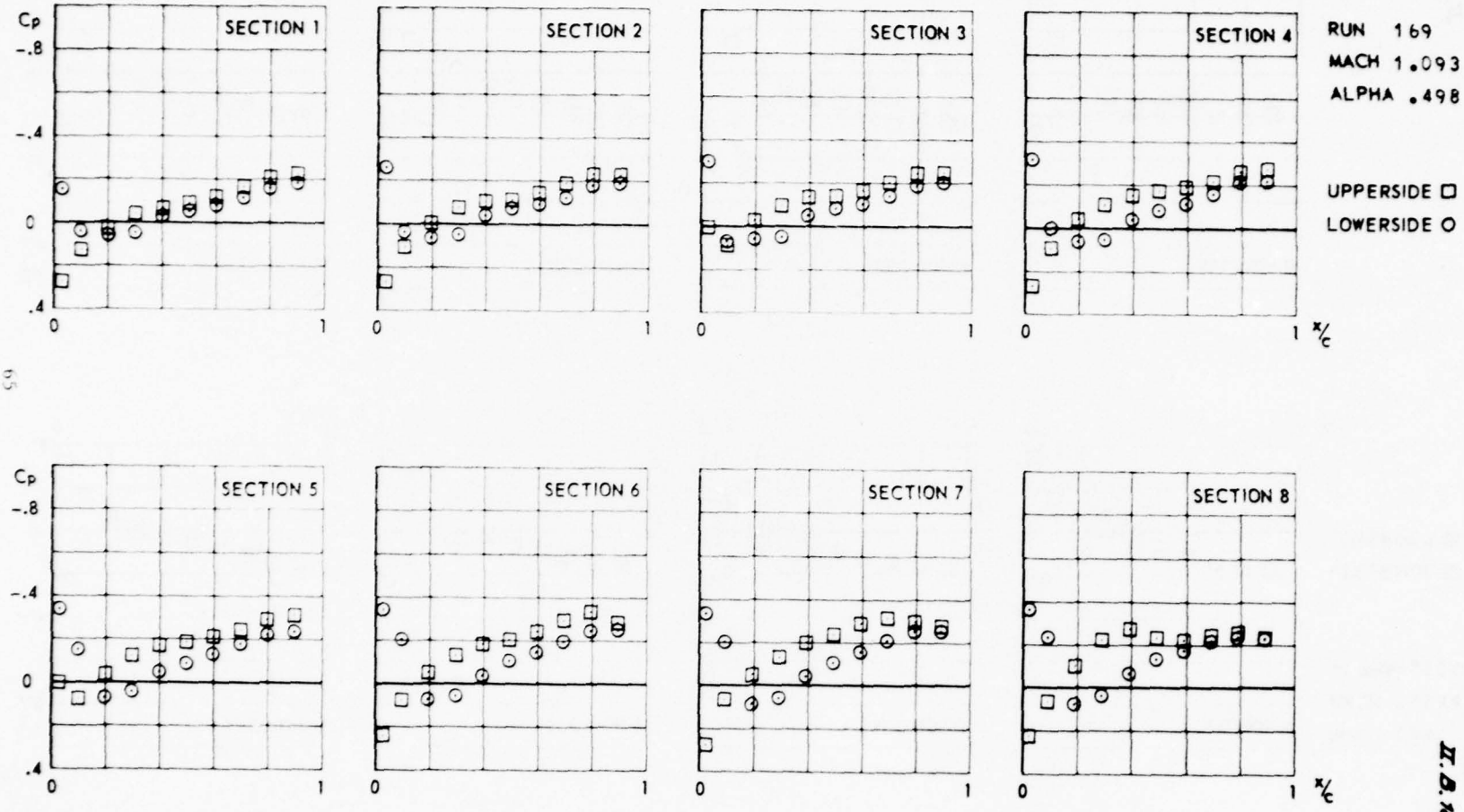

CONF.0 (CLEAN WING)

FIG. II.B.18

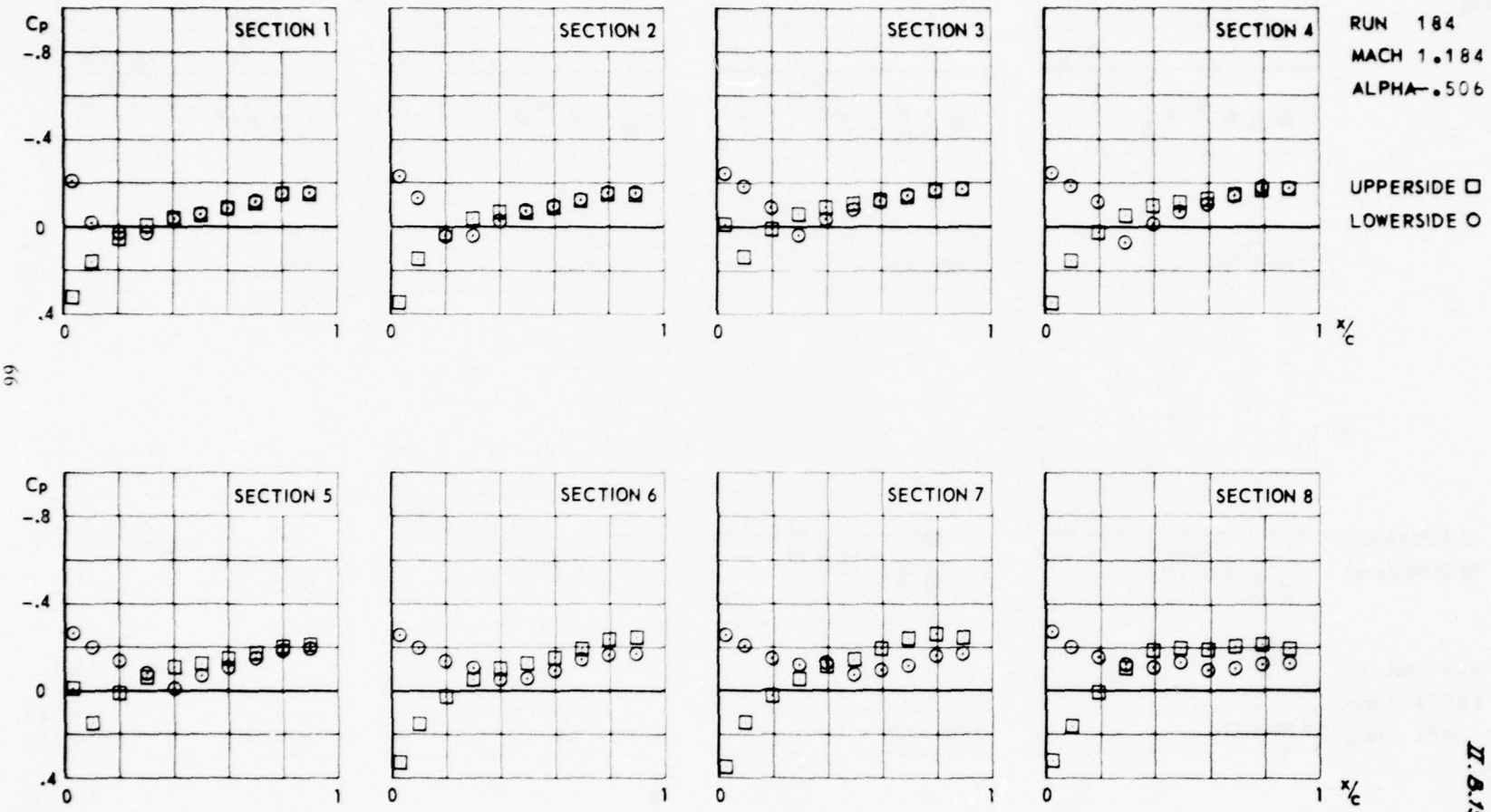

CONF.0 (CLEAN WING)

FIG. II.B.19

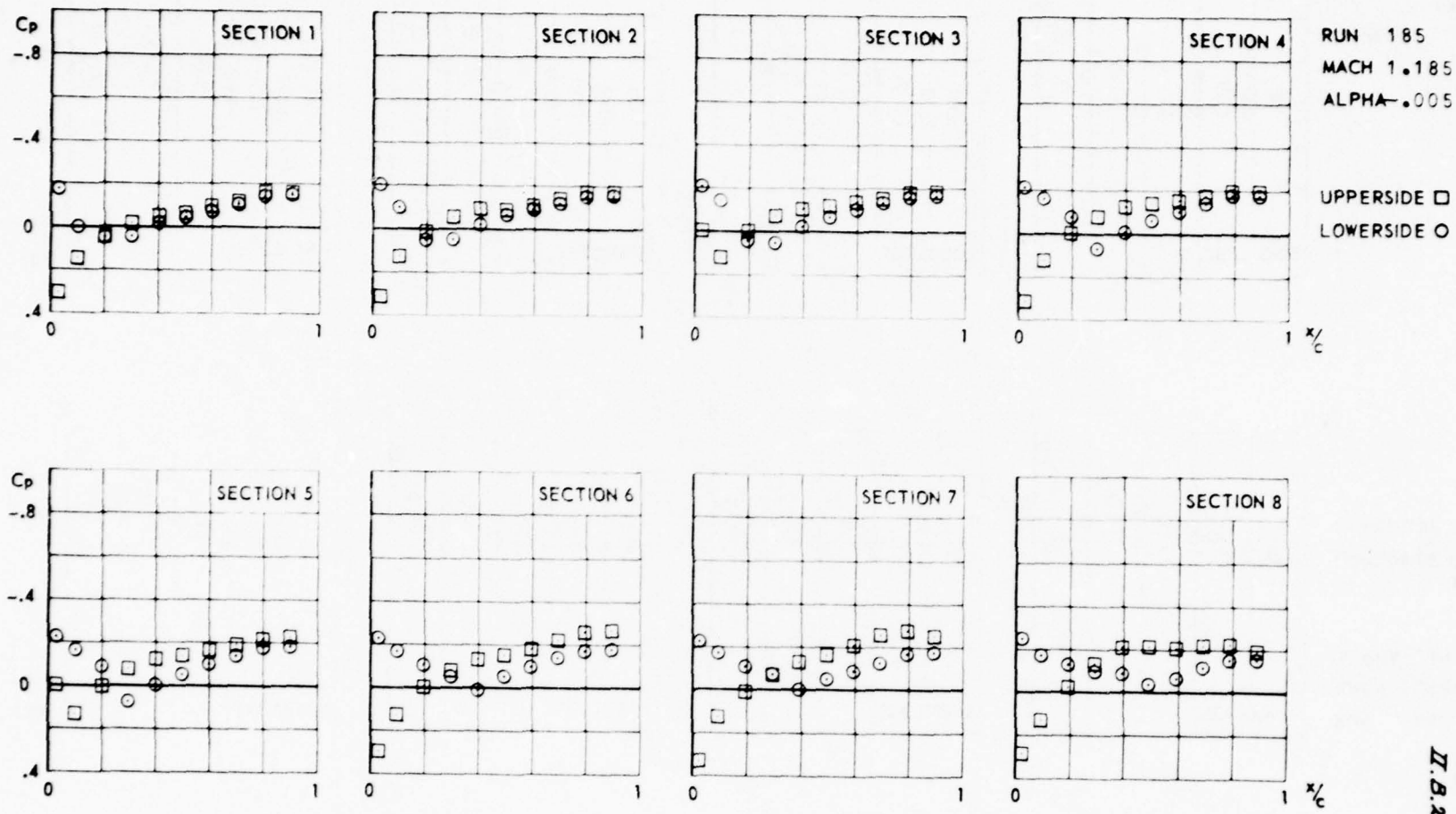

CONF.0 (CLEAN WING)

FIG. II.B.20

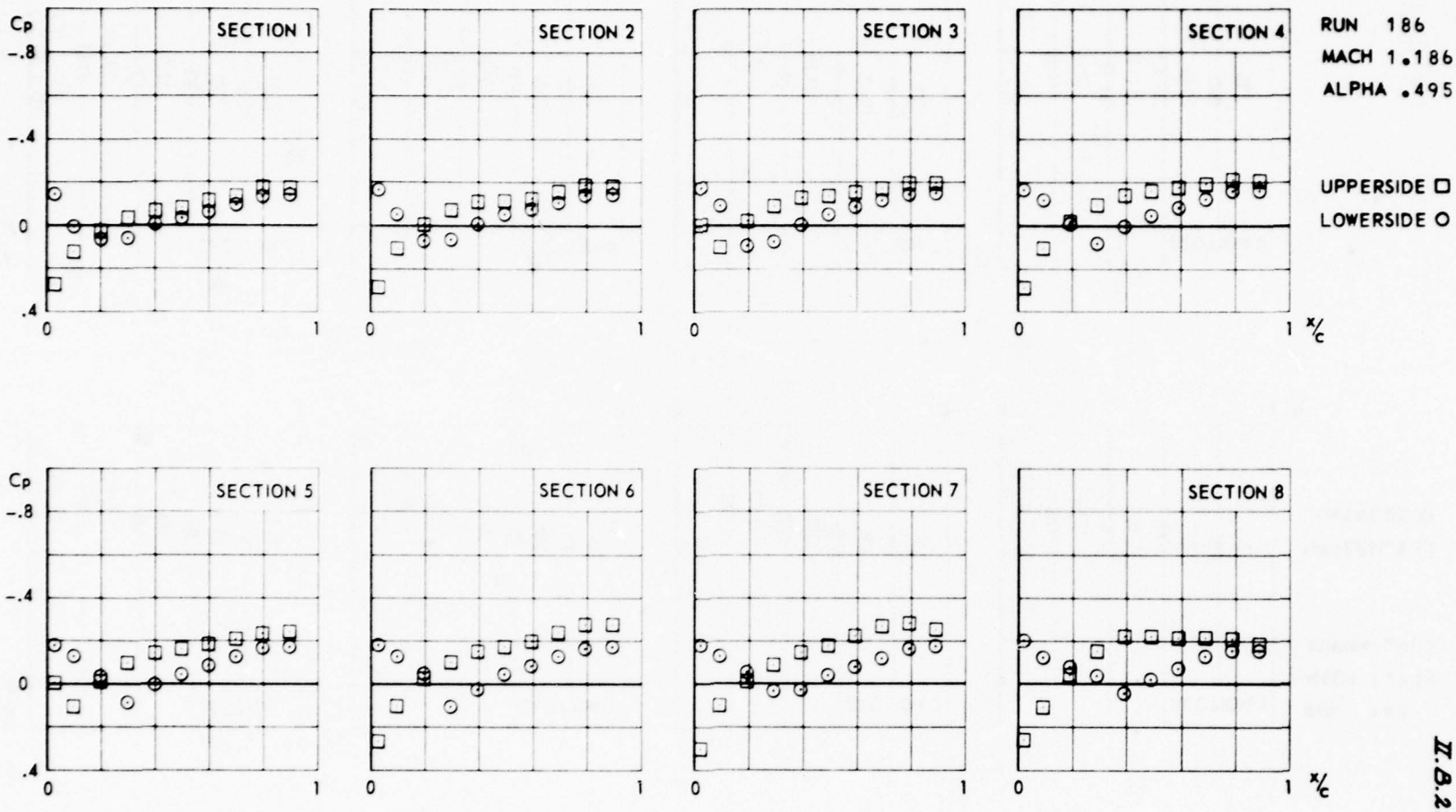

CONF.0 (CLEAN WING)

FIG. IV.B.21

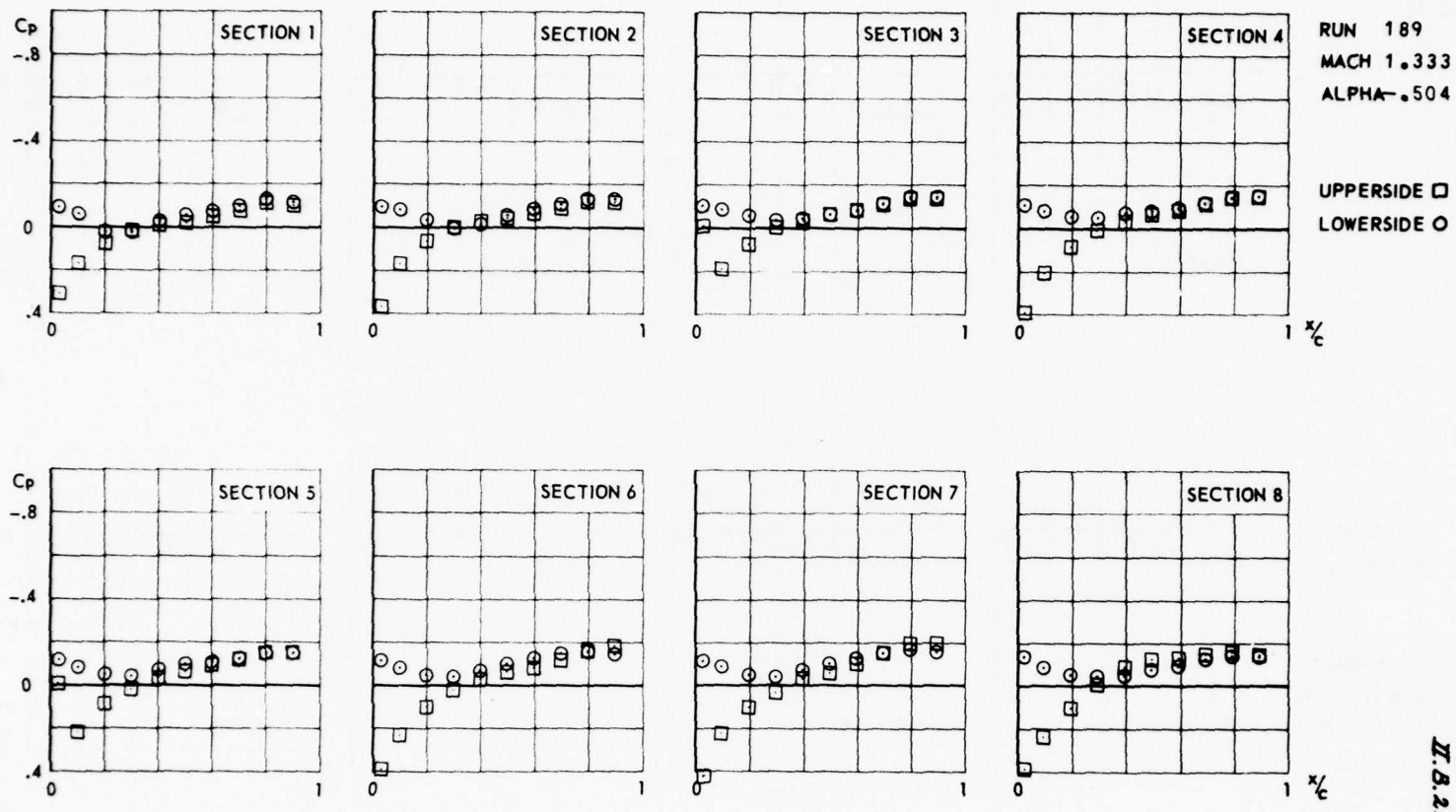

CONF.0 (CLEAN WING)

FIG. II.B.22

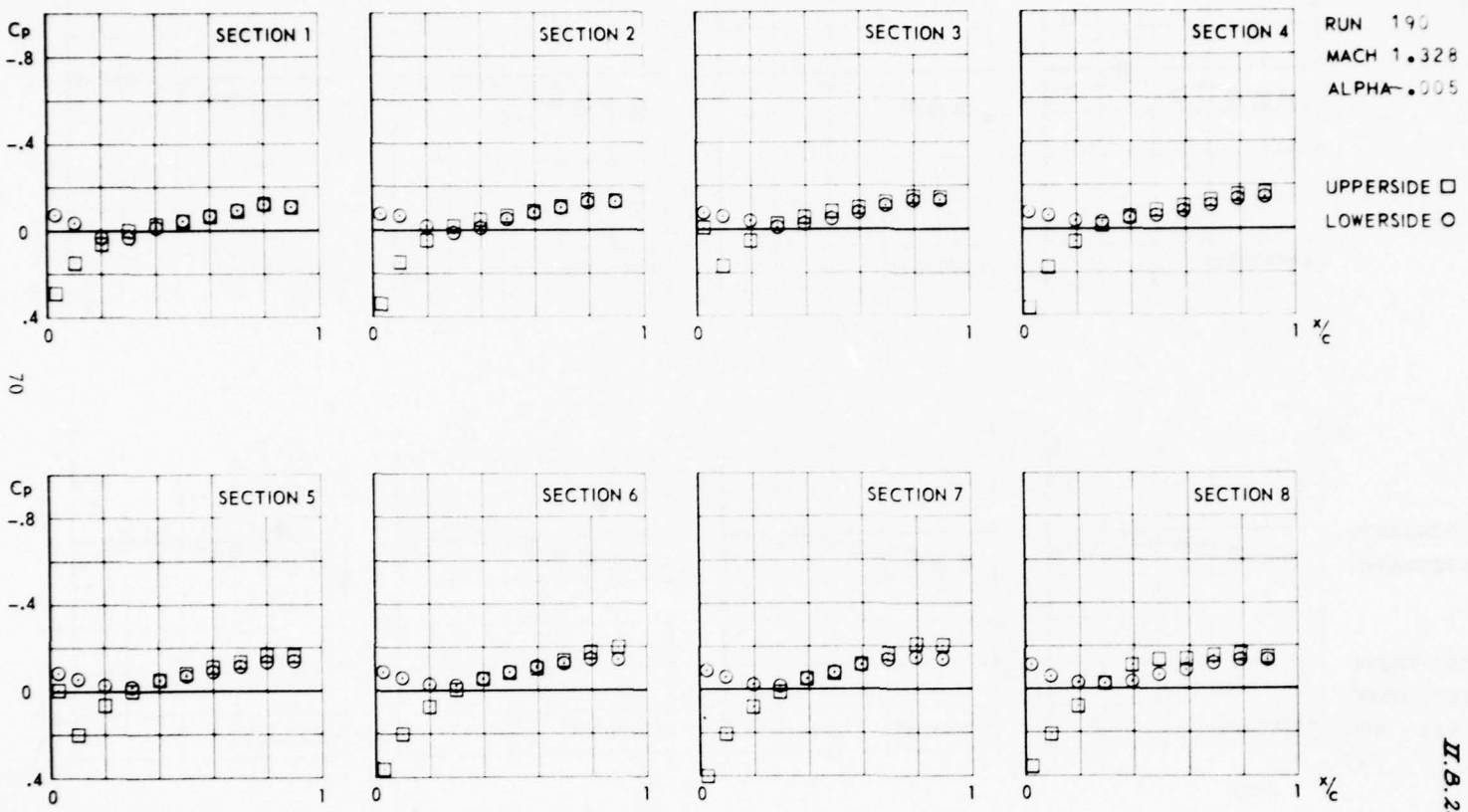

CONF.0 (CLEAN WING)

FIG. II.B.23

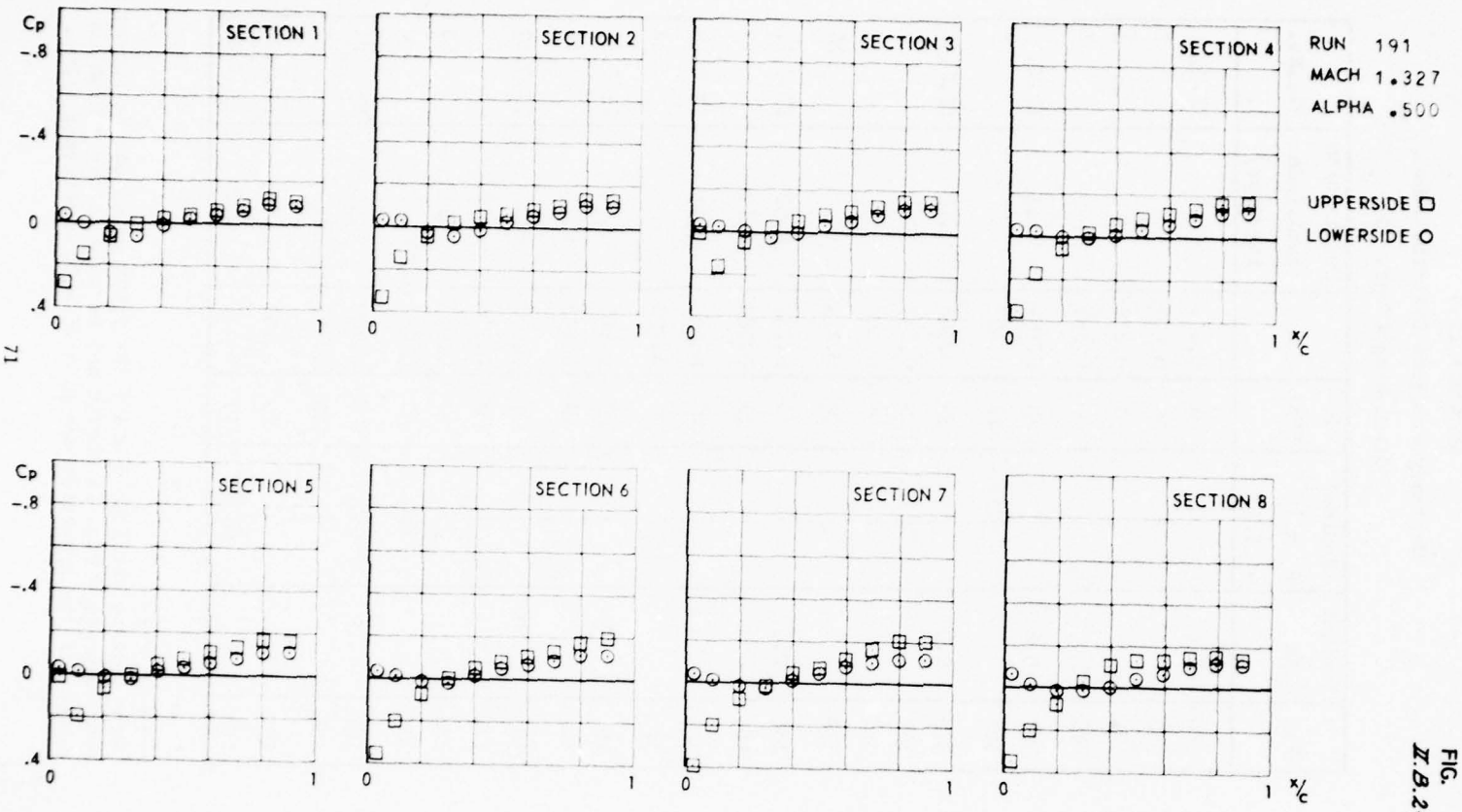

CONF. 0 (CLEAN WING)

FIG. II.B.24

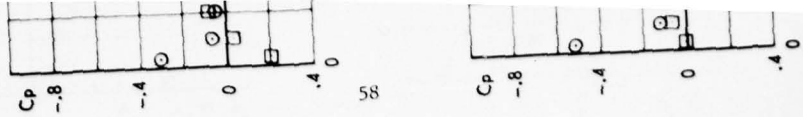

APPENDIX II.C

Unsteady Pressure Distributions

Clean Wing (Conf. 0)

Run	Nominal Ma	Nominal $P_o \times 10^{-5}$ (Pa)	F (Hz)	K	Oscillation amplitude (degrees)	Fig.No.
380	0.6	1.0	10	0.100	0.11	II.C. 1
382			20	0.199		2
381			30	0.299		3
383			40	0.399		4
367	0.8		20	0.153	0.11	II.C. 5
368			40	0.307		6
378	0.9		10	0.068	0.11	II.C. 7
369			20	0.137		8
379			30	0.206		9
370			40	0.275		10
160	0.95		20	0.132	0.52	II.C.11
161			40	0.264	0.22	12
375	1.0		20	0.125	0.11	II.C.13
376			40	0.250		14
165	1.05		20	0.122	0.52	II.C.15
166			40	0.243	0.22	16
373	1.10		10	0.058	0.11	II.C.17
172			20	0.116	0.28	18
374			30	0.173	0.11	19
372		1.0	40	0.231	0.11	20
187	1.20	0.7	20	0.109	0.52	II.C.21
188			40	0.218	0.22	22
192	1.35		20	0.100	0.52	II.C.23
193		0.7	40	0.198	0.22	24

(Note that in sections 3 and 5 the first point on the upperside, showing a zero value, is wrong. It should not be used in any evaluation. Further the values for the upperside are plotted with a reversed sign).

FIG.
II.C.1.a

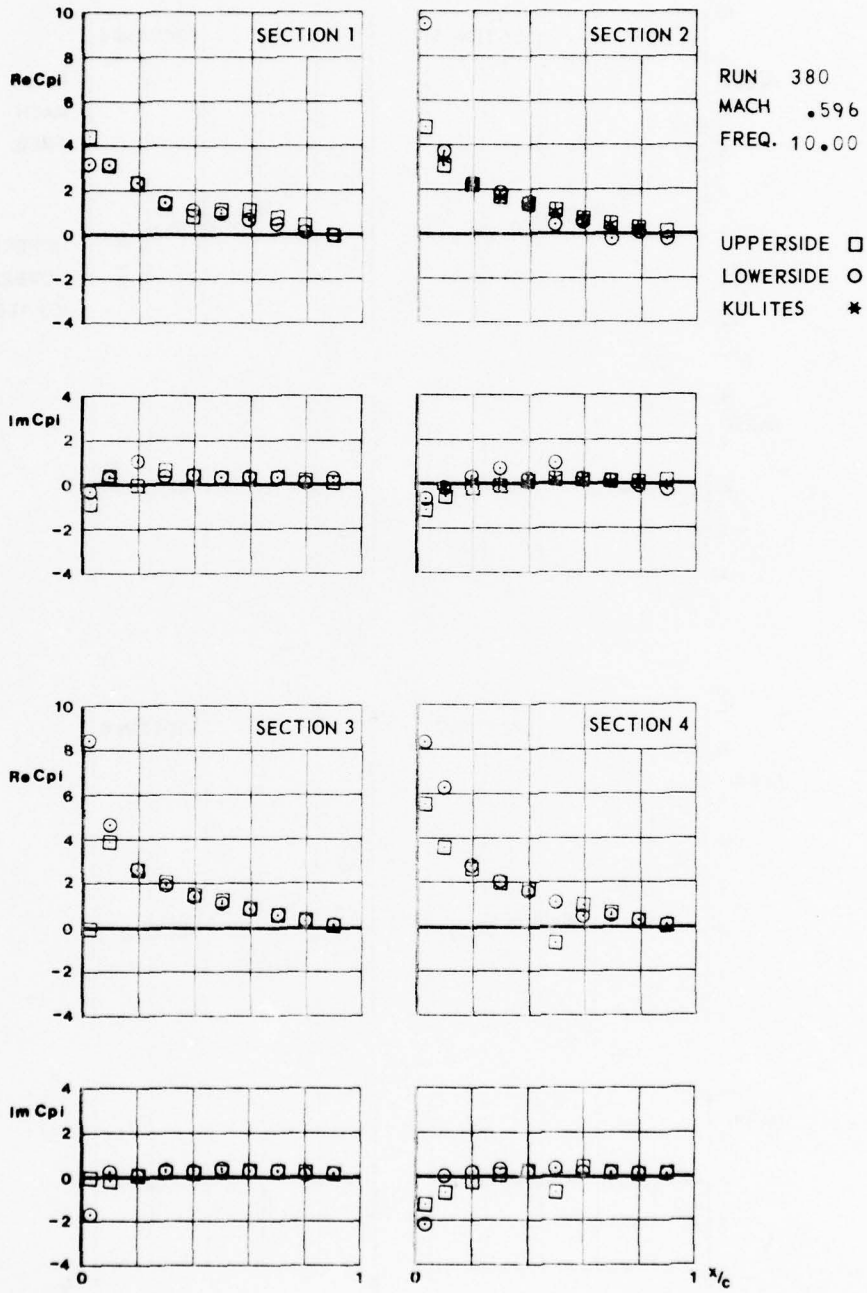

CONF. 0 (CLEAN WING)

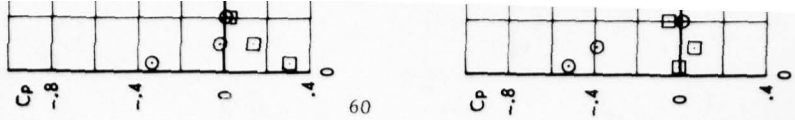

FIG.
II.C.1b

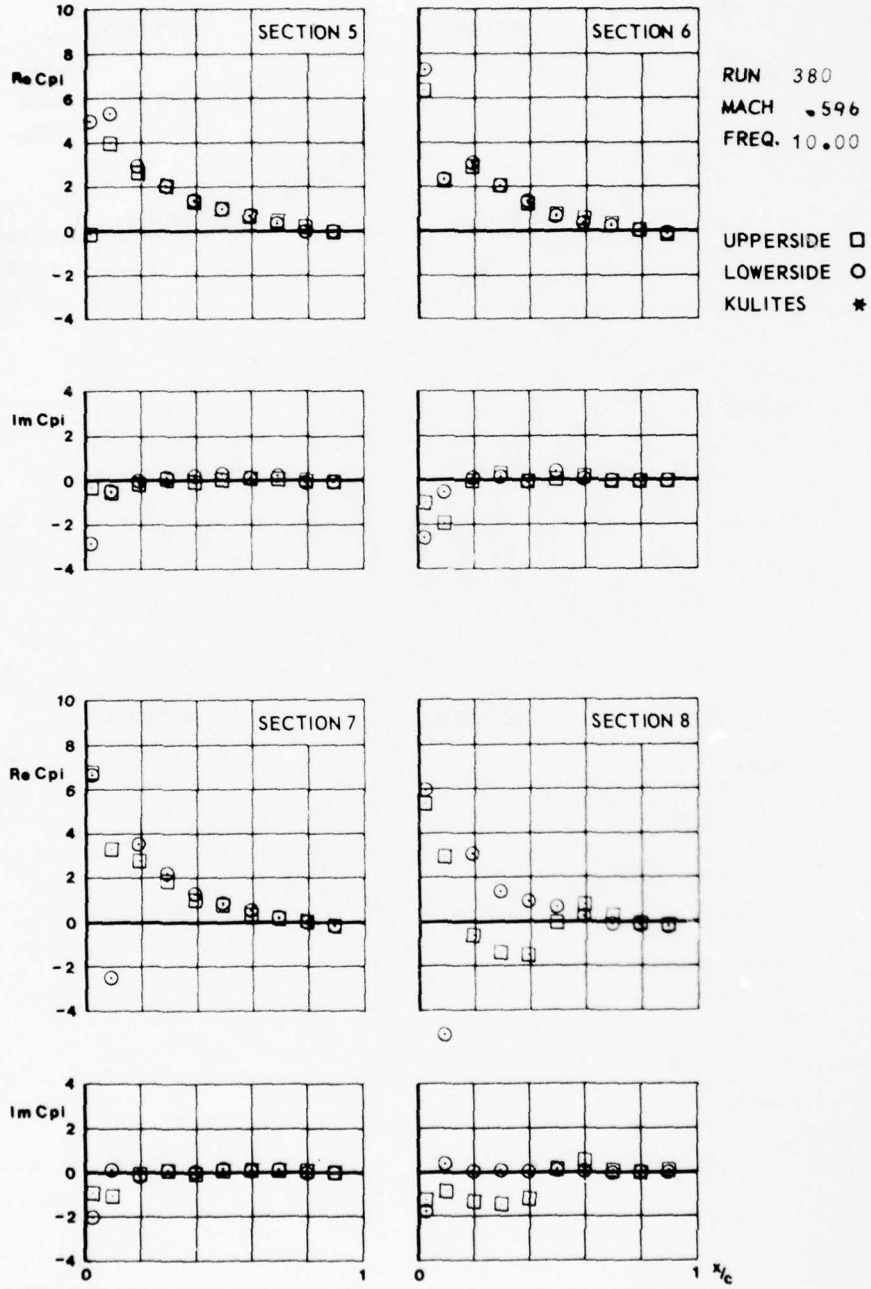

CONF. 0 (CLEAN WING)

FIG.
II.C.2.a

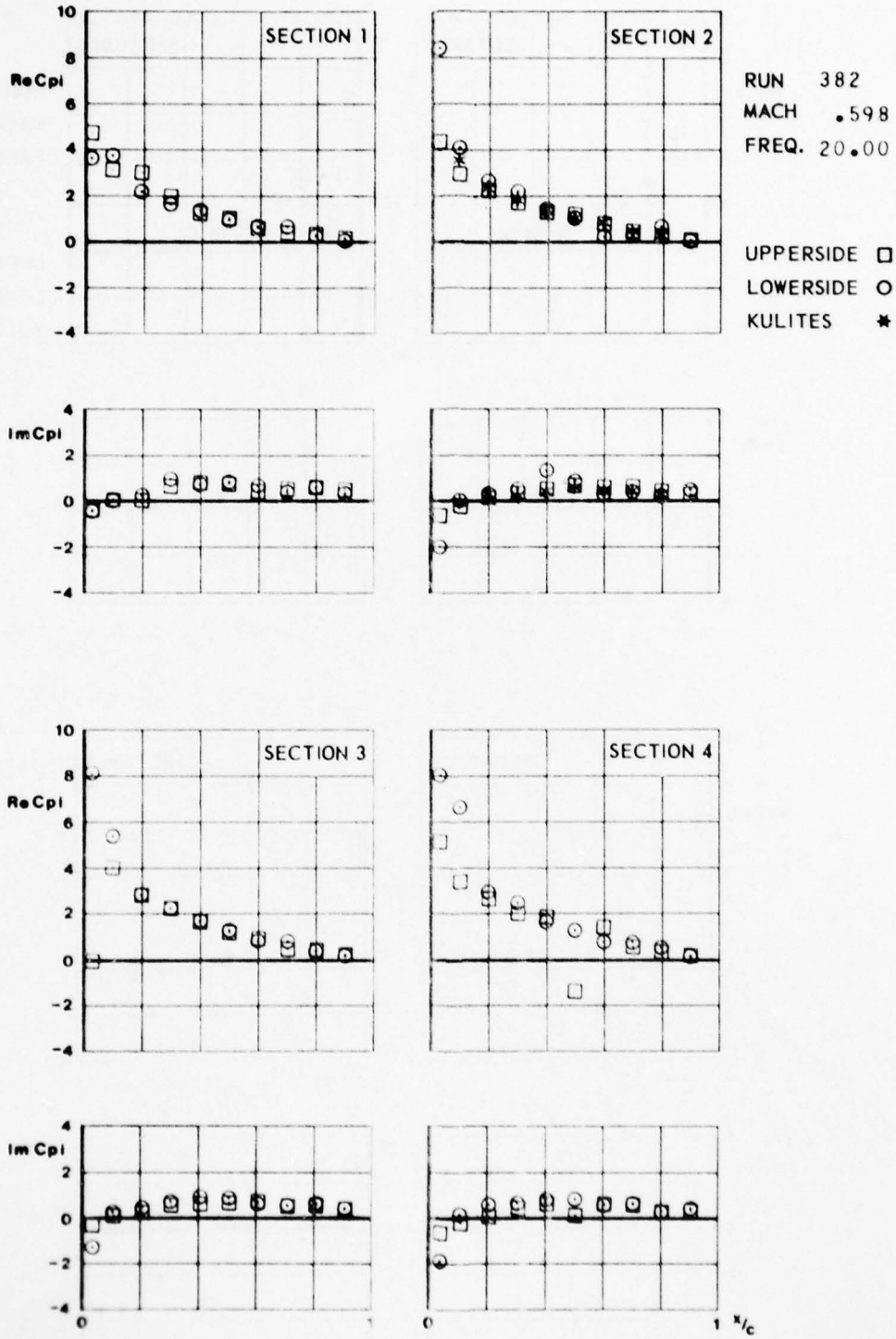

CONF. 3 (CLEAN WING)

FIG.
II.C.2.6

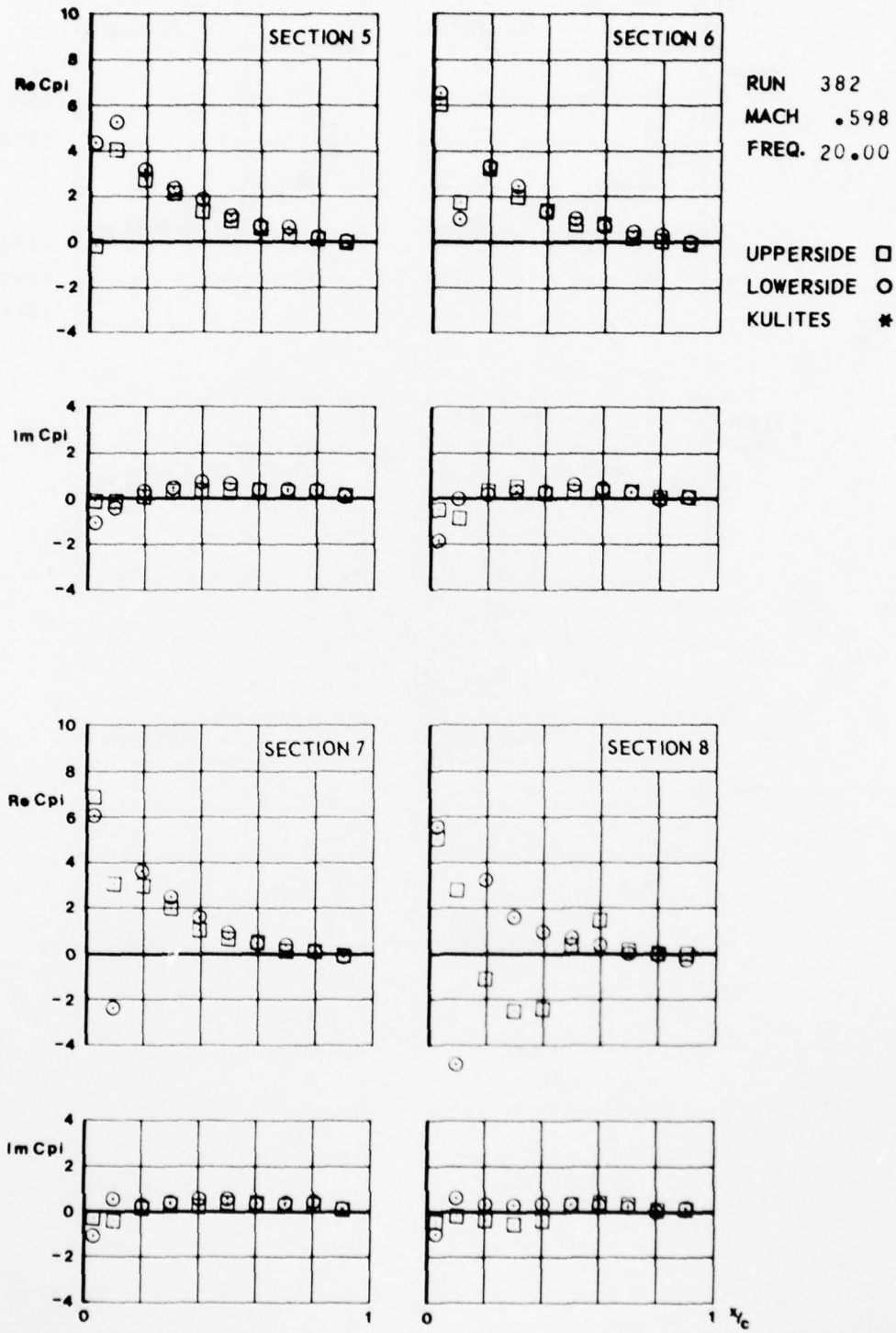

CONF. 0 (CLEAN WING)

FIG.
II.C.3.a

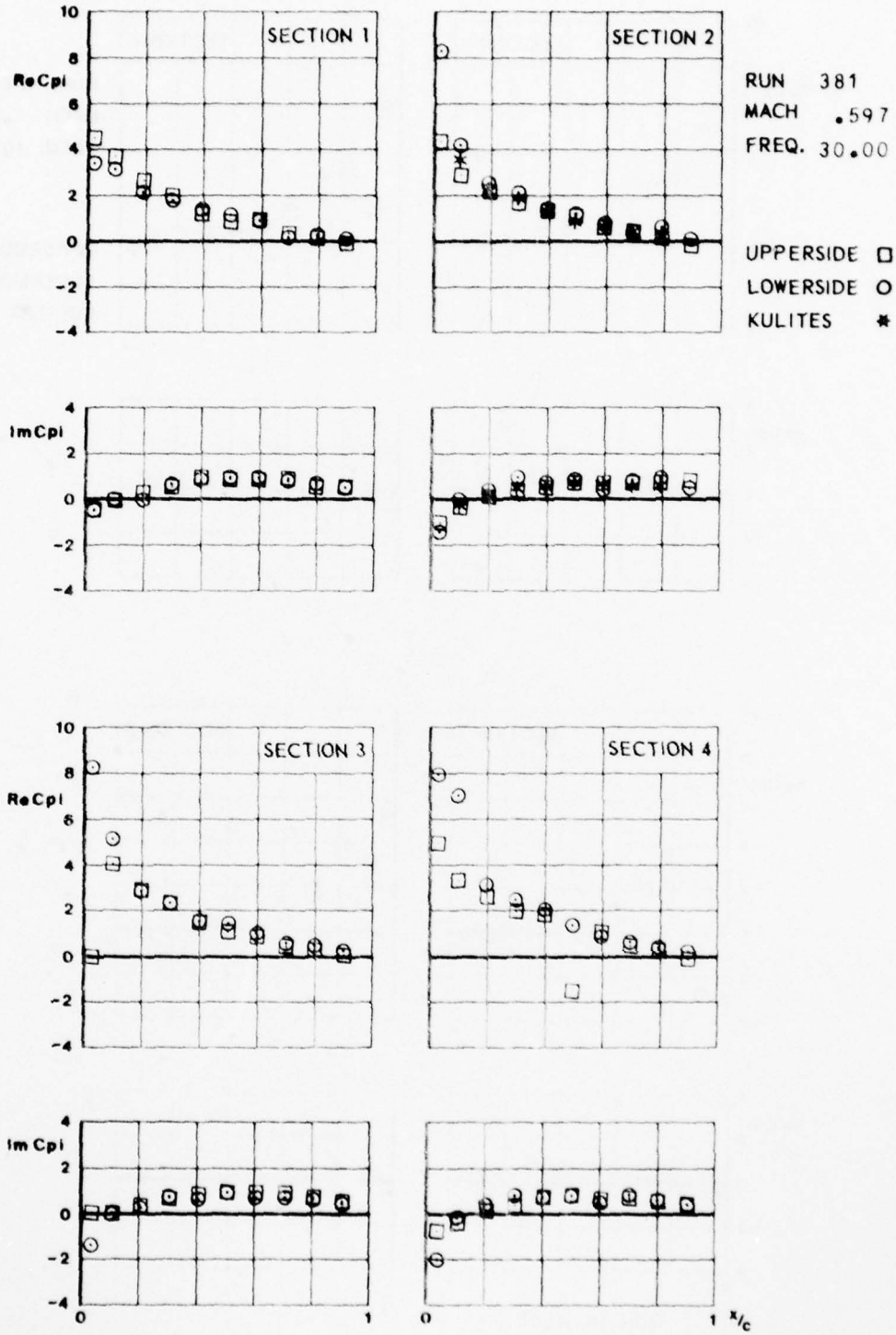

CONF. 0 (CLEAN WING)

FIG.
II.C.3.b

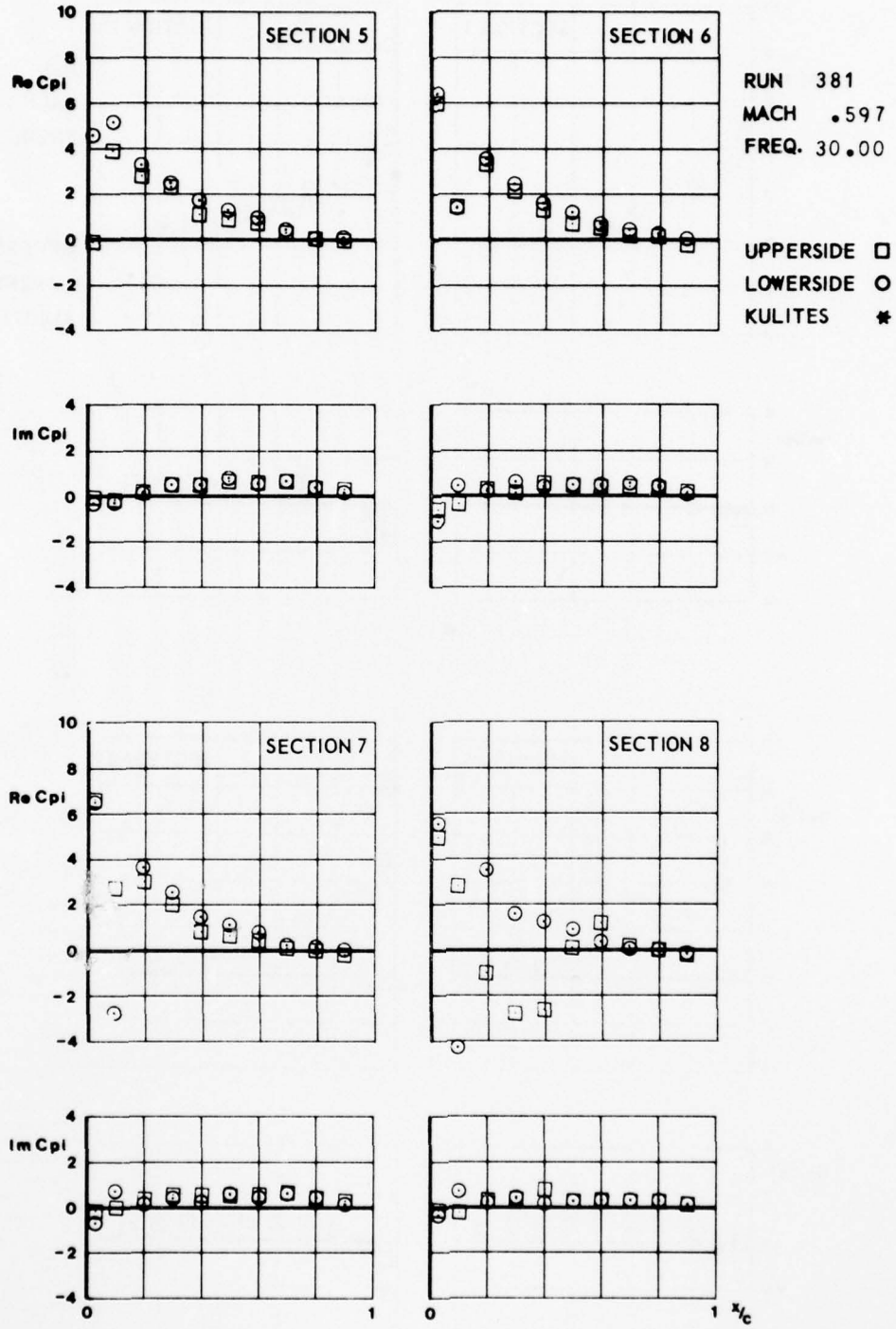

CONF. C (CLEAN WING)

FIG.
II.C.4.a

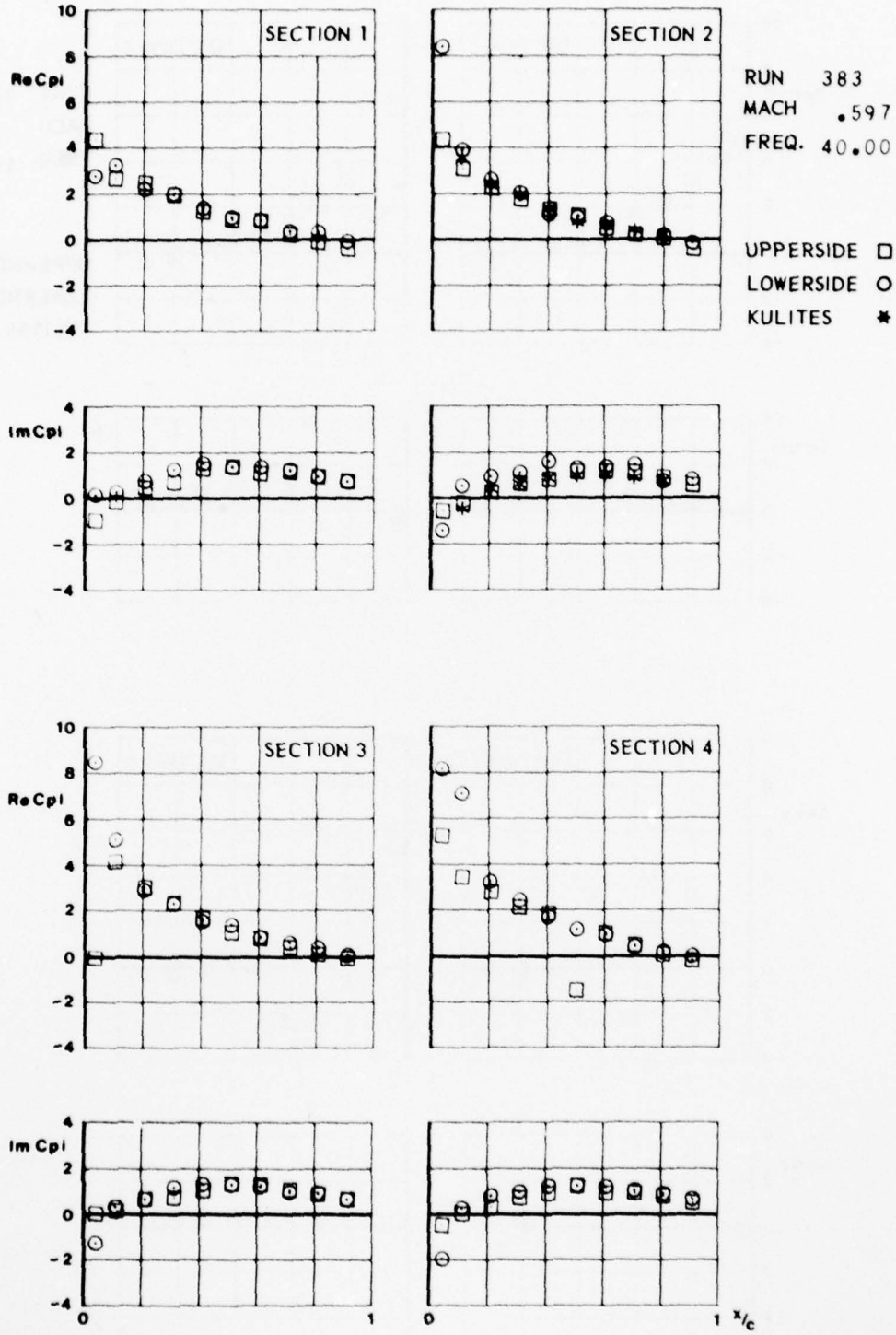

CONF. 0 (CLEAN WING)

FIG.
II.C.4.b

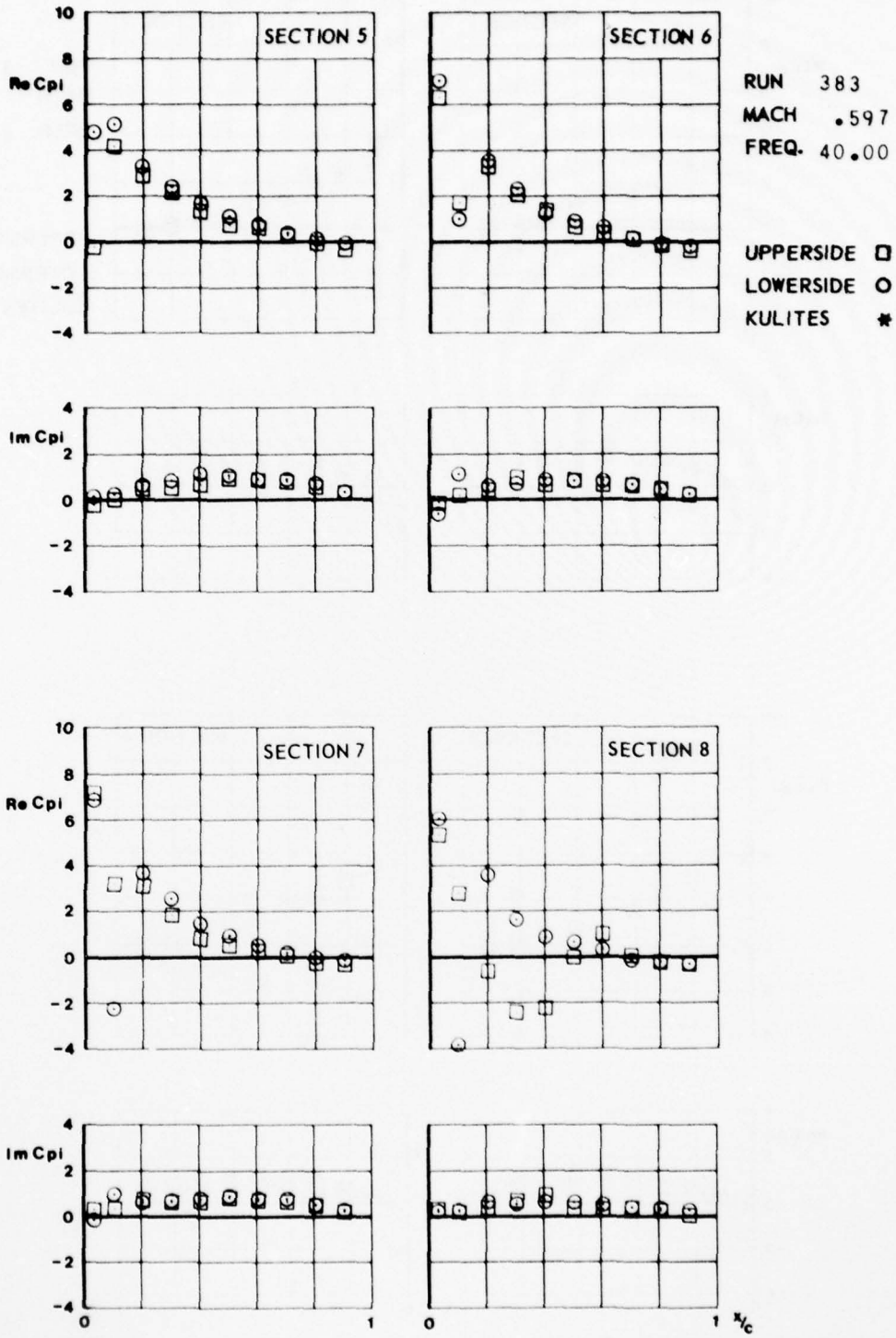

CONF. 0 (CLEAN WING)

FIG.
II.C.5.a

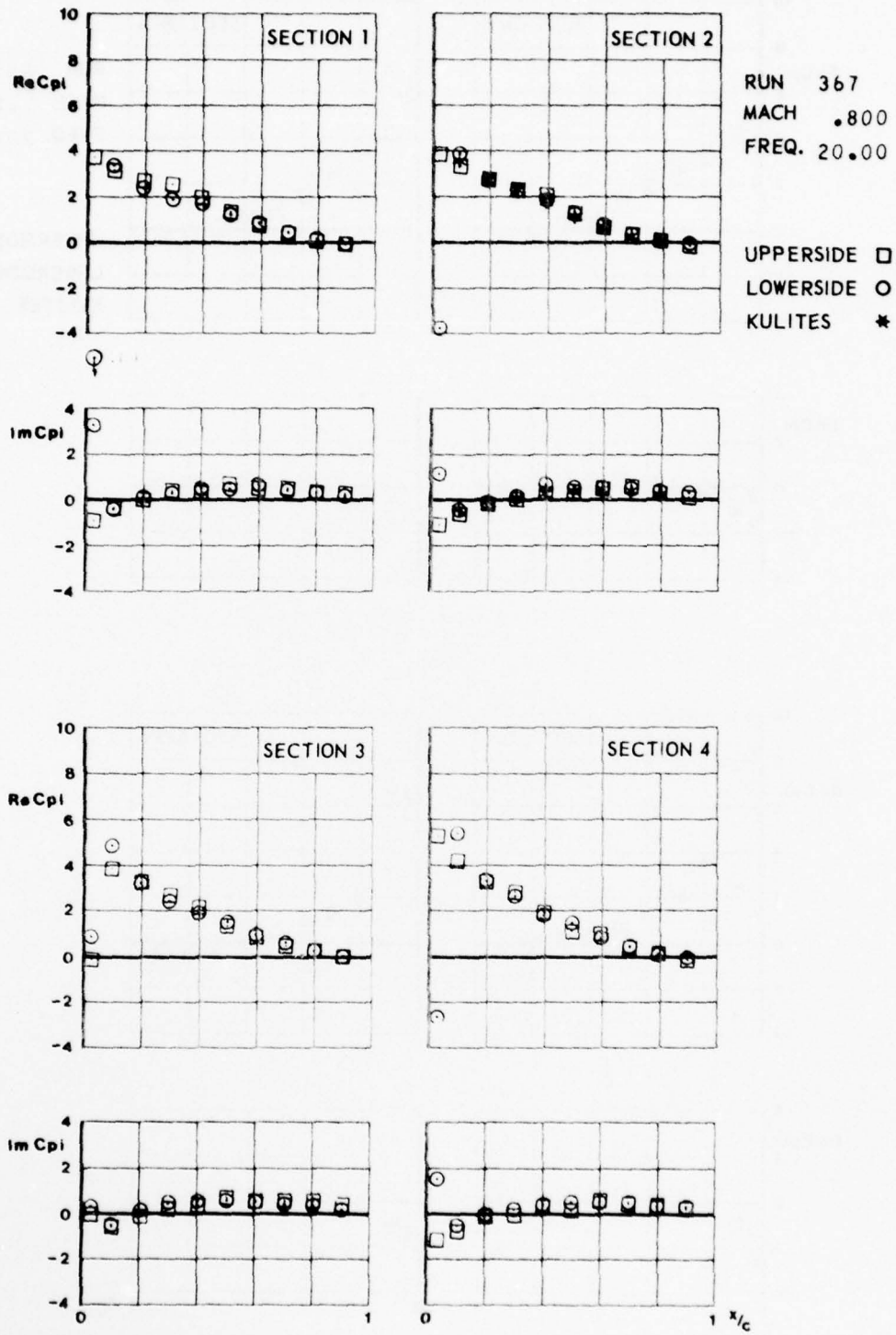

CONF. 0 (CLEAN WING)

FIG.
II.C.5.b

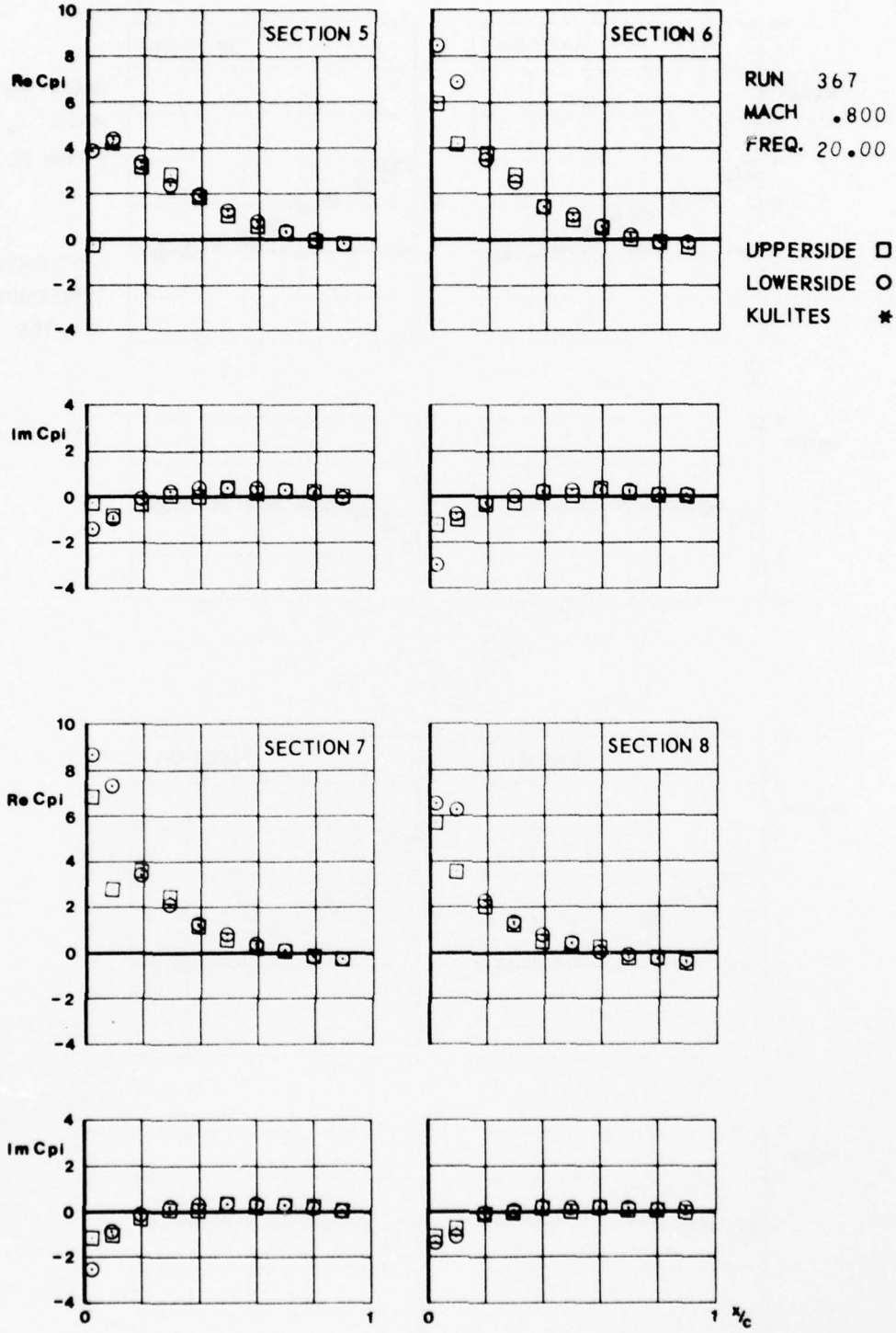

CONF. 0 (CLEAN WING)

FIG.
II.C.6.a

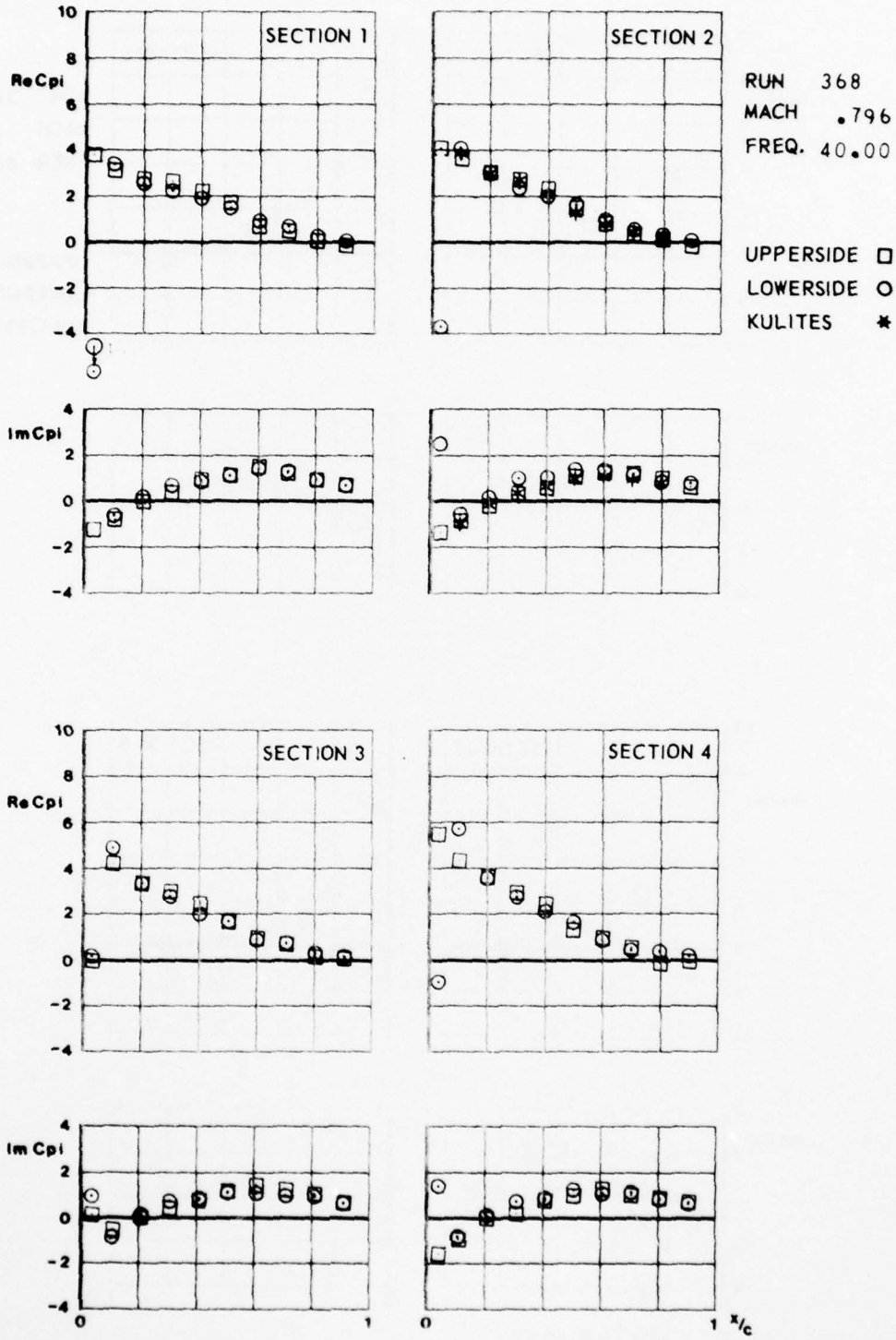

CONF. 0 (CLEAN WING)

FIG.
II.C.6.6

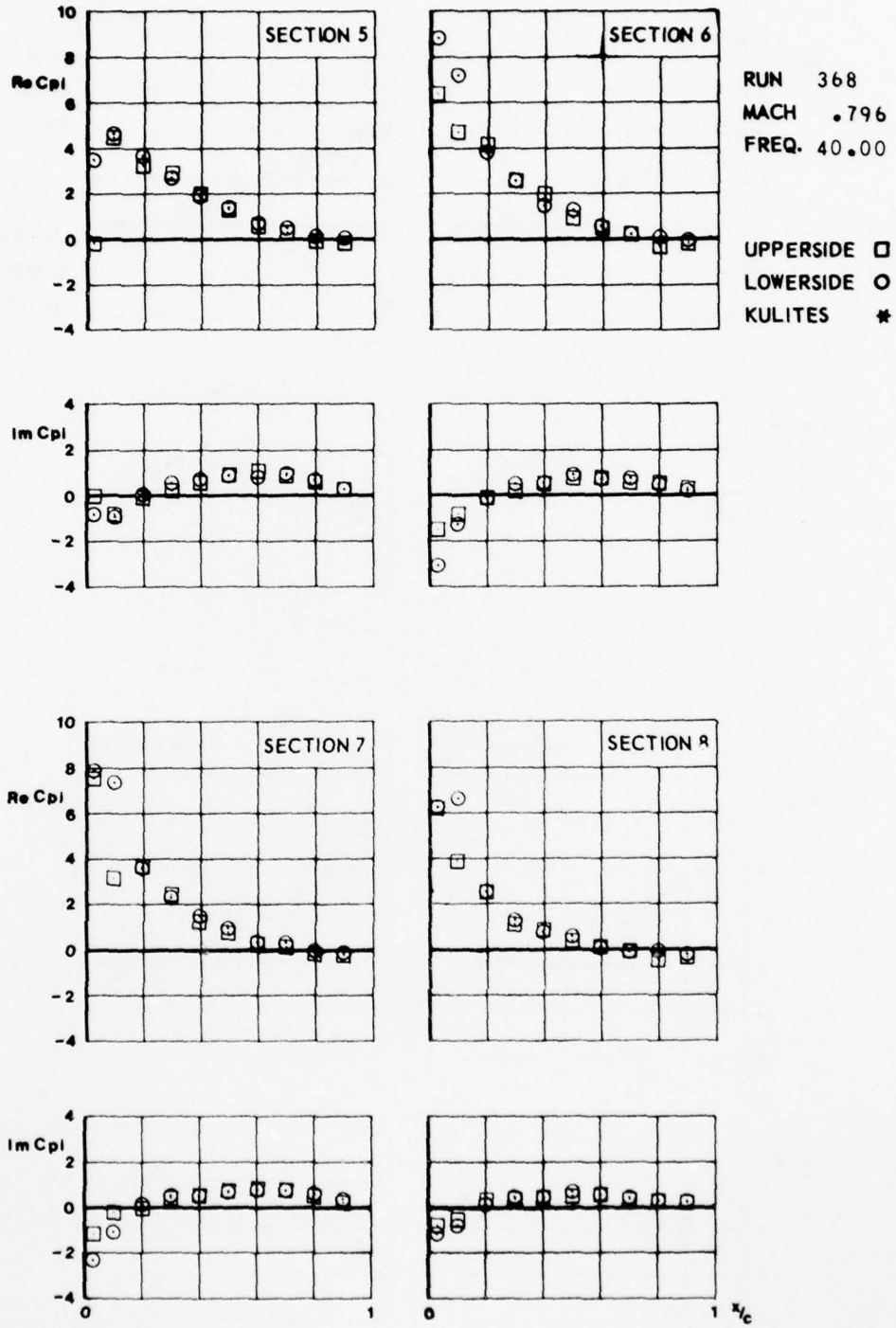

CONF. 0 (CLEAN WING)

FIG.
II.C.7.a

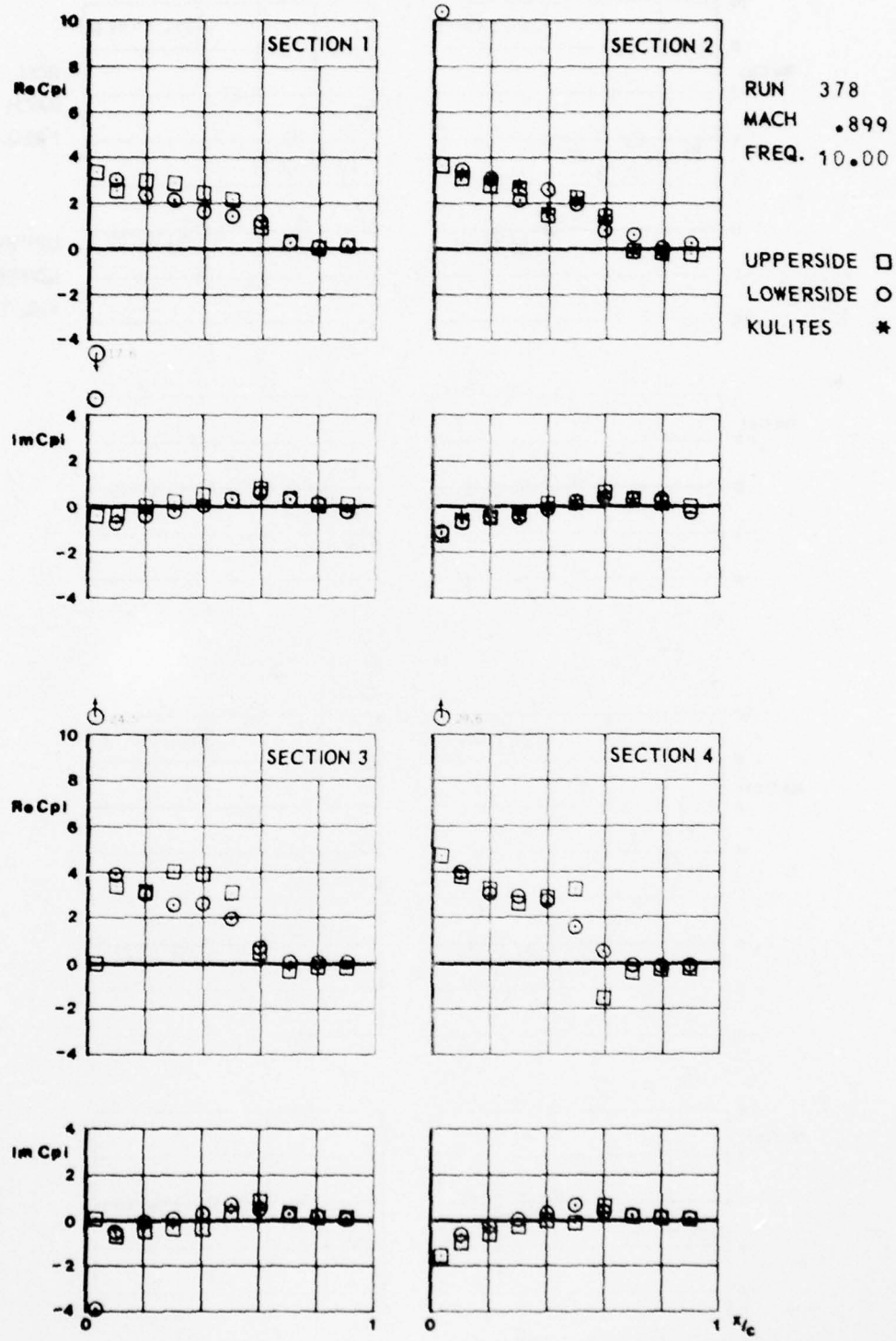

CONF.0 (CLEAN WING)

FIG.
III.C.7.6

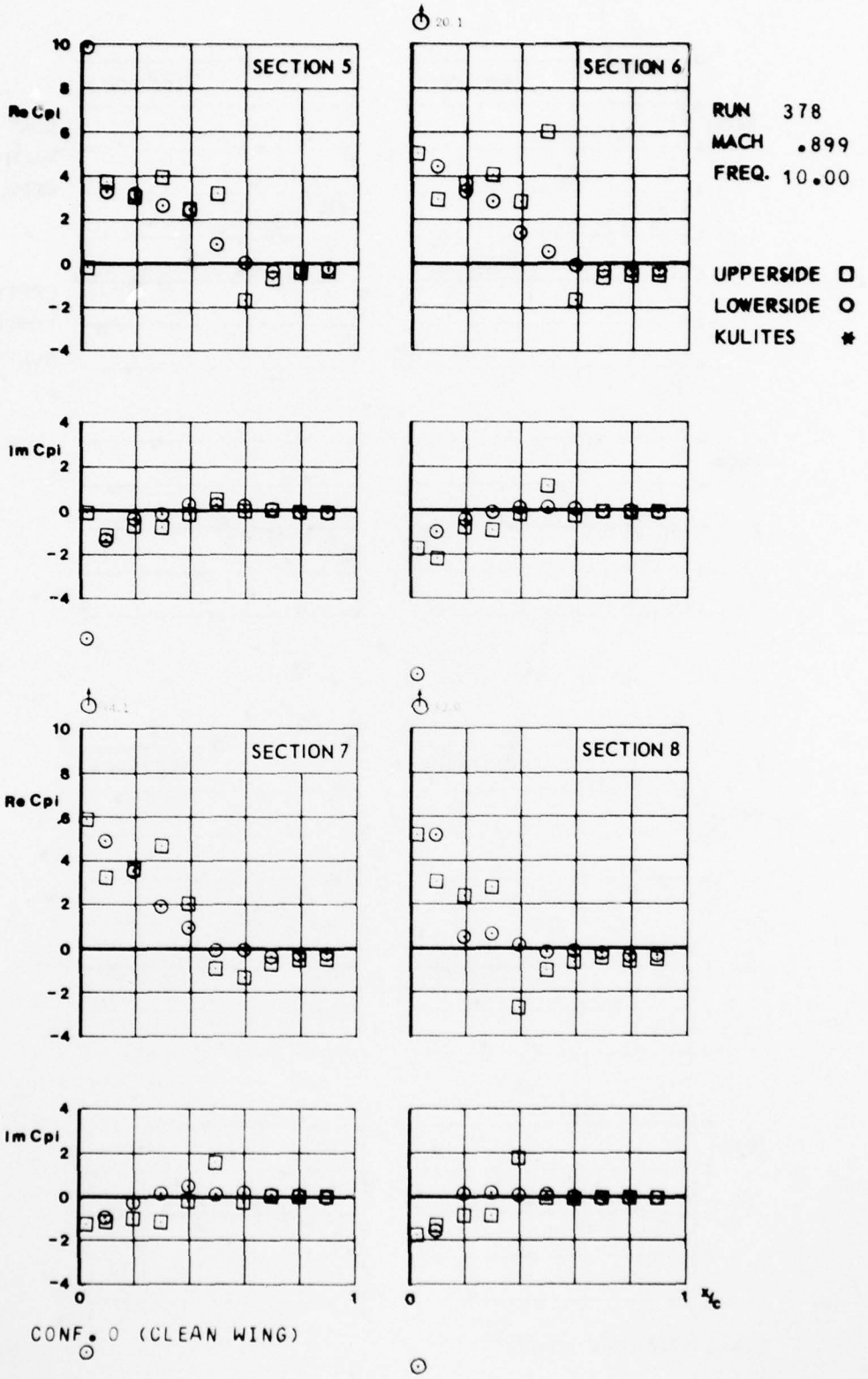
SECTION 5
SECTION 6
SECTION 7
SECTION 8
Re Cpi
Im Cpi
RUN 378
MACH .899
FREQ. 10.00
UPPERSIDE □
LOWERSIDE ○
KULITES ✱
x/c
CONF. 0 (CLEAN WING)

FIG.
II.C.8.a

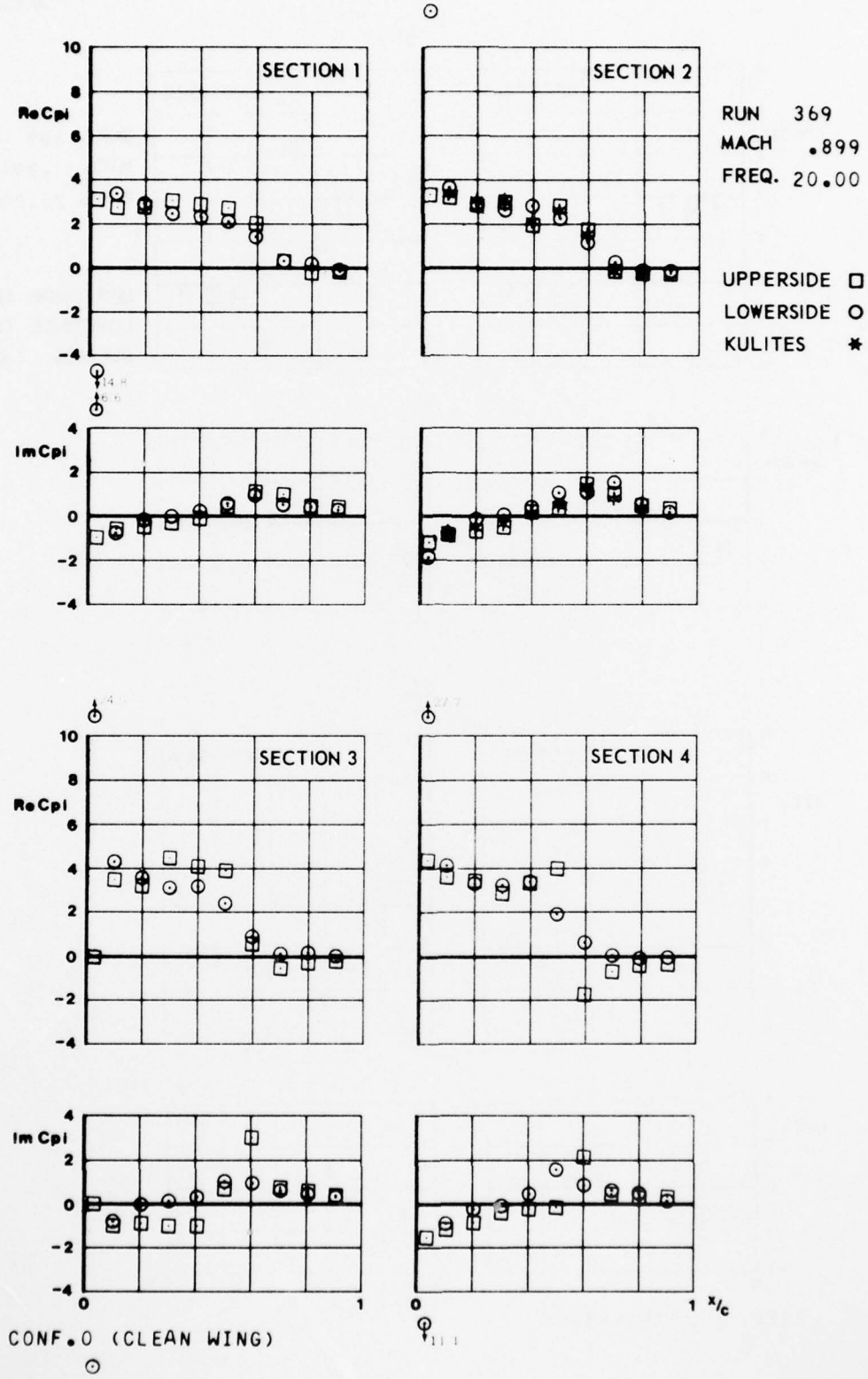
SECTION 1
SECTION 2
SECTION 3
SECTION 4
ReCpi
ImCpi
RUN 369
MACH .899
FREQ. 20.00
UPPERSIDE □
LOWERSIDE ○
KULITES ✱
x/c
CONF.0 (CLEAN WING)

FIG.
II.C.8.b

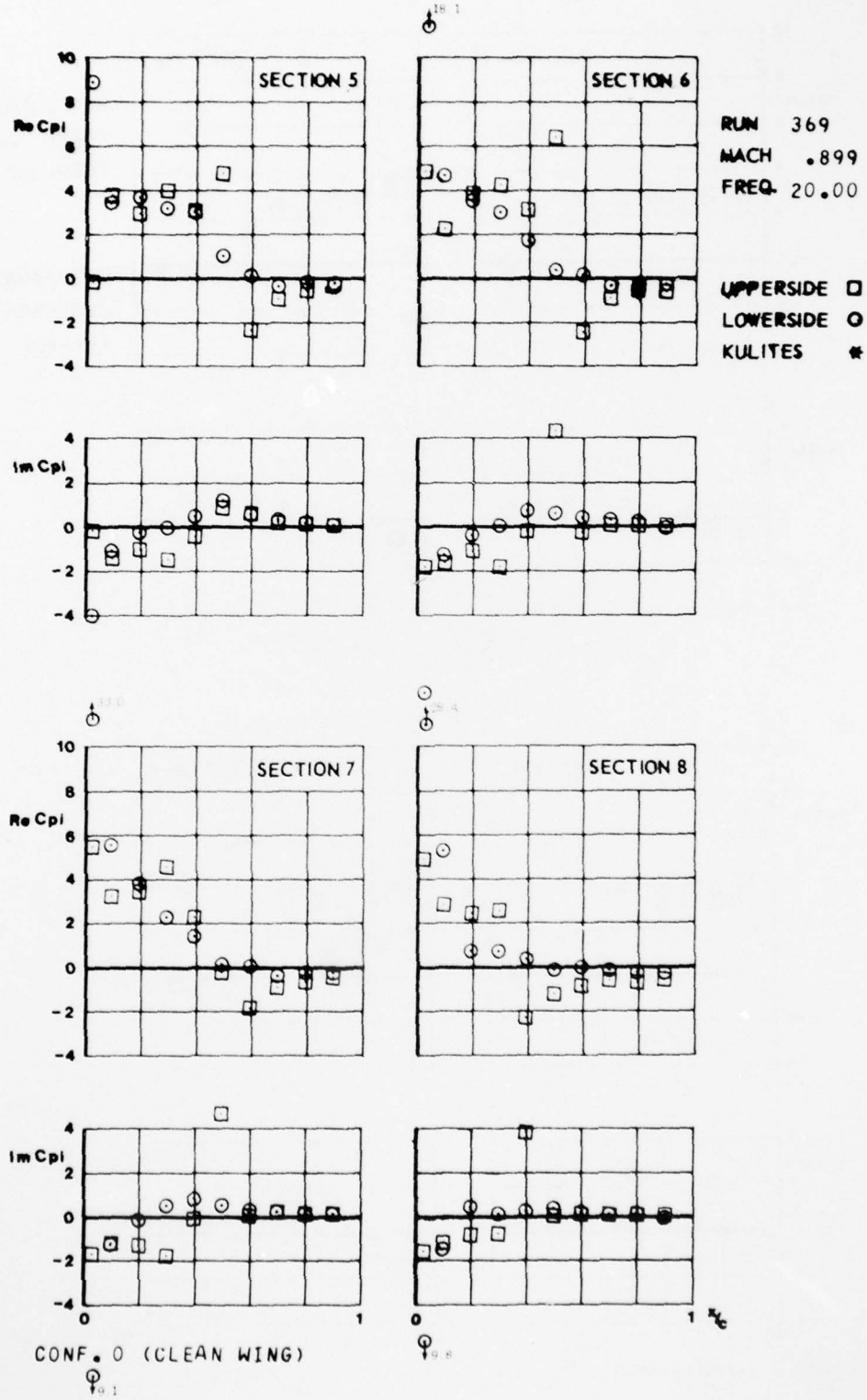

CONF. 0 (CLEAN WING)

AD-A071 420 NATIONAL AEROSPACE LAB AMSTERDAM (NETHERLANDS) F/G 20/4
TRANSONIC WIND TUNNEL TESTS ON AN OSCILLATING WING WITH EXTERNA--ETC(U)
MAR 79 H TIJDEMAN, J W VAN NUNEN, A N KRAAN AFOSR 77-3233
UNCLASSIFIED NLR-TR-78106-U-PT-2 AFFDL-TR-78-194-PT-2 NL

2 OF 2
AD
A071420

END
DATE
FILMED
9-79
DDC

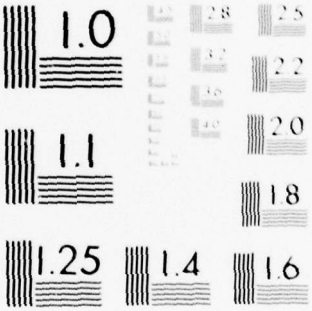

MICROCOPY RESOLUTION TEST CHART
NATIONAL BUREAU OF STANDARDS 1963-A

FIG.
II.C.9.a

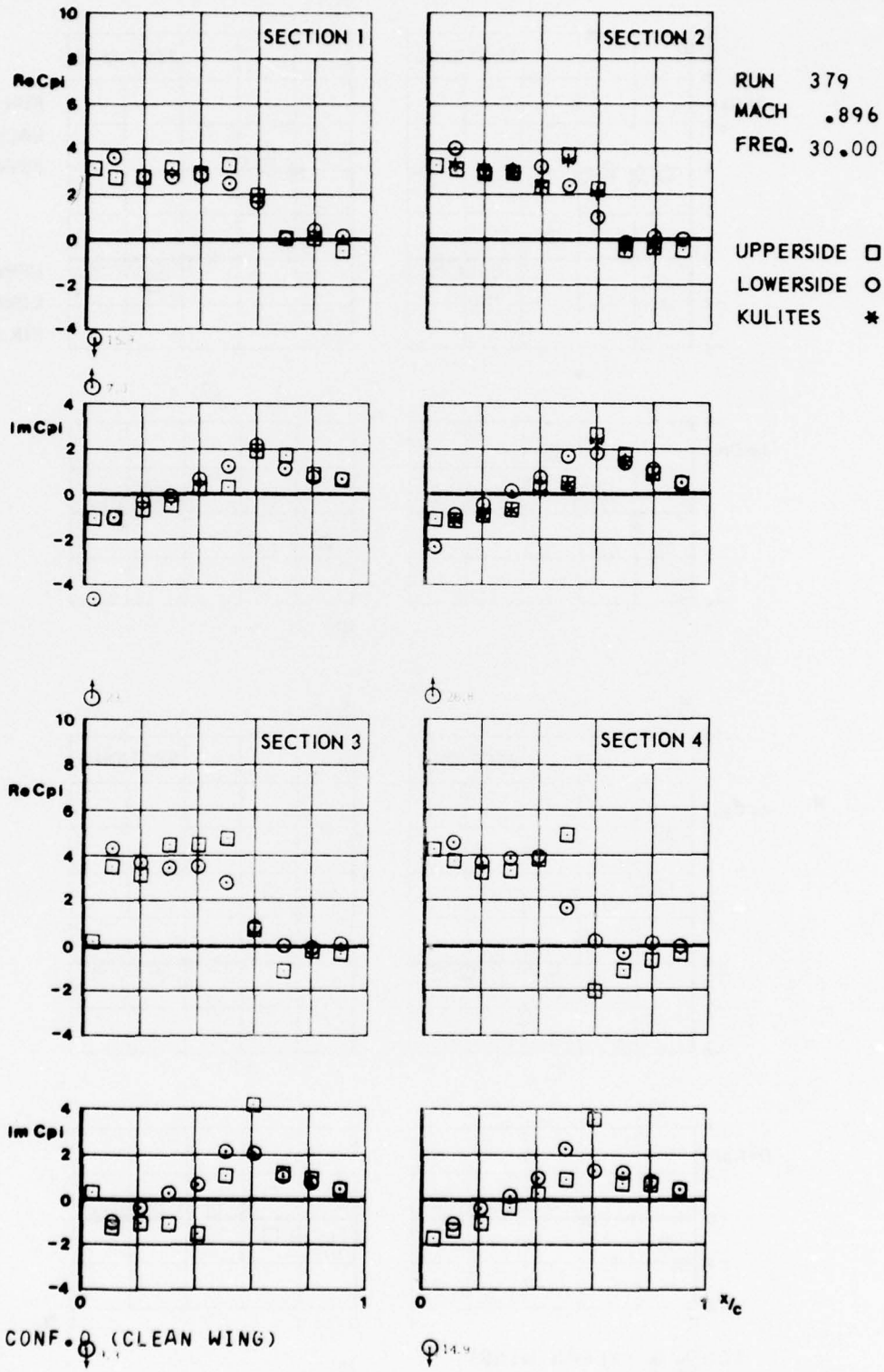

CONF. 0 (CLEAN WING)

FIG.
II.C.9.6

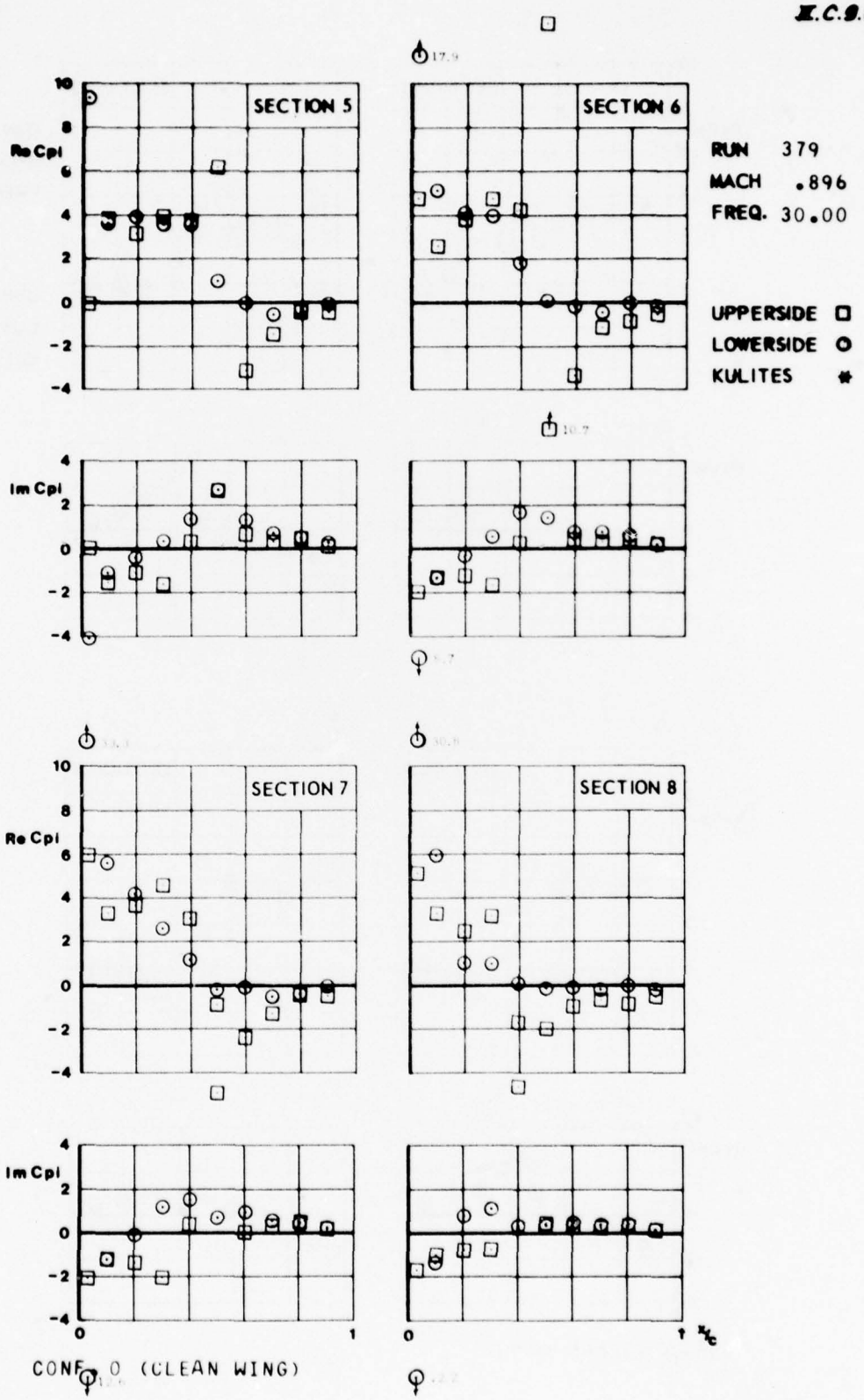

CONFIG. 0 (CLEAN WING)

FIG.
II.C.10.a

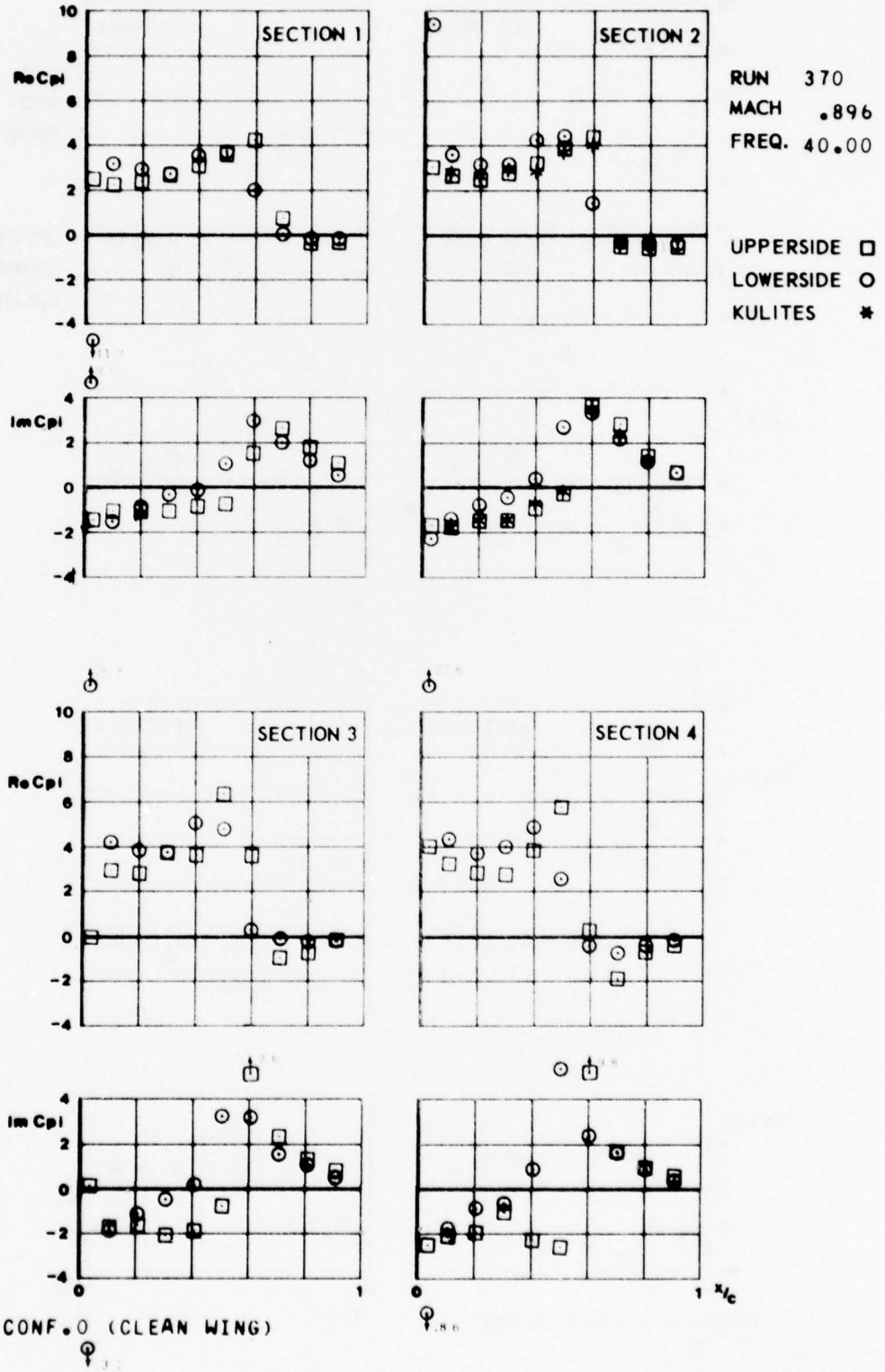
SECTION 1
SECTION 2
SECTION 3
SECTION 4
ReCpl
ImCpl
RUN 370
MACH .896
FREQ. 40.00
UPPERSIDE □
LOWERSIDE ○
KULITES ✱
x/c
CONF. 0 (CLEAN WING)

FIG.
II.C.10.b

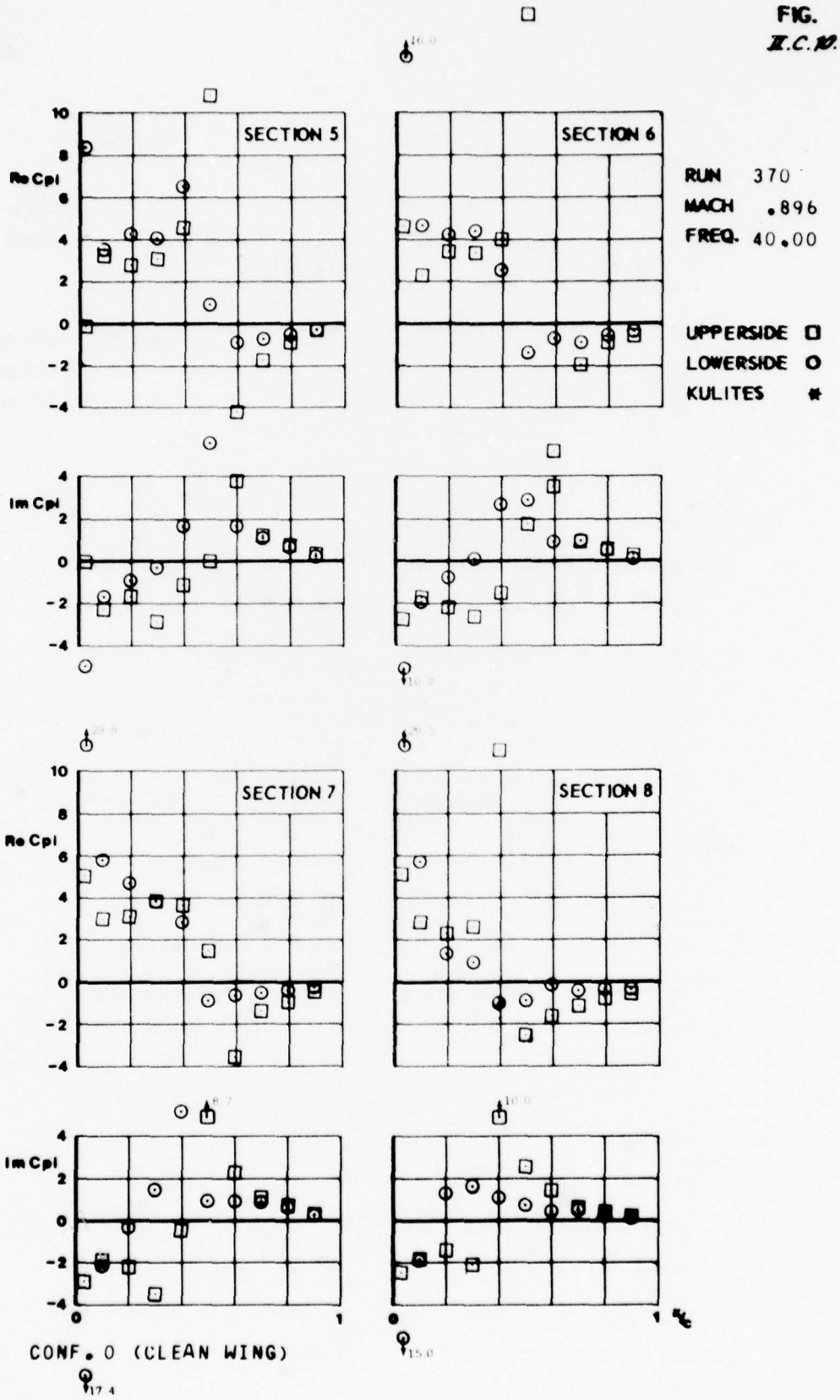
SECTION 5
SECTION 6
SECTION 7
SECTION 8
Re Cpl
Im Cpl
RUN 370
MACH .896
FREQ. 40.00
UPPERSIDE
LOWERSIDE
KULITES
CONF. 0 (CLEAN WING)

FIG.
II.C.11.a

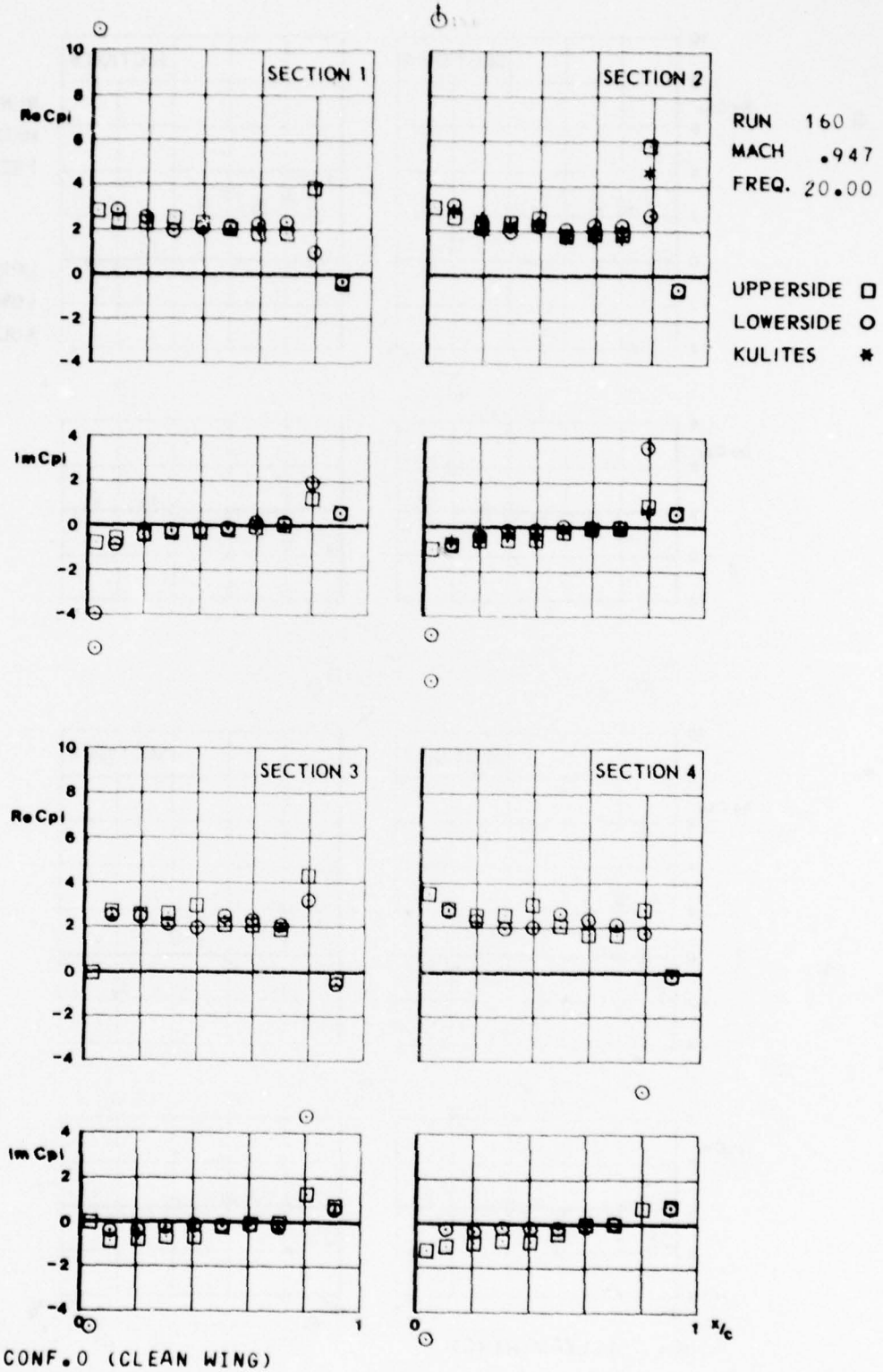

CONF.0 (CLEAN WING)

FIG.
II.C.11.b

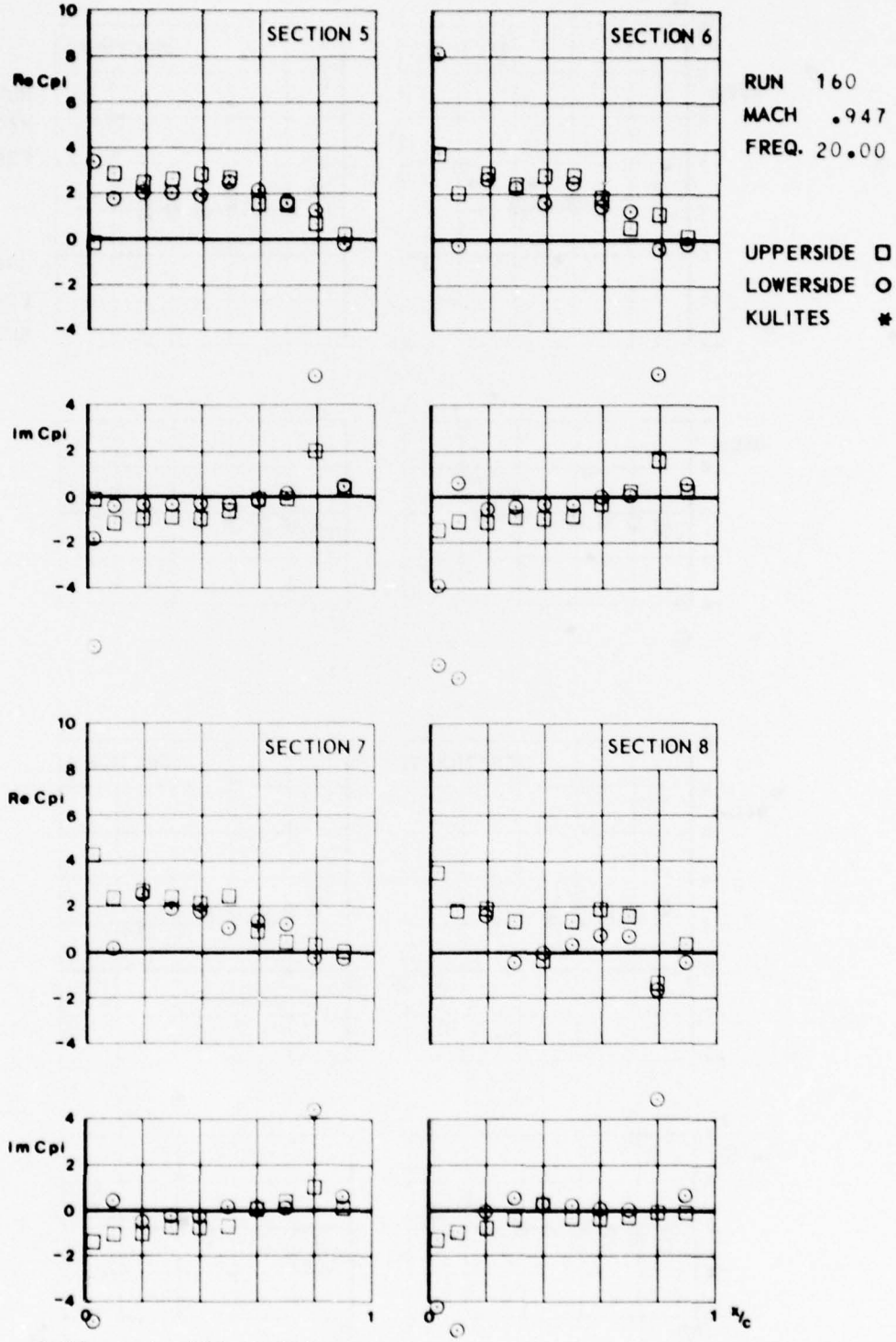

CONF. 1 (CLEAN WING)

FIG.
II.C.12.a

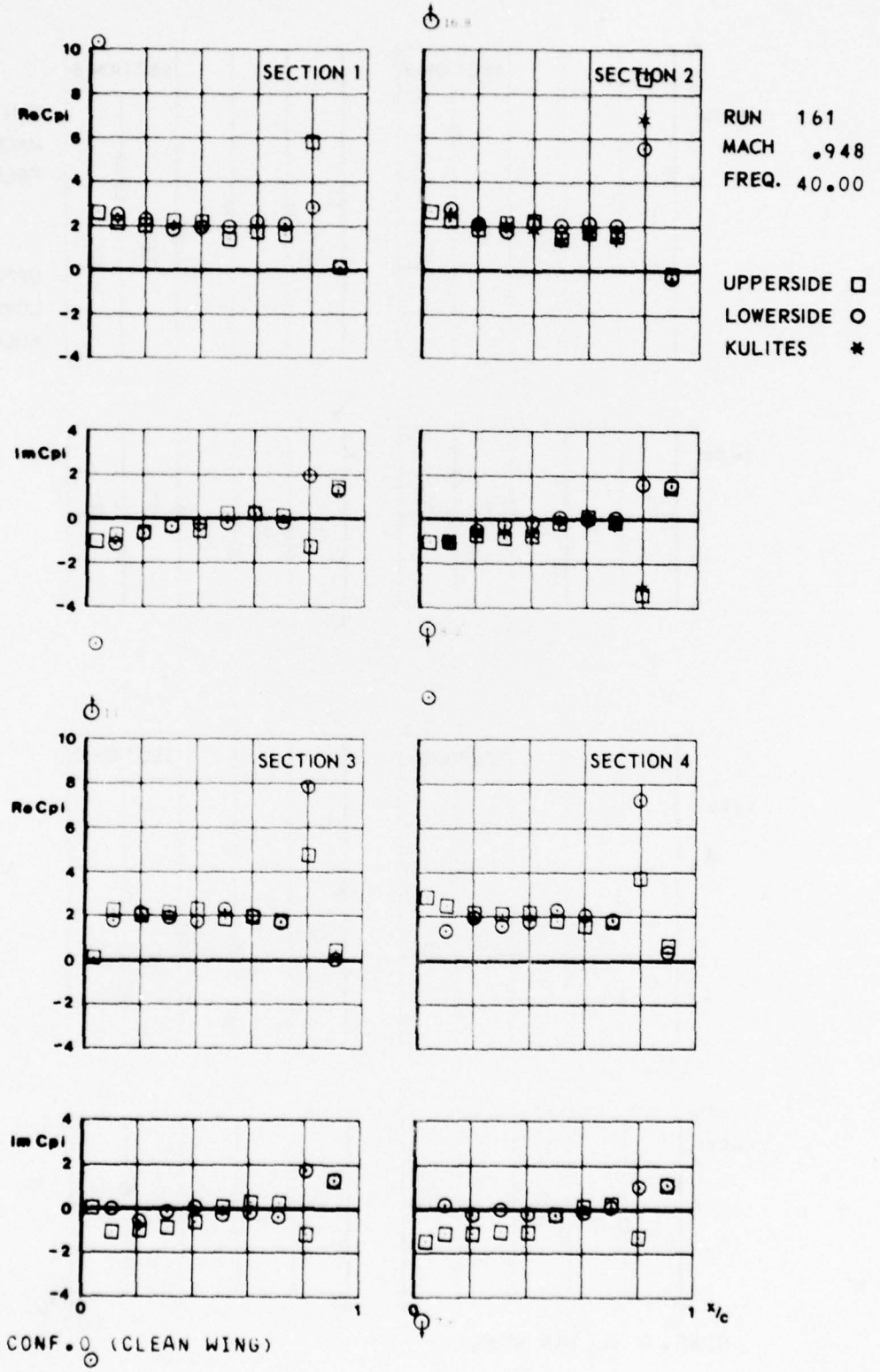
SECTION 1
SECTION 2
SECTION 3
SECTION 4
ReCpl
ImCpl
RUN 161
MACH .948
FREQ. 40.00
UPPERSIDE □
LOWERSIDE ○
KULITES ✱
x/c
CONF. 0 (CLEAN WING)

FIG.
II.C.12.b

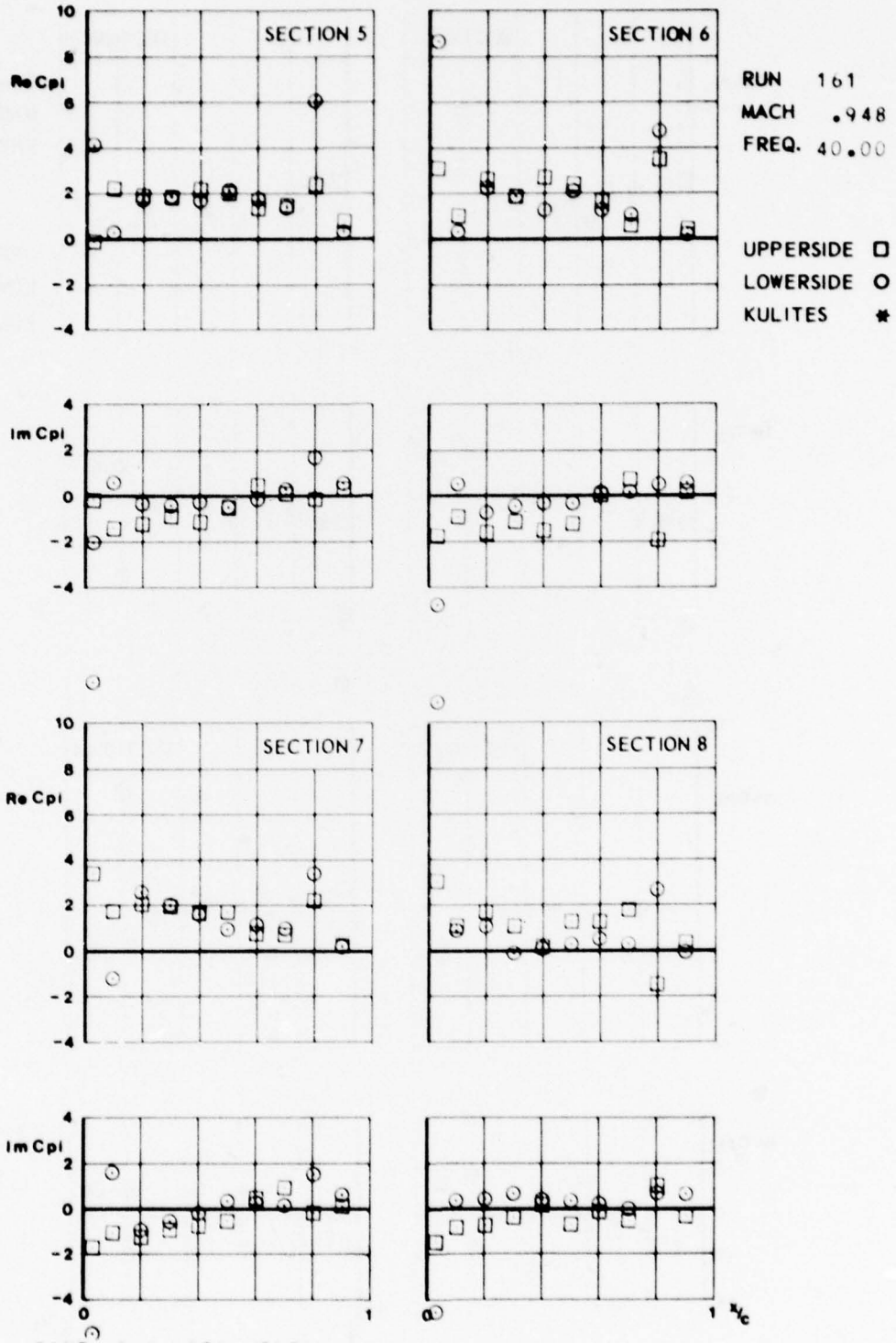

CONF. 0 (CLEAN WING)

FIG.
II.C.13.a

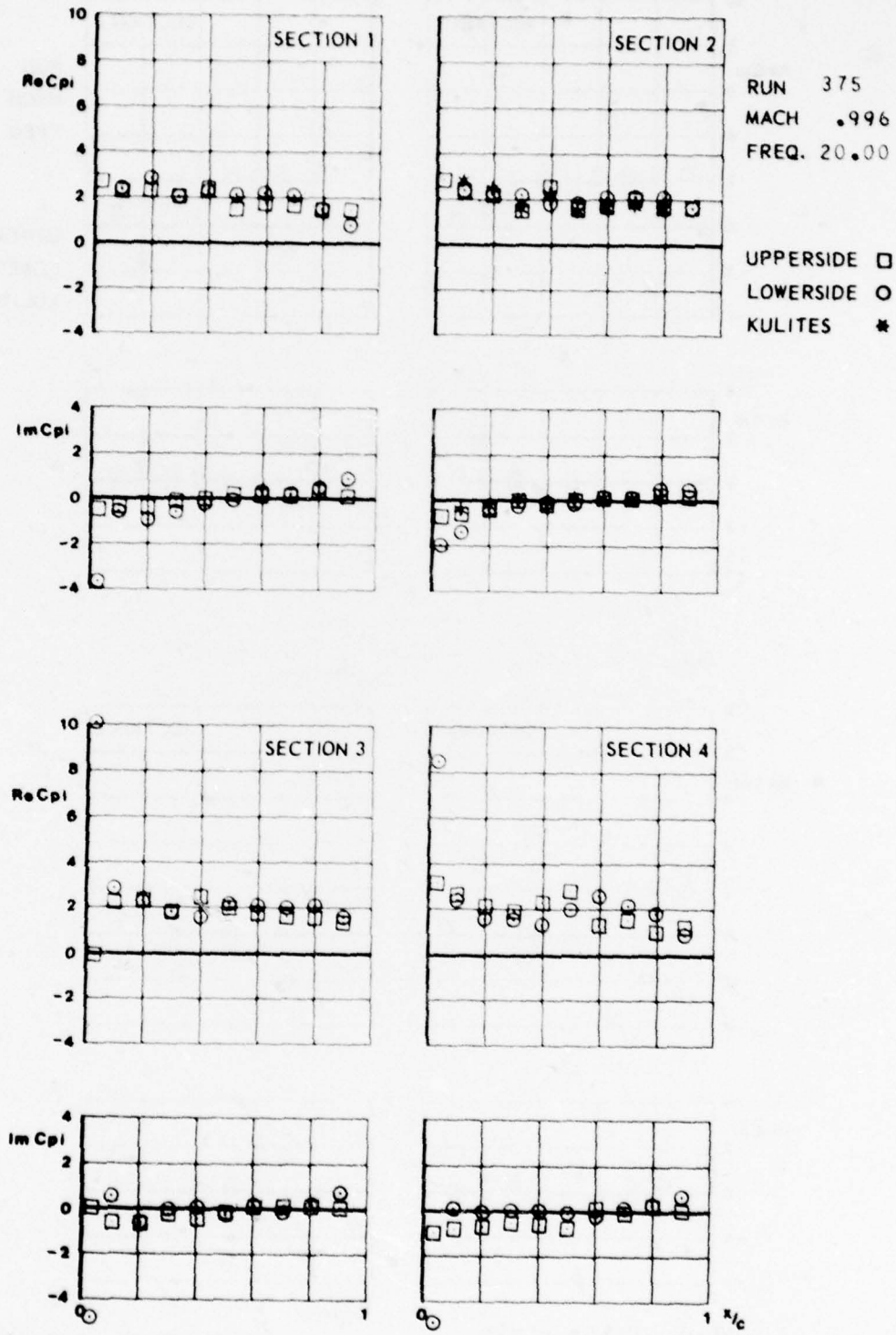

CONF.0 (CLEAN WING)

FIG.
II.C.13.b

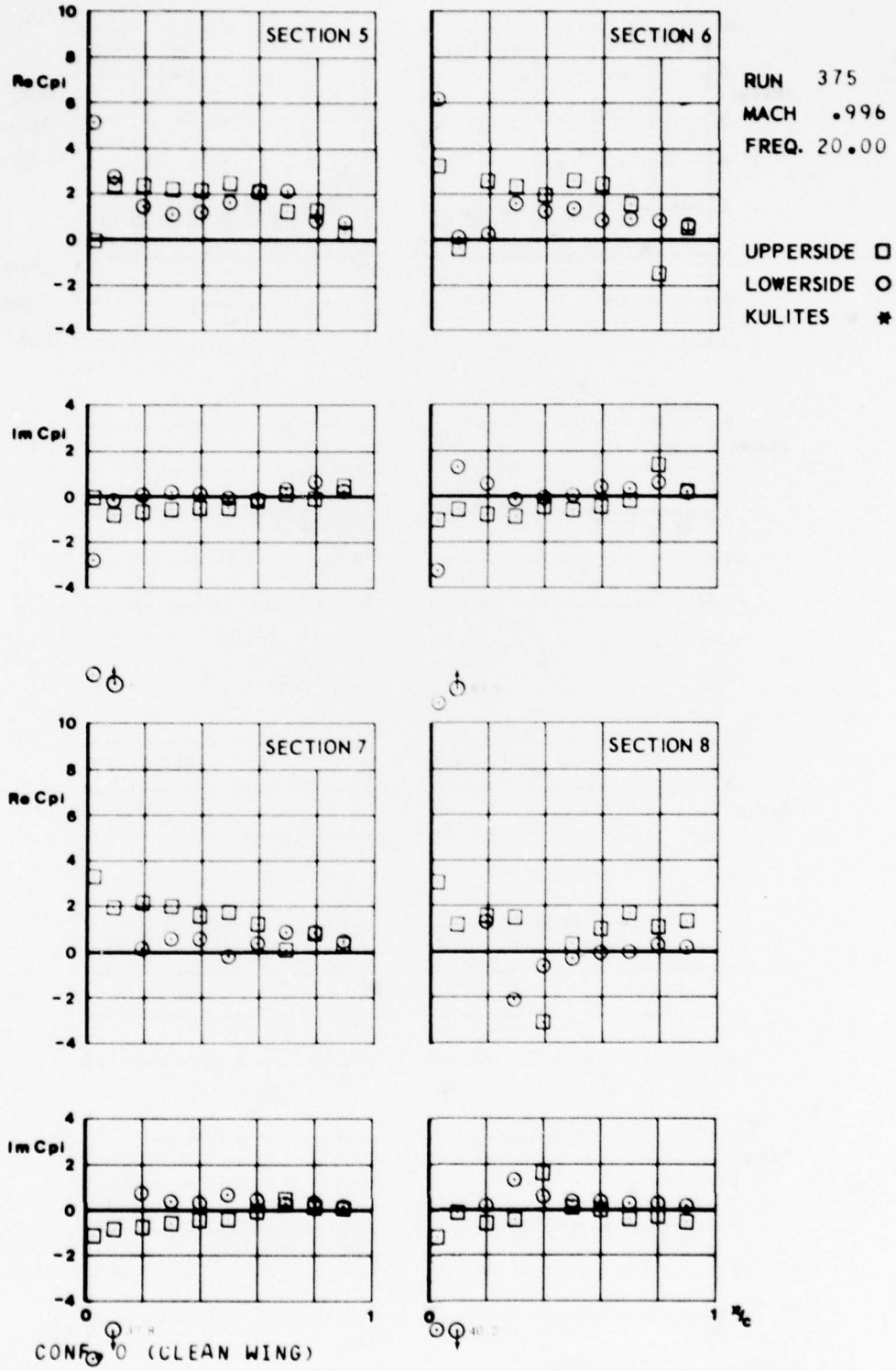

CONFIG 0 (CLEAN WING)

FIG.
II.C.14.a

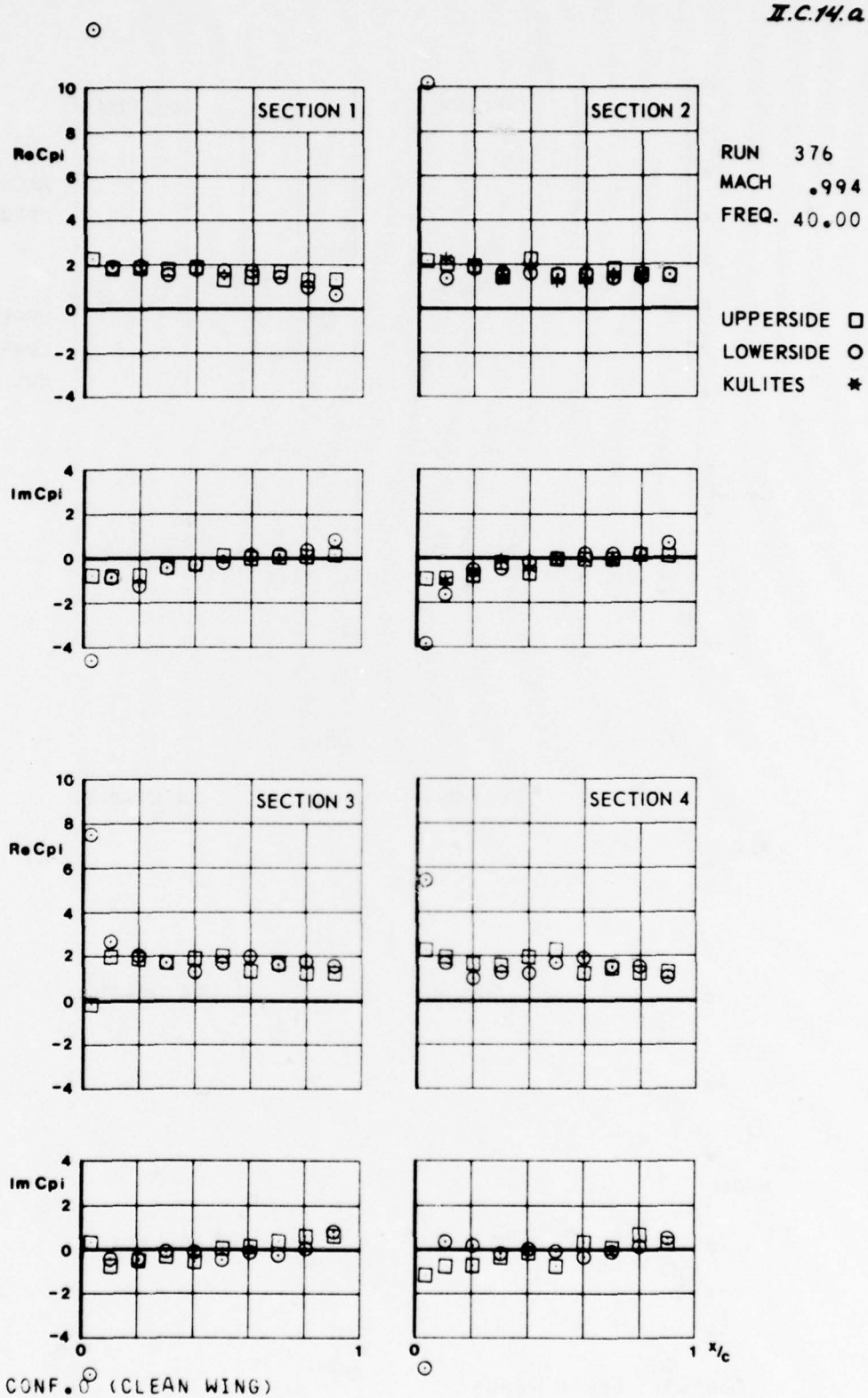
SECTION 1
SECTION 2
SECTION 3
SECTION 4
ReCpi
ImCpi
RUN 376
MACH .994
FREQ. 40.00
UPPERSIDE □
LOWERSIDE O
KULITES ✱
x/c
CONF. 0 (CLEAN WING)

FIG.
II.C.14.b

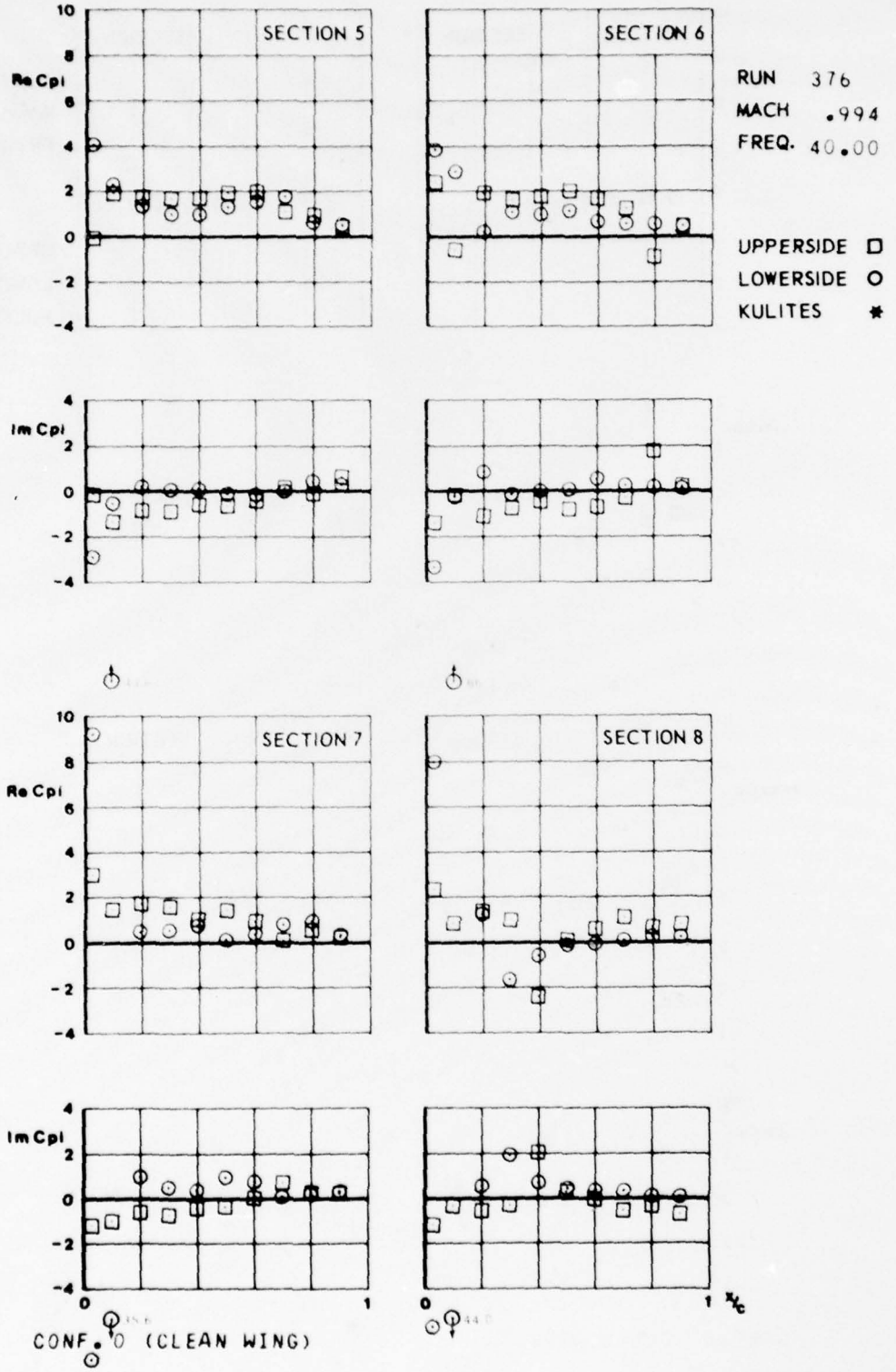
SECTION 5
SECTION 6
SECTION 7
SECTION 8
Re Cpi
Im Cpi
RUN 376
MACH .994
FREQ. 40.00
UPPERSIDE □
LOWERSIDE ○
KULITES ✱
x/c
CONF. 0 (CLEAN WING)

FIG.
II.C.15.a

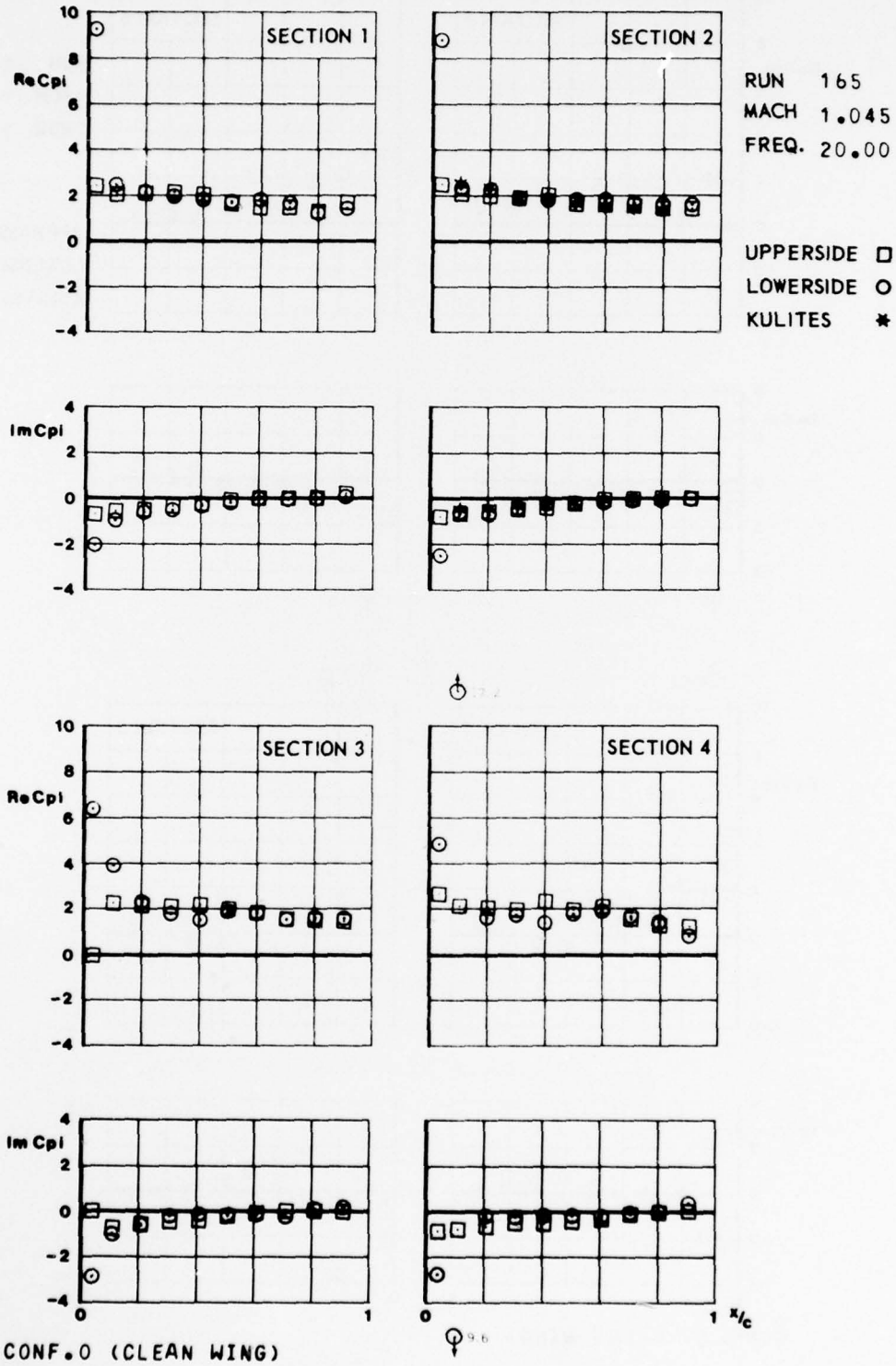

CONF.0 (CLEAN WING)

FIG.
II.C.15.b

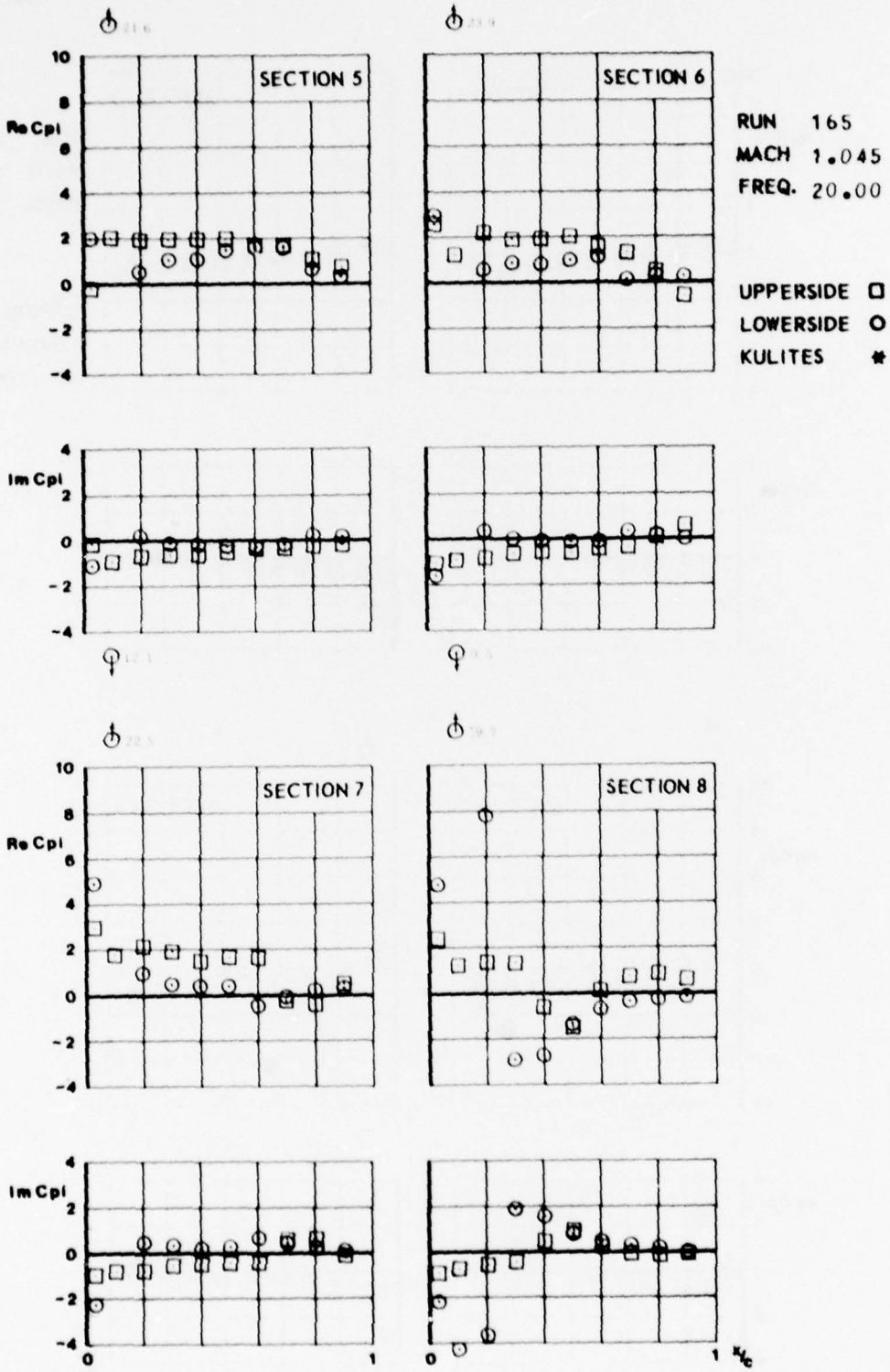

CONF. (CLEAN WING)

FIG.
II.C.16.a

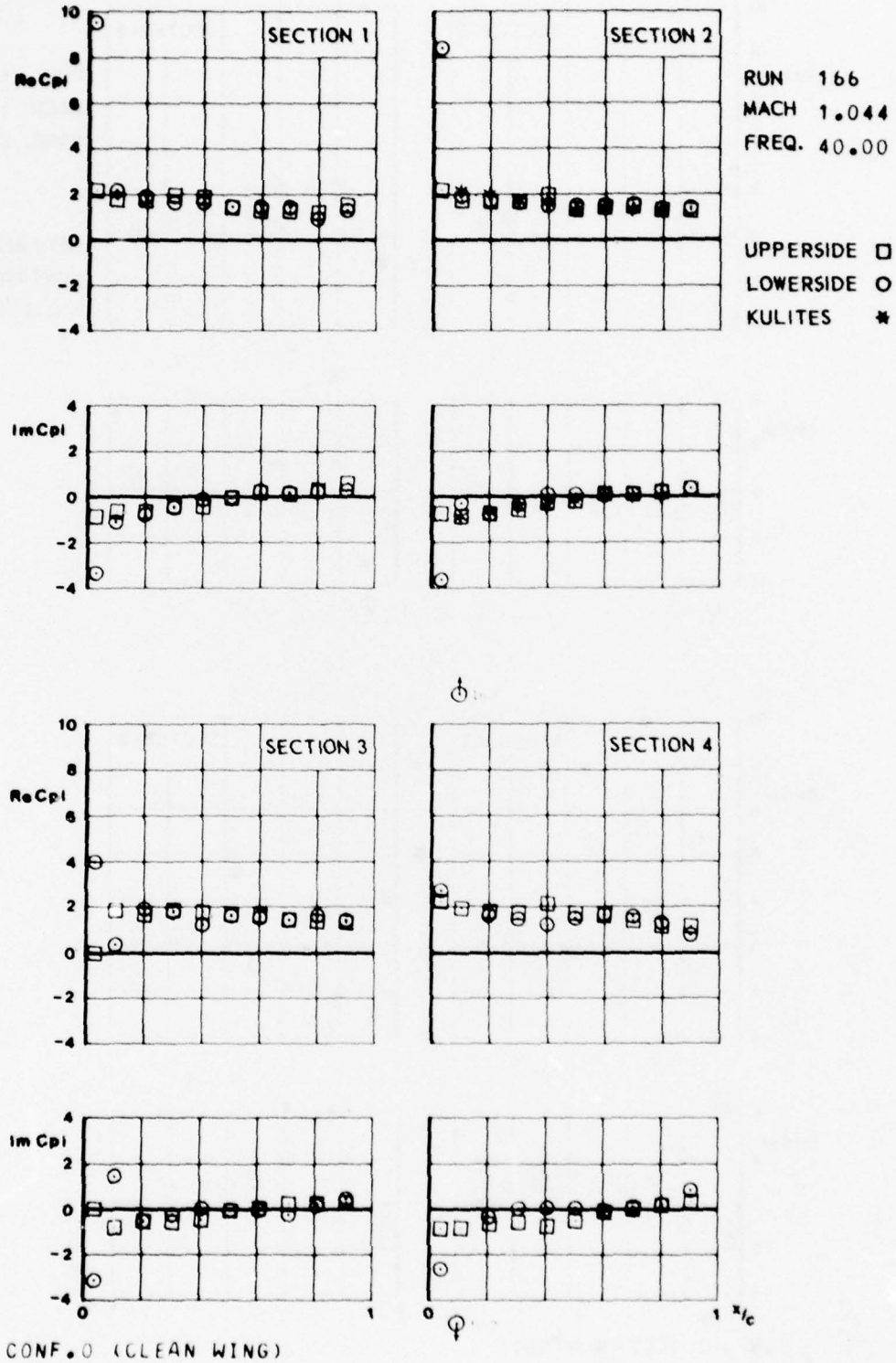

CONF. 0 (CLEAN WING)

FIG.
II.C.16.b

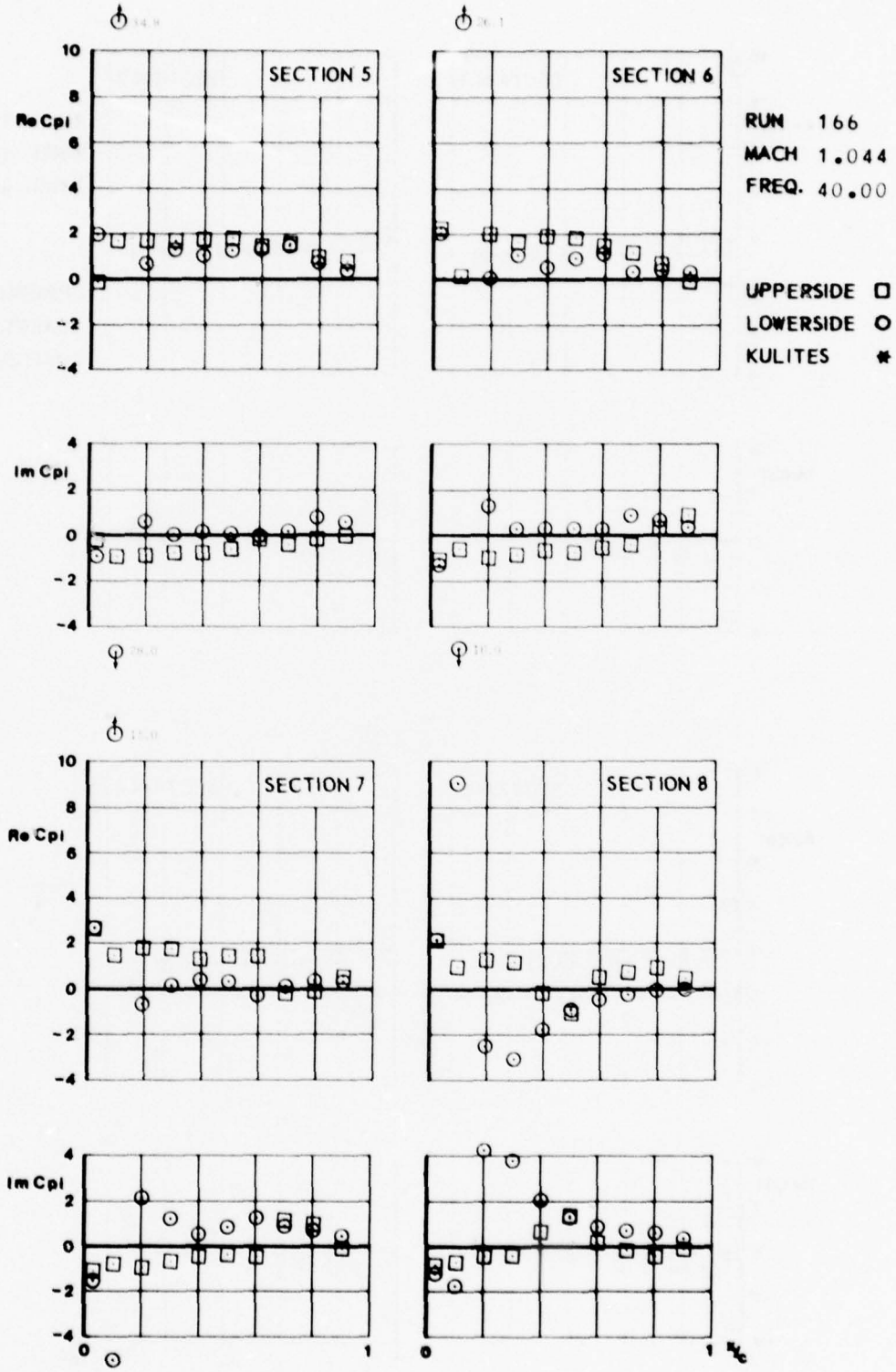

CONF. 0 (CLEAN WING)

FIG.
II.C.17.a

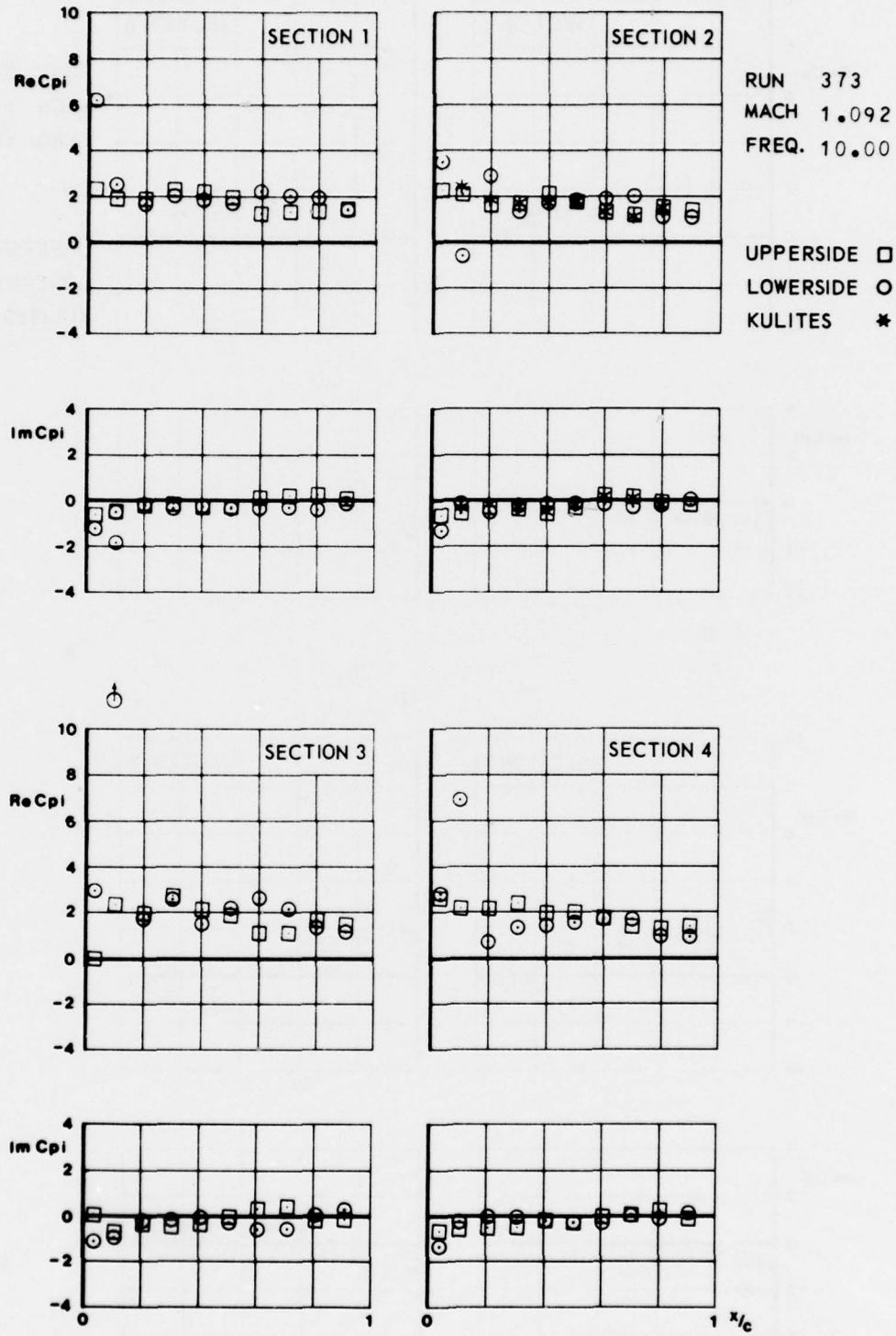

CONF.0 (CLEAN WING)

FIG.
II.C.17.b

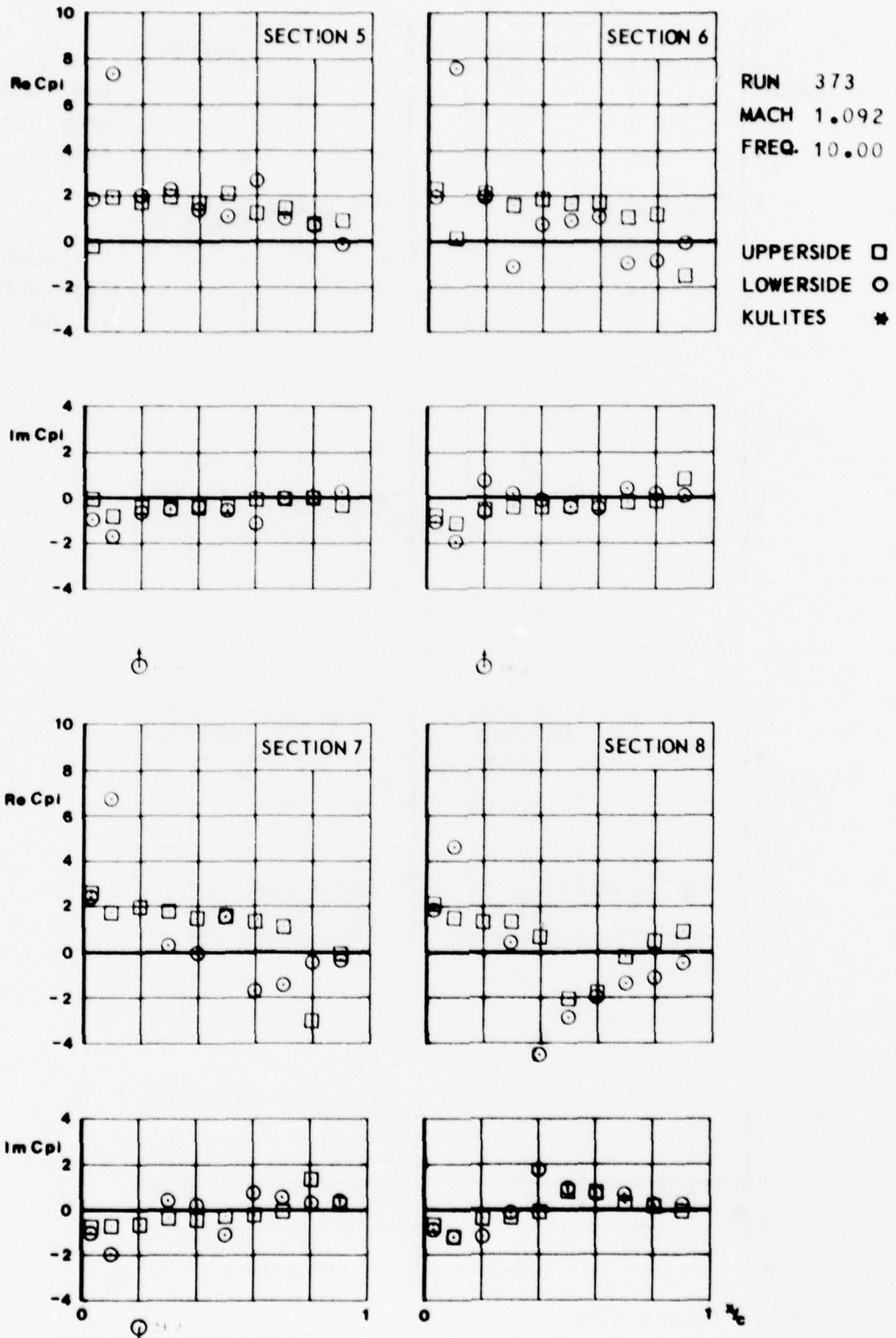

CONF. 0 (CLEAN WING)

FIG.
II.C.18.a

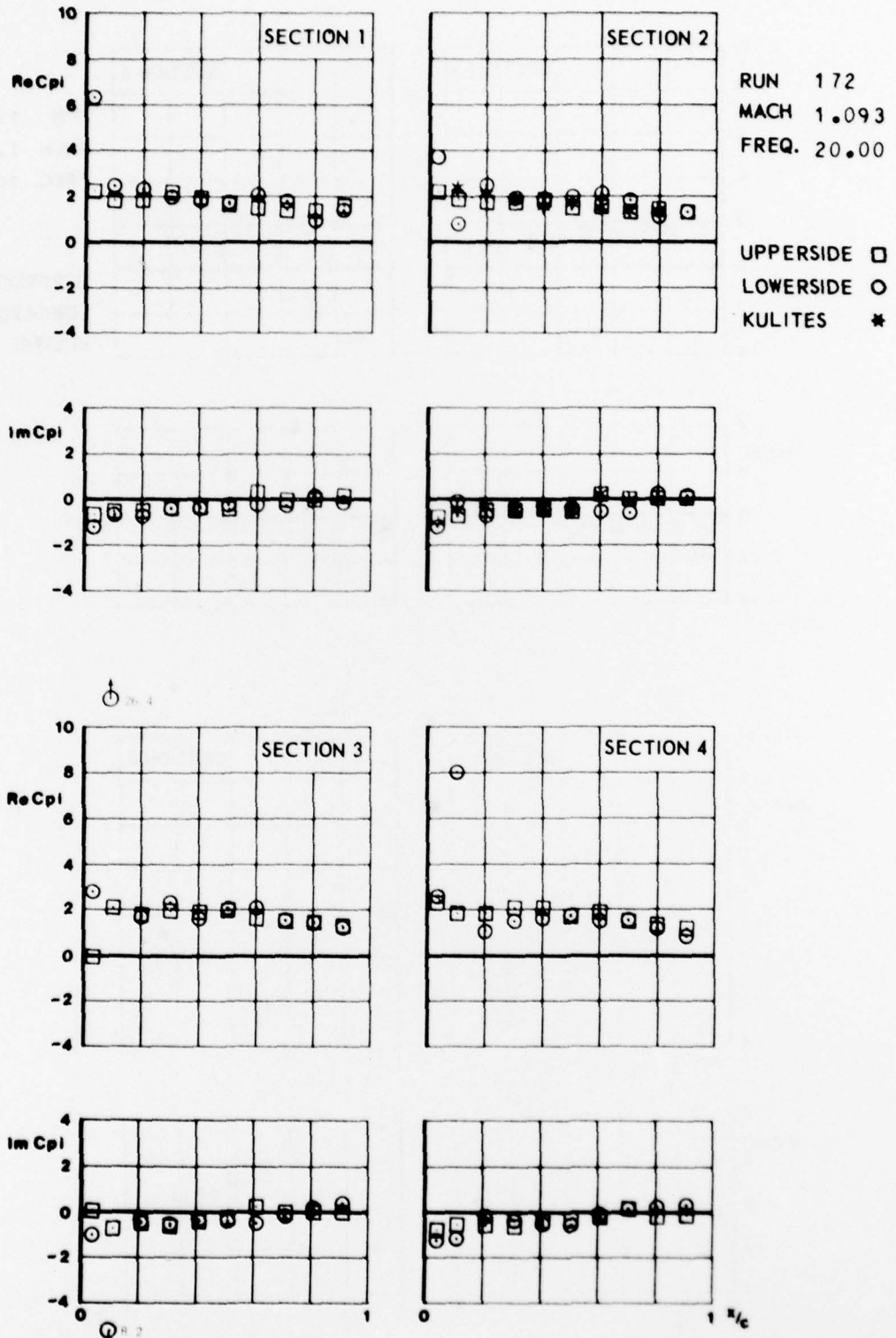

CONF.0 (CLEAN WING)

FIG.
II.C.18.b

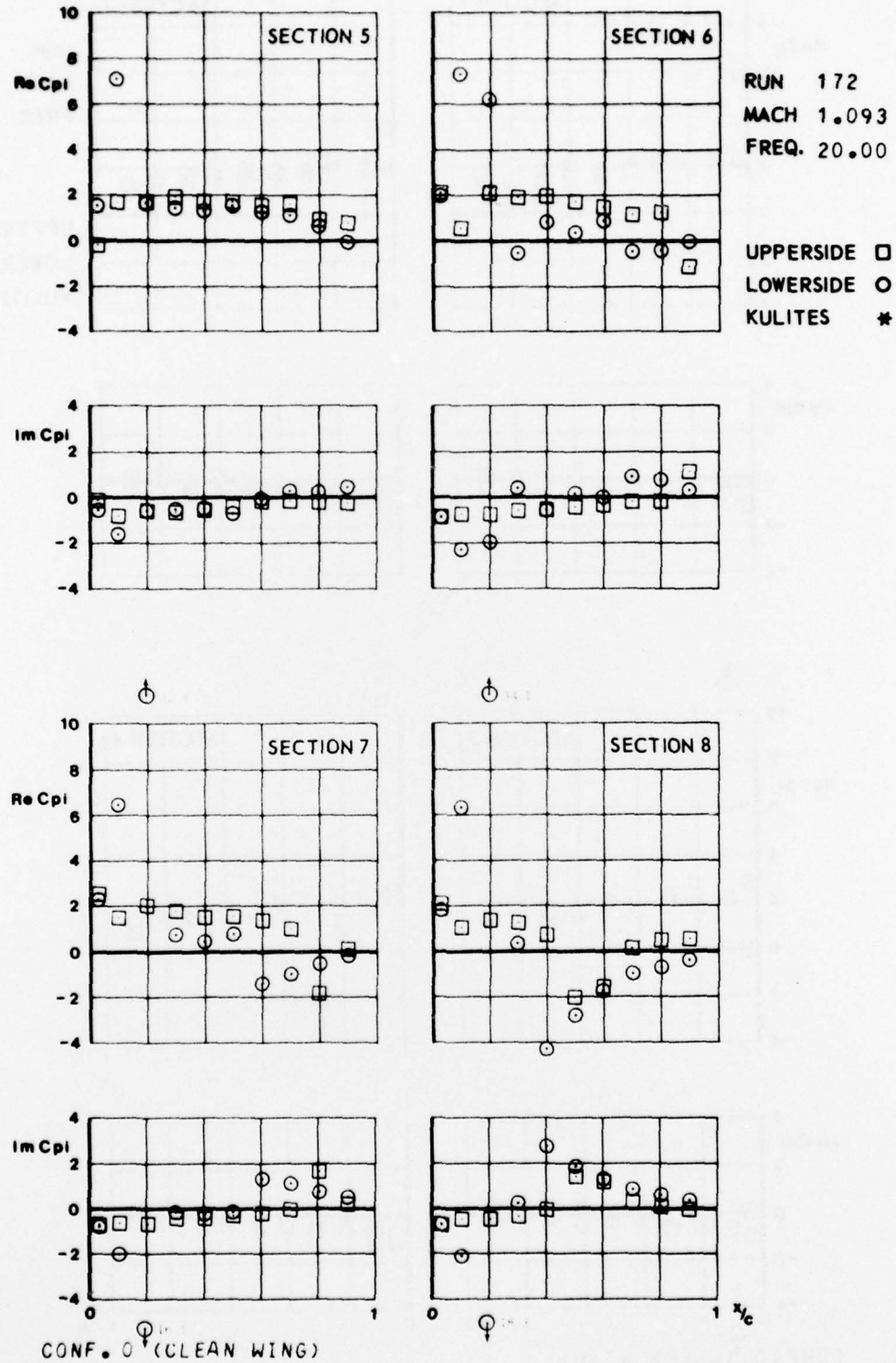
SECTION 5
SECTION 6
SECTION 7
SECTION 8
Re Cpi
Im Cpi
RUN 172
MACH 1.093
FREQ. 20.00
UPPERSIDE □
LOWERSIDE ○
KULITES ✱
x/c
CONF. 0 (CLEAN WING)

FIG.
II.C.19.a

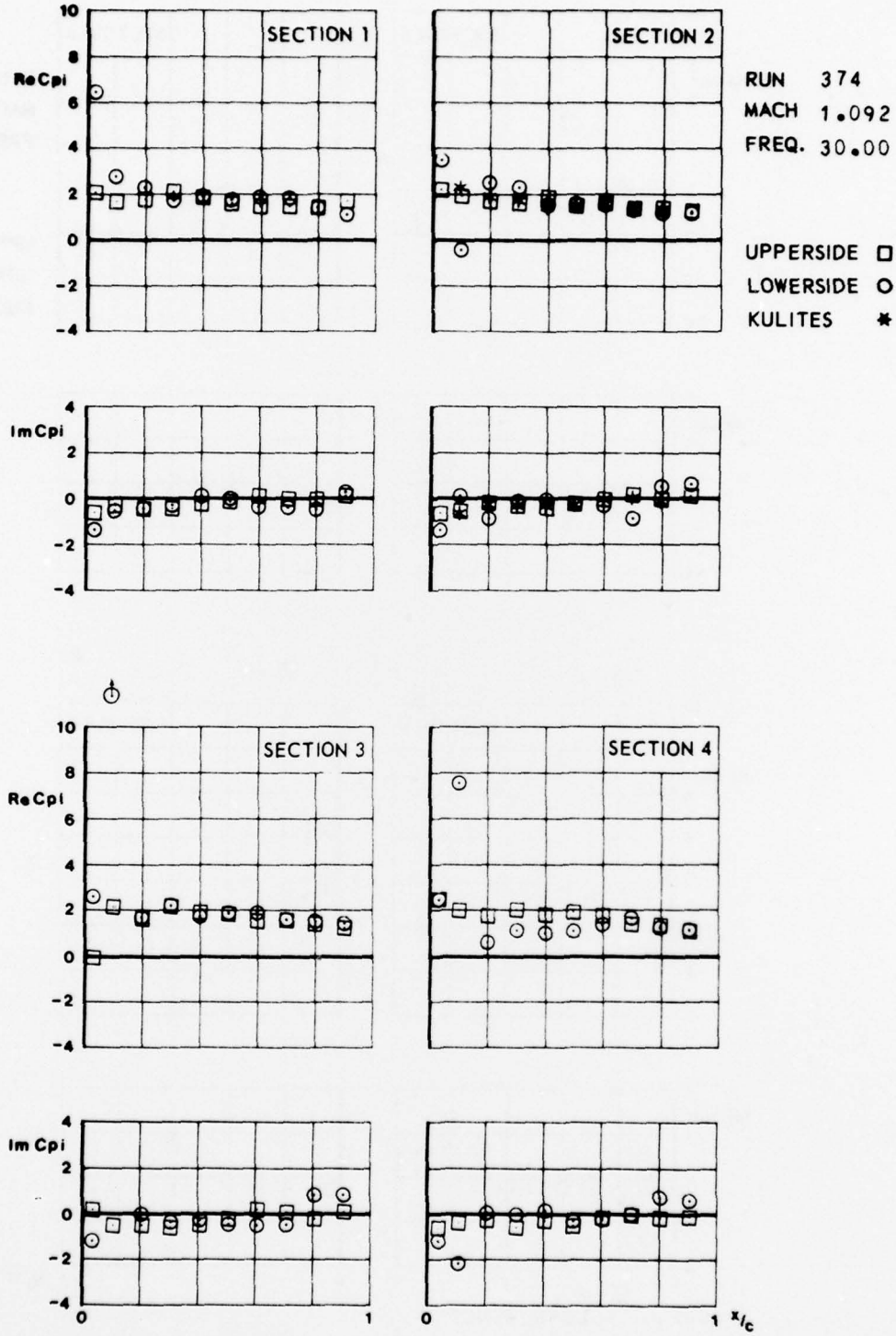

CONF. 0 (CLEAN WING)

FIG.
II.C.19.b

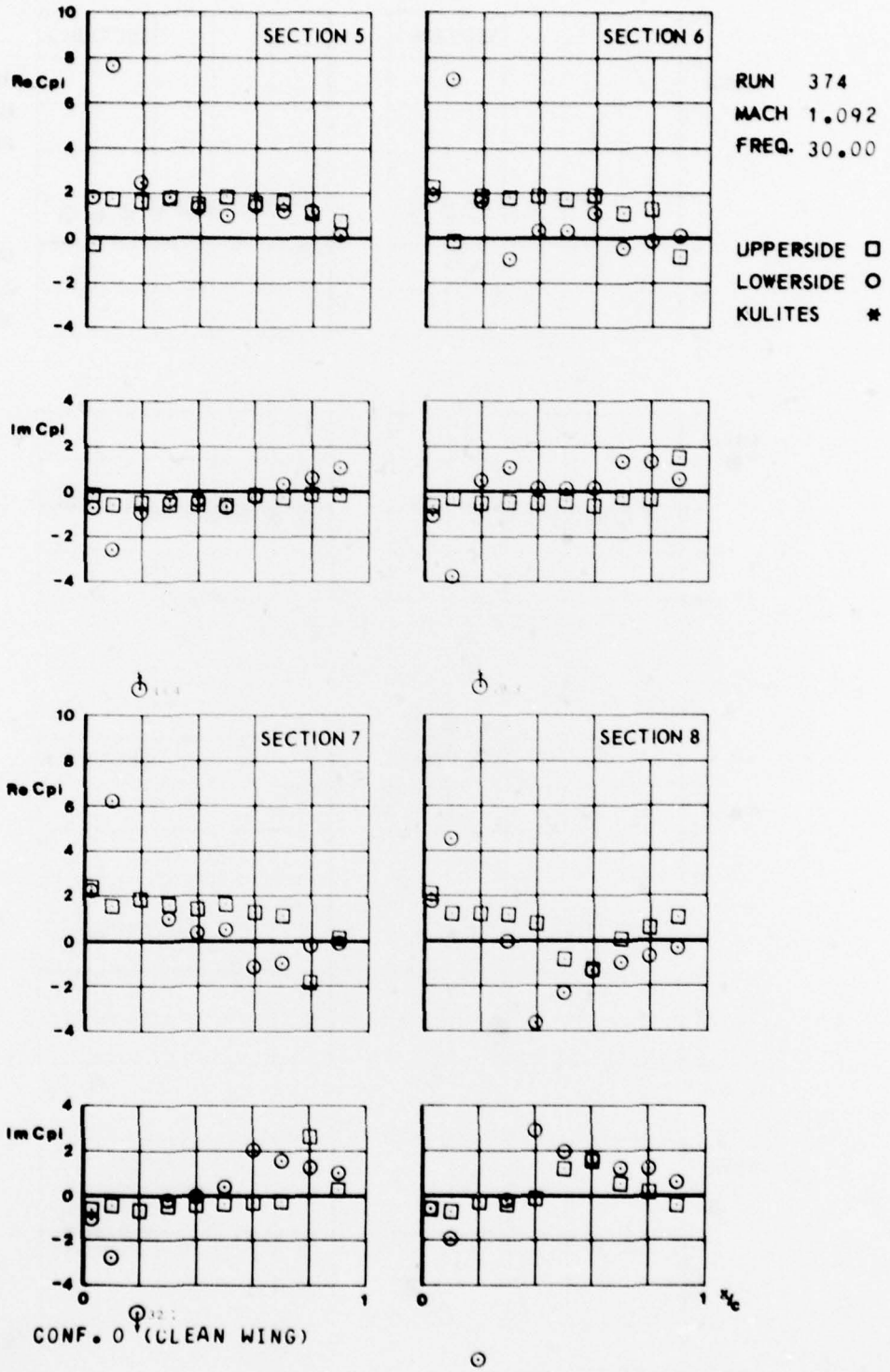

CONF. 0 (CLEAN WING)

FIG.
II.C.20.a

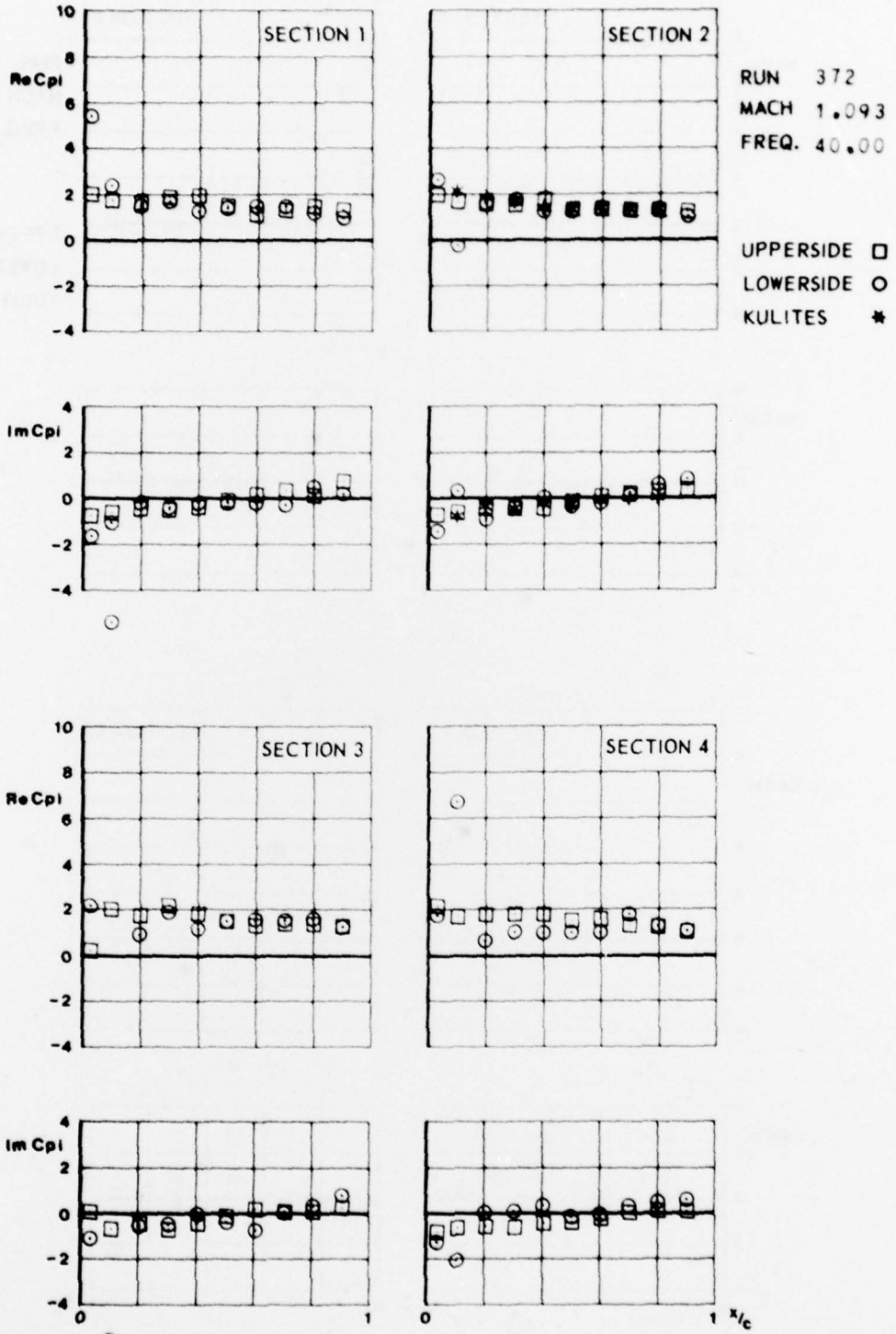

CONF. 0 (CLEAN WING)

FIG.
II.C.20.6

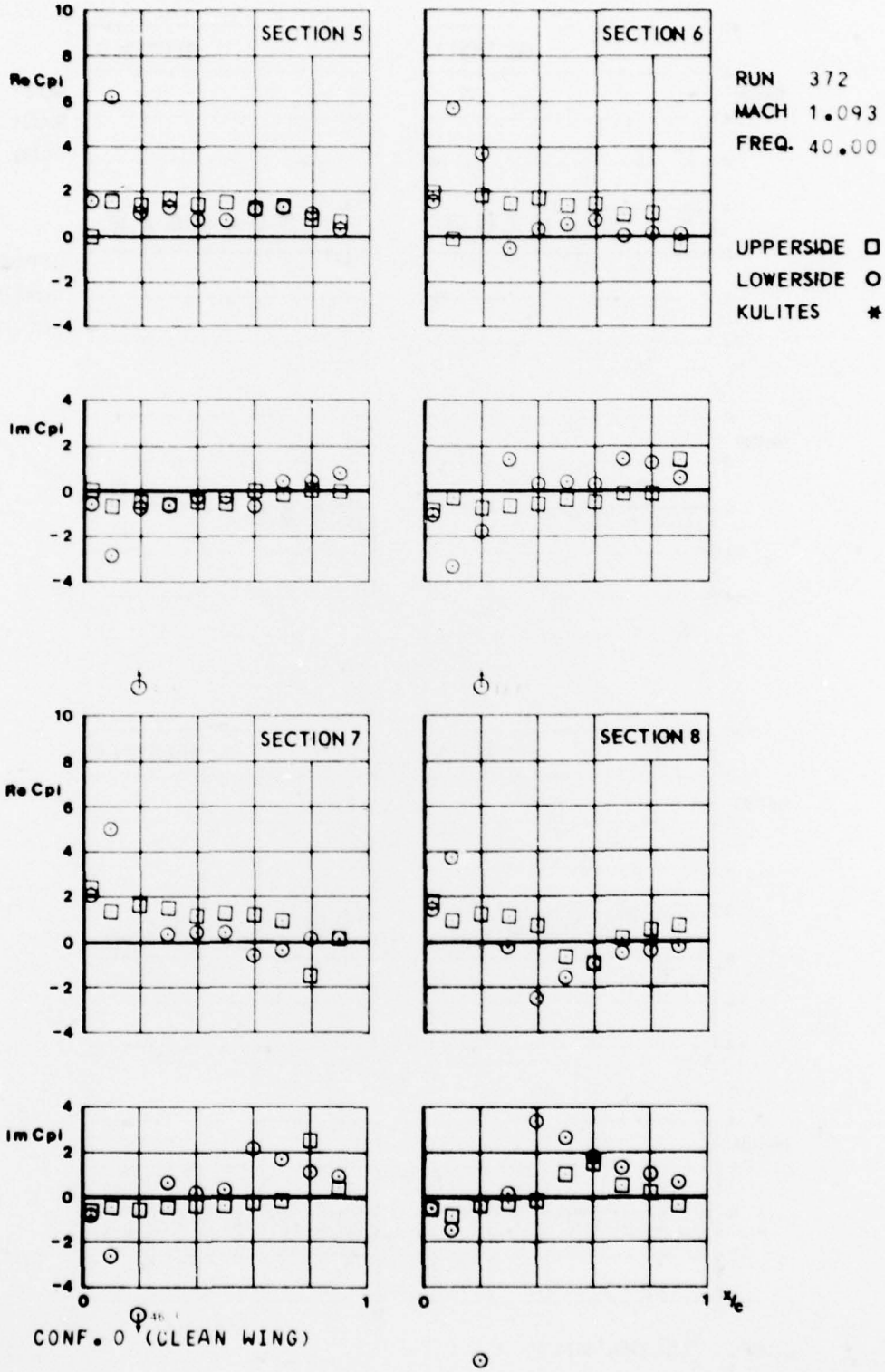
SECTION 5
SECTION 6
SECTION 7
SECTION 8
Re Cpi
Im Cpi
RUN 372
MACH 1.093
FREQ. 40.00
UPPERSIDE □
LOWERSIDE O
KULITES ✱
x/c
CONF. 0 (CLEAN WING)

FIG.
II.C.21.a

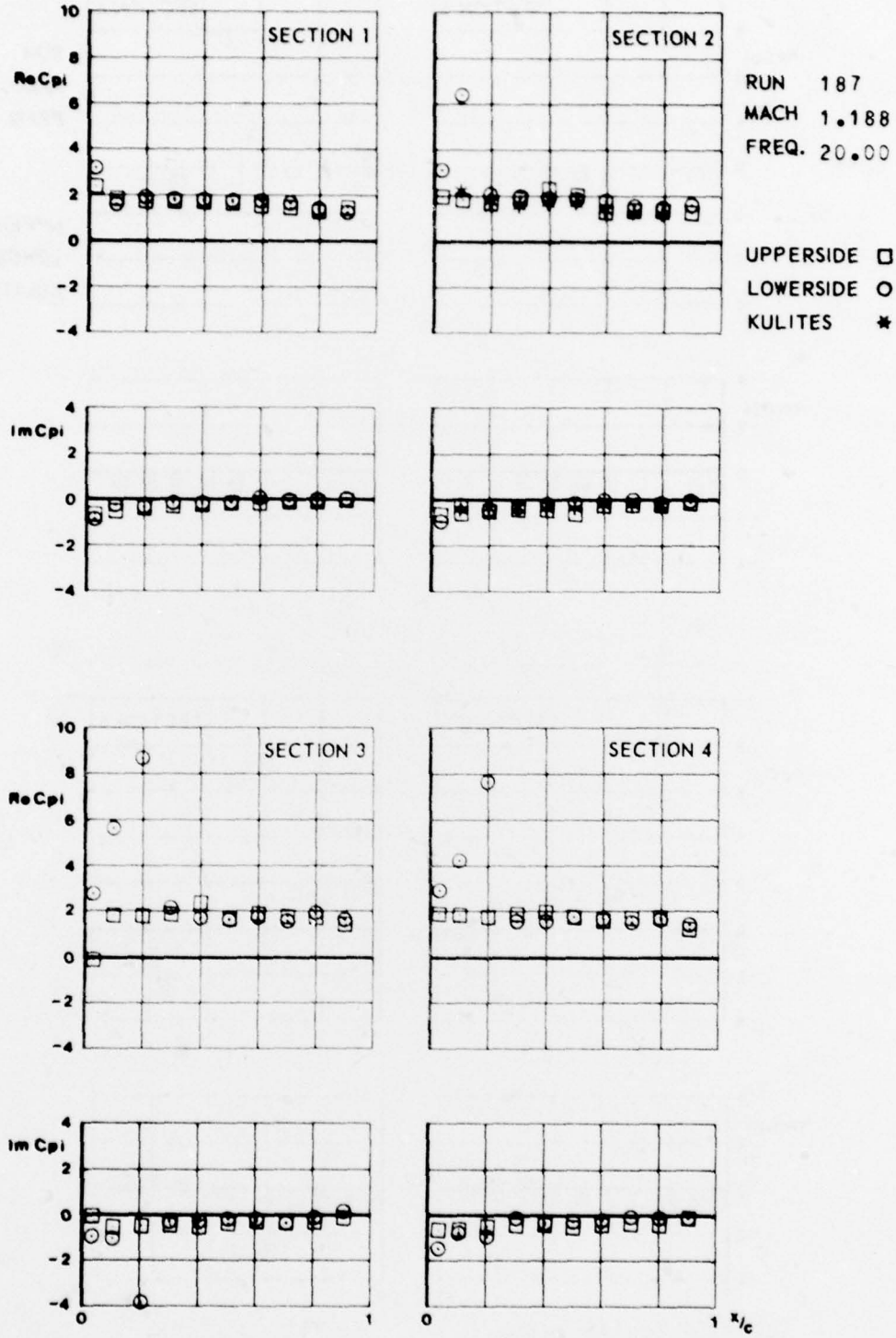

CONF. C (CLEAN WING)

FIG.
II.C.21.b

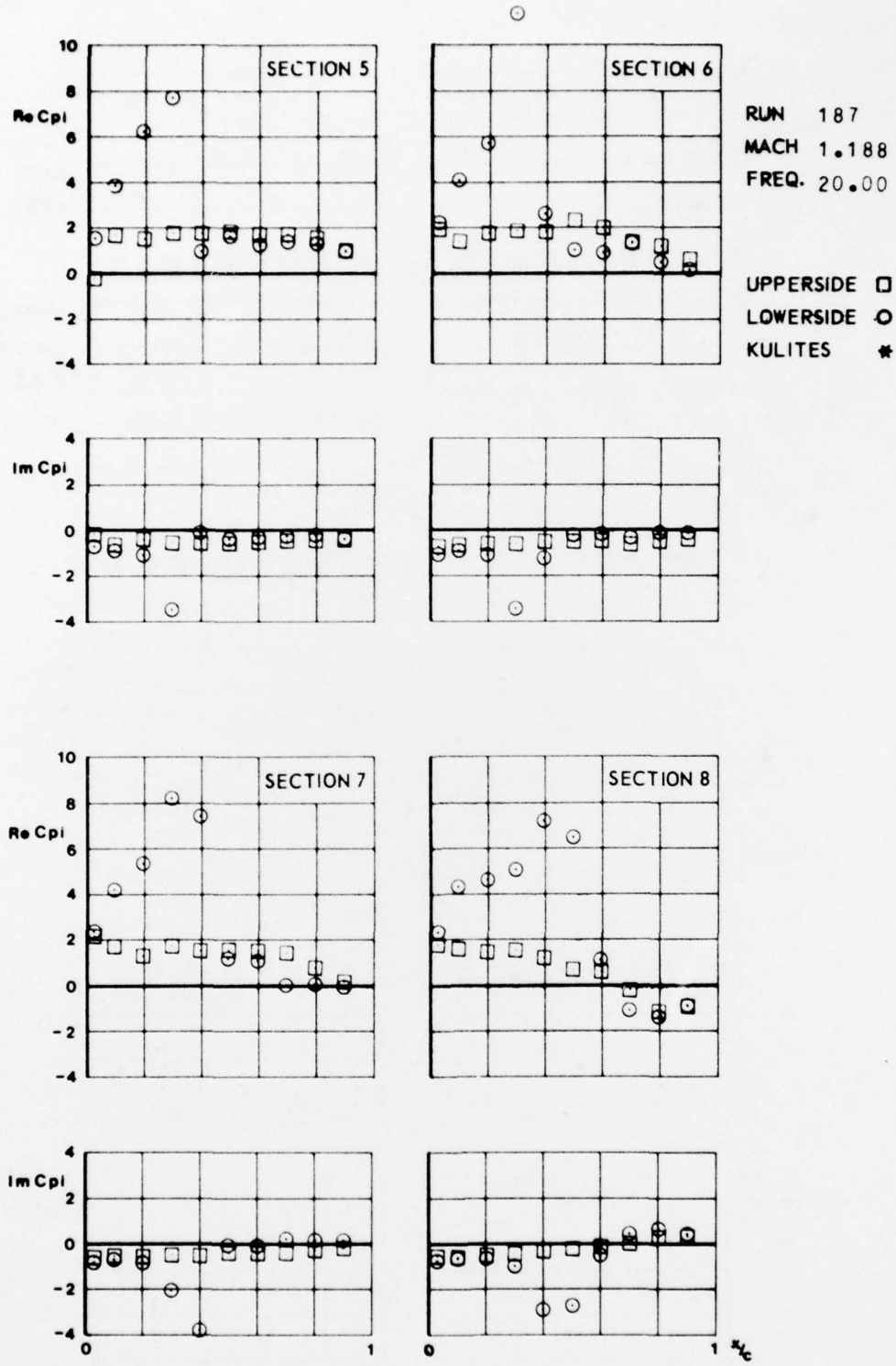

CONF. 0 (CLEAN WING)

FIG.
II.C.22.a

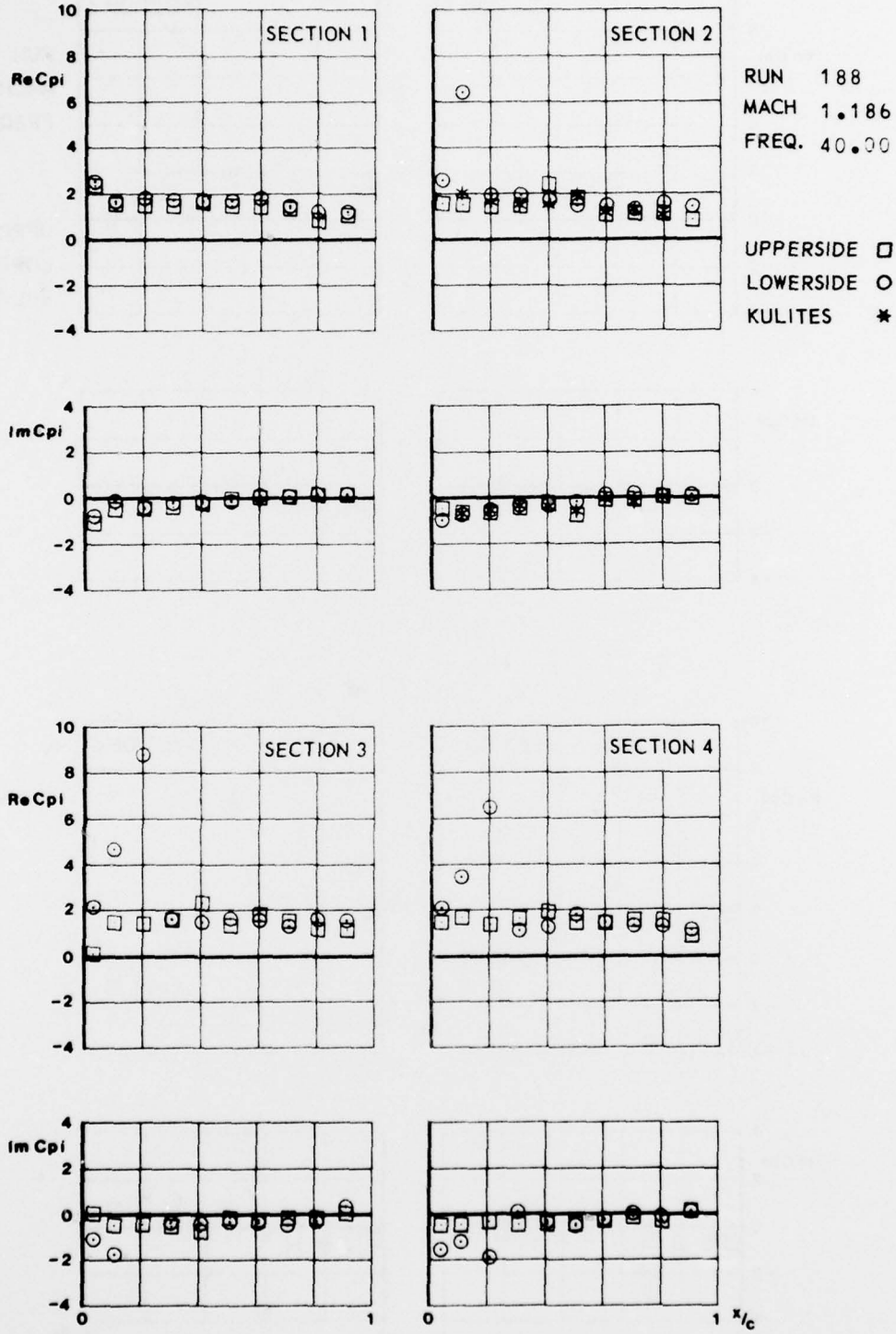

CONF. 0 (CLEAN WING)

FIG.
II.C.22.6

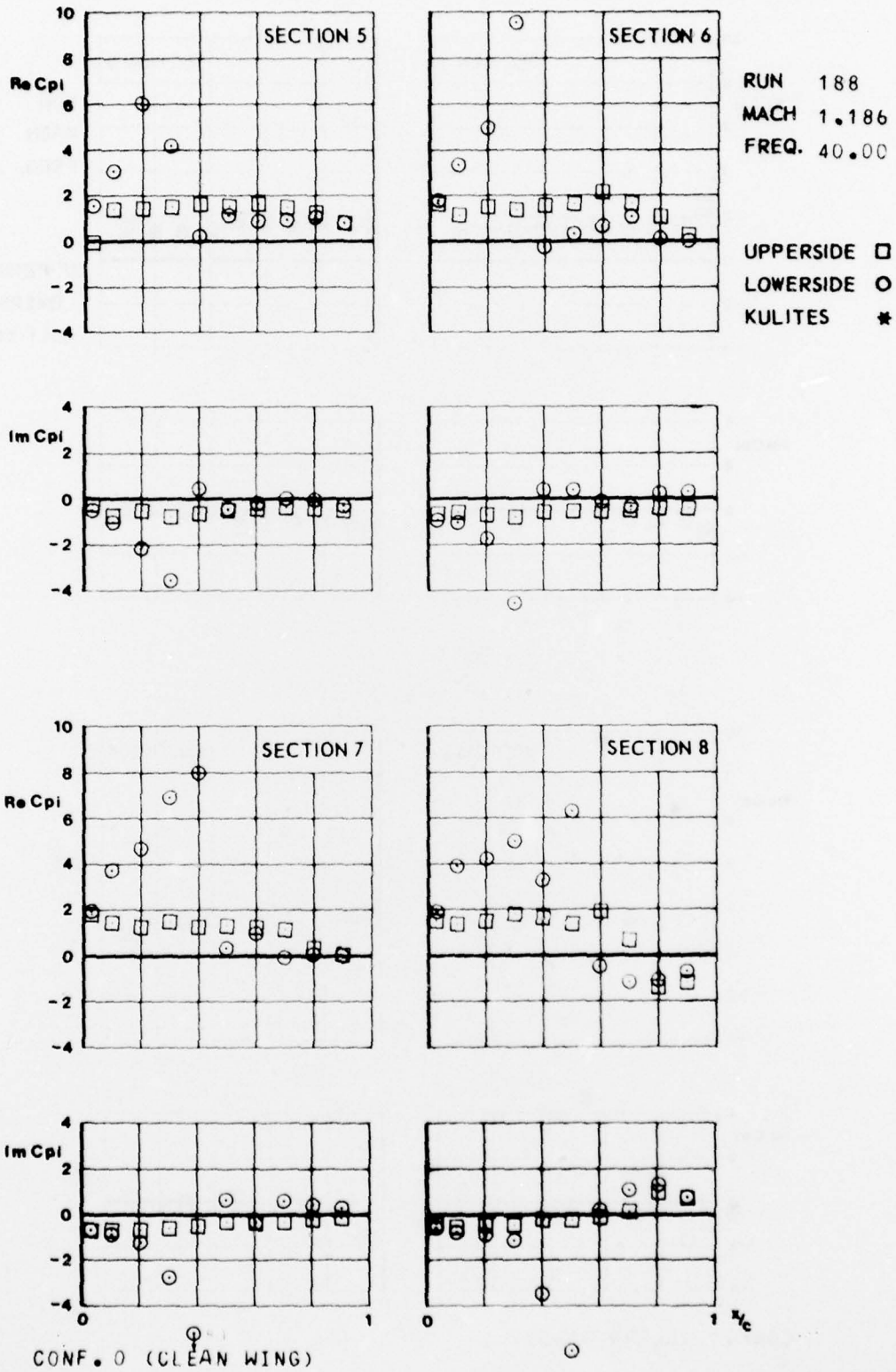

CONF. 0 (CLEAN WING)

FIG.
II.C.23.a

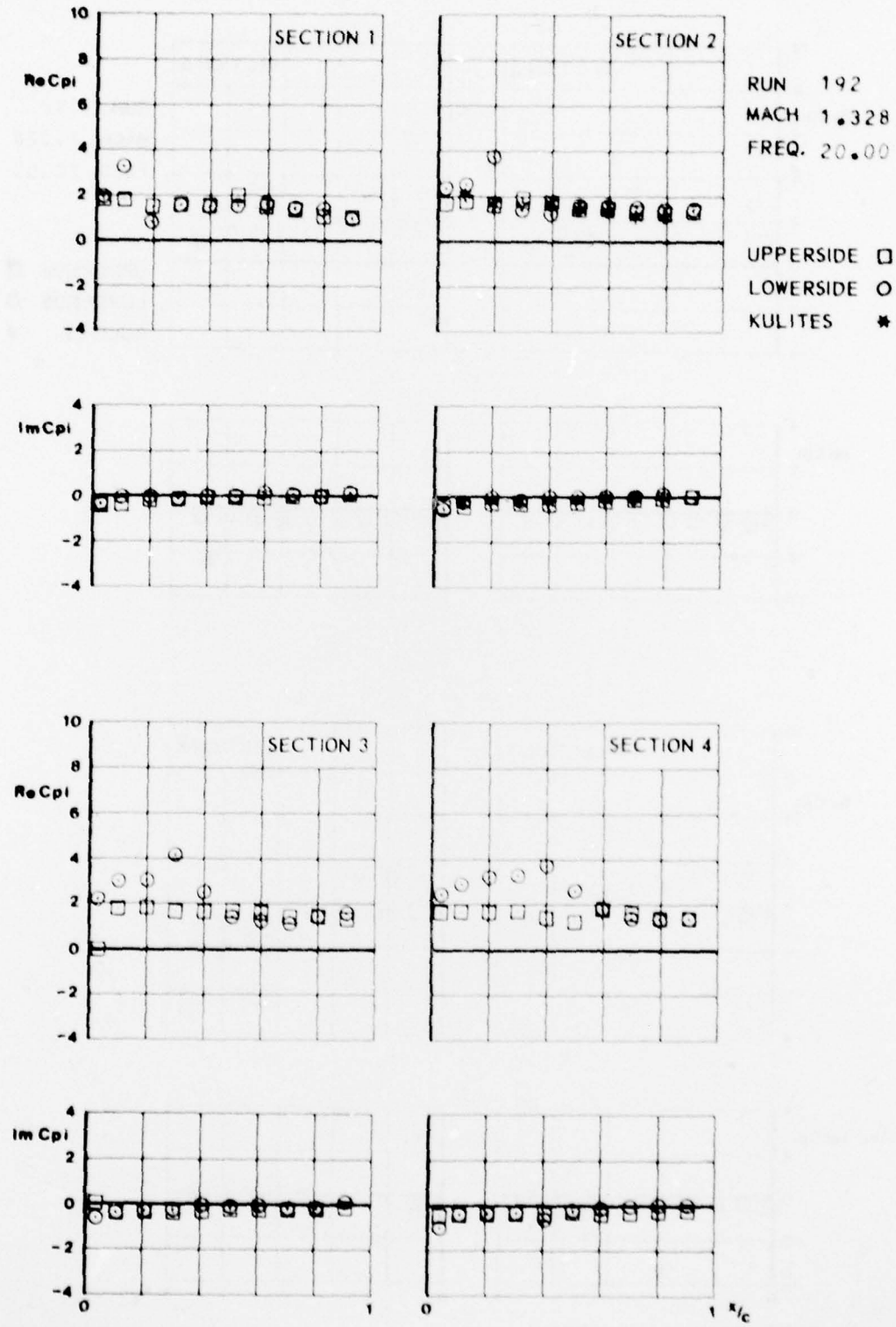

CONF.0 (CLEAN WING)

FIG.
II.C.23.b

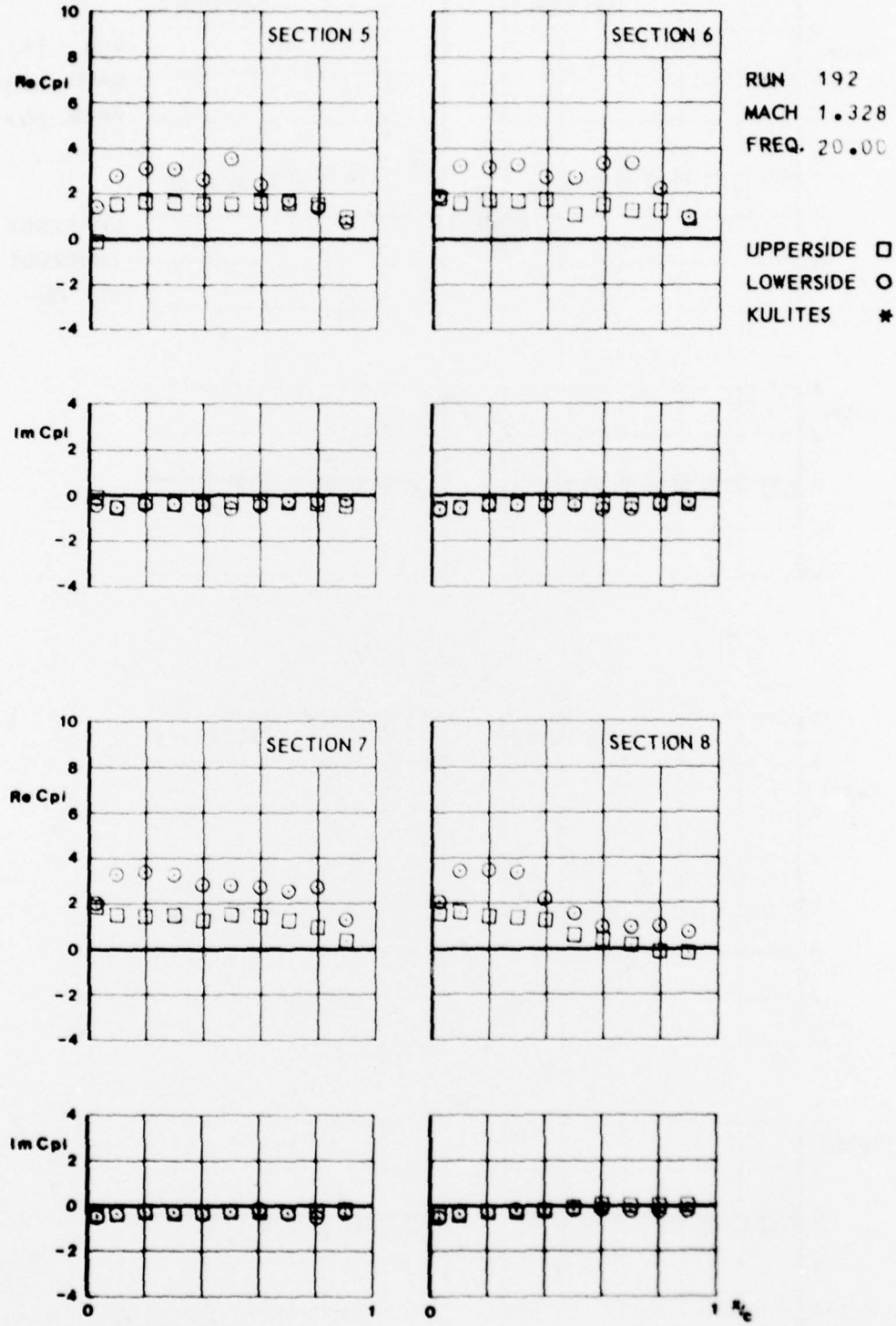

CONF. 0 (CLEAN WING)

FIG.
II.C.24a

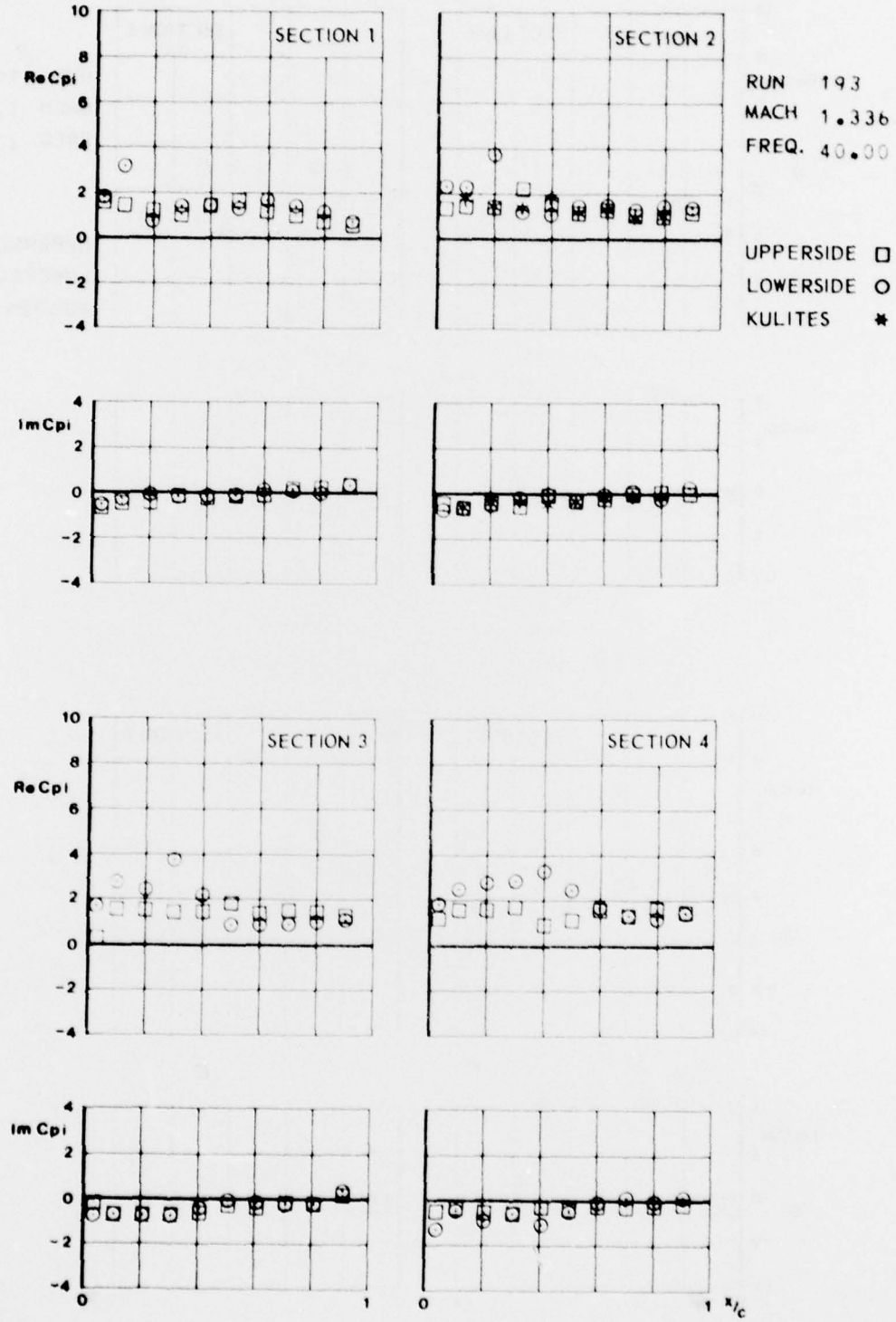

CONF. 0 (CLEAN WING)

FIG.
II.C.24.b

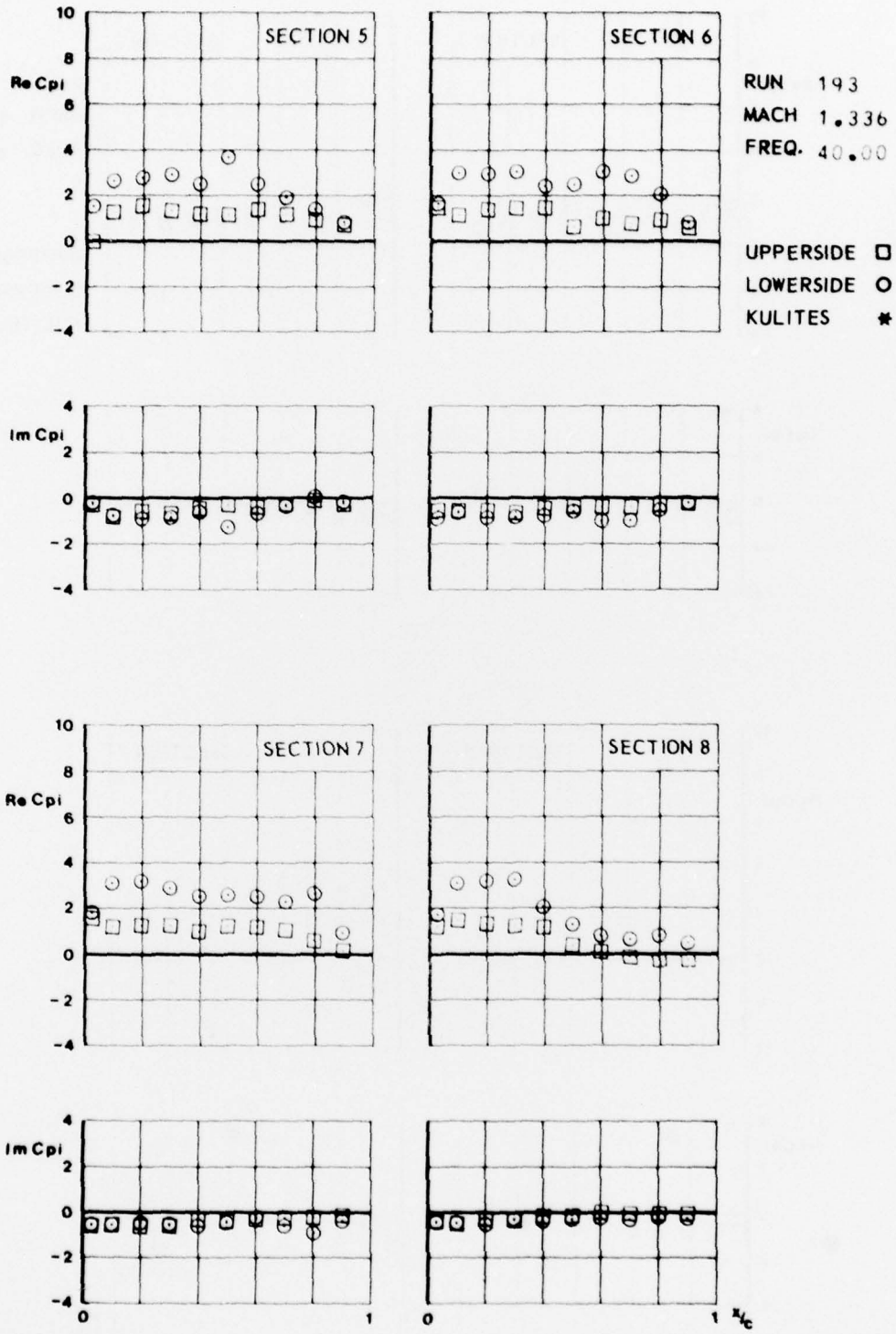

CONF. 0 (CLEAN WING)

☆U.S.Government Printing Office: 1979 — 657-002/608